공학박사학위논문

Fabrication of Gold Nanoparticle Microcapsules *via* Self-assembly of α-Synuclein and Their Application for Cargo Delivery System

알파-시뉴클레인의 자가조립을 통한 금 나노입자 마이크로캡슐의 제작 및 적재물 전달 체계로의 응용

2018 년 8 월

서울대학교 대학원

화학생물공학부

홍 철 석

Fabrication of Gold Nanoparticle Microcapsules *via* Self-assembly of α-Synuclein and Their Application for Cargo Delivery System

알파-시뉴클레인의 자가조립을 통한 금 나노입자 마이크로캡슐의 제작 및 적재물 전달체계로의 응용

지도교수 백 승 렬

이 논문을 공학박사 학위논문으로 제출함

2018년 8월

서울대학교 대학원

화학생물공학부

홍 철 석

홍철석의 박사학위논문을 인준함

2018년 7월

위 원 장	김 병기	(인)
부 위 원 장	백 승렬	(인)
위 원	김 병수	(인)
위 원	정 선호	(인)
위 원	유 동원	(인)

Abstract

Fabrication of Gold Nanoparticle Microcapsules *via* Self-assembly of α-Synuclein and Their Application for Cargo Delivery System

Chul-Suk Hong

School of Chemical and Biological Engineering

The Graduate School

Seoul National University

Bio-applicable cargo delivery system requires biocompatibility, *in vivo* stability, and controlled cargo release responding to external stimuli at target site. Here, the strategy for manufacturing Pickering emulsions of various

nano-sized particles including gold nanoparticles (AuNPs), silver nanoparticles (AgNPs), quantum dots (QDs) and magnetic nanoparticles (MNPs) by adjusting the surface property using self-assembly protein of α-synuclein (αS), and the αS-mediated fabrication of microcapsule as a cargo carrier derived from the Pickering emulsions were introduced. Both processes of the Pickering emulsion formation and the microcapsule fabrication are entirely due to the property of the αS conjugates onto nanoparticle. By encapsulating the nanoparticles with αS, the particles have a much higher detachment energy, which allows the particles to stably keep the Pickering emulsions structure from coalescence or degradation. As the organic solvent-induced β-sheet structures between the αS are formed, the emulsions could be derived into mechanically and chemically stable microcapsules. With Rhodamine 6G (R6G) loaded, the microcapsules exhibited controlled release of R6G by triggers such as proteases, pH and specific metal ion. Additionally, a rapid and localized heat generating photothermal activity of the microcapsules composed of AuNPs was investigated and the effectiveness of the hyperthermia therapy was confirmed by *in vitro* cell viability test. Furthermore, the microcapsules could obtain additional functions such as orthogonal cargo loading, imaging property, and targeting characteristic by taking inverted micelles, other nanoparticles, or antibodies, respectively. Taken together, fabrication of the AuNP microcapsule for cargo delivery

system are suggested, and the resulting multi-functional microcapsules could be served as ideal cargo carriers that exhibit appropriate properties in the applications for their uses.

Keywords

***α*-Synuclein, Cargo delivery system, Gold nanoparticles, Multimodal microcapsules, Pickering emulsion, Protein self-assembly**

Student number: 2010-23336

Contents

Part II

Microcapsule composed of Gold Nanoparticles *via* Self-assembly of α-Synuclein

List of Tables

List of Figures

Part I

Pickering Emulsion Formation of α-Synuclein-Nanoparticle Complex

I-1. Introduction

(1) Microencapsulation

Microencapsulation is a process in which cargoes (chemicals, particles, droplets, etc.) are surrounded by a coating material, or embedded in a homogeneous or heterogeneous matrix, to give micro-sized capsules (microcapsules) [1]. The microcapsules exhibit various useful properties depending on the characteristics of the coating materials. Although micro-capsules could be made of synthetic polymers [2-5] and natural biomolecules such as lipids [6, 7], proteins [8, 9], and polysaccharides [10], nanoparticles are advantageous as a coating material since they have mechanical and chemical stability as well as reactivity to physical stimuli such as light, heat, electricity, and magnetic fields. In fact, nanoparticles have been assembled into various structures of multiple dimensions and shapes in order to enhance

their optical, electrical, catalytic and magnetic properties more effectively. In particular, if microcapsules assembled with nanoparticles are utilized in cargo delivery systems, the properties of nanoparticles could be exploited in the overall process of fabricating, functionalizing, transporting and operating microcapsules.

(2) Pickering emulsion

In order to fabricate microcapsules composed of nanoparticles, Pickering emulsion [11] can be employed. Pickering emulsion is an emulsion stabilized by solid particles which adsorb onto the interface between two immiscible phases, where the solid particles lower the surface energy of the emulsions and prevent the emulsions from coalescence [12]. The lower surface energy of the emulsion can then be expressed as the energy required to detach the particles from the interface, which is called detachment energy. When the particle is located at the interface as shown in **Figure 1**, the detachment energy E_d is given by

$$E_d = \pi R^2 \gamma_{ow} (1 \pm \cos\theta)^2 \qquad \textbf{(Equation 1)}$$

in which the sign inside the bracket is negative when detach the particle to the water phase and positive when detach the particle to the oil phase [13]. The steps for obtaining **Equation 1** are represented in **Figure 1**. E_d shows the

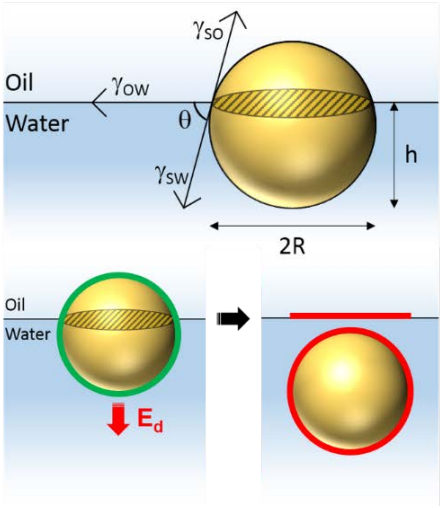

$h = R(1 + \cos\theta)$

$A_w = 2\pi Rh = 2\pi R^2(1 + \cos\theta)$

$A_o = 2\pi R(2R\text{-}h) = 2\pi R^2(1 - \cos\theta)$

A_i ( ) $= \pi R^2 \sin^2\theta = \pi R^2(1 - \cos^2\theta)$

In o/w system, $(0° \leq \theta \leq 90°)$

$E_d = \{(A_w + A_o)\gamma_{sw} + A_i\gamma_{ow}\} - (A_w\gamma_{sw} + A_o\gamma_{so})$

$= 2\pi R^2(1 - \cos\theta)(\gamma_{sw} - \gamma_{so}) + \pi R^2(1 - \cos^2\theta)\gamma_{ow}$

By Young's equation, $(\gamma_{so} = \gamma_{sw} + \gamma_{ow}\cos\theta)$

$E_d = \pi R^2\gamma_{ow}(1 - \cos\theta)^2 \qquad (0° \leq \theta \leq 90°)$

Figure 1. Schematic representation for obtaining detachment energy. When particles at the interface are moved to one phase, the detachment energy is expressed as the energy difference of the system before and after the movement. In water-in-oil (w/o) system ($90° \leq \theta \leq 180°$), the minus sign in the equation representing detachment energy is changed to plus sign. The subscripts 'w', 'o', 'i' and 's' mean 'water phase', 'oil phase', 'interface' and 'solid particle', respectively.

largest value when $\theta = 90°$, which means that it is advantageous to form a Pickering emulsion when the particles have similar wettability in both the water and oil phases. Since E_d is proportional to the square of the particle radius, it is an essential process to manipulate the surface properties of the particles in nano-sized particles. For this purpose, particles could be coated using coating materials such as polymer [14-16], lipid [17], starch [18], and protein [19] to effectively form Pickering emulsion. In this study, Pickering emulsion was prepared using a protein of α-synuclein (αS) with self-assembly property as a coating material.

(3) α-Synuclein

αS is an amyloidogenic protein comprised of 140 amino acids, and its primary structure is separated into three regions [20]: (i) an amphipathic N-terminal region (residues 1-60) suggested to interact with lipid membrane; (ii) a hydrophobic central region (residues 61-95) containing the non-Aβ component (NAC) segment; and (iii) a highly acidic C-terminal stretch (residues 96-140). This protein is an intrinsically disordered protein (IDP) which is a protein that lacks a fixed or ordered three-dimensional structure [21-23] and have been characterized by multiple partner interactions enabled by their structural plasticity [22, 24, 25]. Unlike other structured proteins,

IDP does not have a specific structure. When proteins interact with other materials such as ligands, however, they become structured and functional through structural changes [26]. αS is known to form an α-helical structure when directly biding to the negatively charged lipid membrane [27-31] with its four 11-residue repeats including the consensus sequence KTKEGV in N-terminal region [32]. Interestingly, when αS interacts with the neutral lipid membrane, it has been reported that the αS forms a β-sheet structure by forming radiating amyloid fibrils (RAFs) [33]. It could be also structured in a β-sheet formation when assembled into amyloid fibrils [34, 35] through self-assembly. Mechanisms of the self-assembly of αS are classified into two types, nucleation-dependent assembly and unit-assembly. The nucleation-dependent fibrillation model has been widely accepted as a mechanism of amyloidogenesis [36, 37]. Once the monomers form into the nucleus, they experience a conformational transition to an amyloidogenic form and then grow into a fibrillar structure [38]. Besides this type of self-assembly, the αS has a tendency to assemble rapidly by formidable cross-β-sheet structures *via* unit-assembly when it is exposed to stimuli such as organic solvent [39] or shear stress [40]. Based on this assembly model, the fibril formation is achieved via assembly of oligomers resulting from association of monomers, where the oligomers act as a growing unit for the fibril formation in the absence of template [39-41]. Furthermore, through this unit-assembly, αS

could be assembled into not only amyloid fibril structures but also various types of structures. It was actually proven by producing pea-pod type 1D nanochains of gold nanoparticles (AuNPs) conjugated with αS in the presence of either 5 % hexane or pH change [42] and fabricating free-floating 2D film of AuNP by the self-associative property of αS upon contact with chloroform [43, 44]. When preparing a water-in-oil (w/o) Pickering emulsion, contact between the solid particles absorbed on the emulsion surface and the organic solvent is inevitable. Therefore, αS could be applied as a coating material of nanoparticles for foaming Pickering emulsion by taking several advantages such as amphipathicity and unit-assembly propensity.

I-2. Results and Discussion

(1) Preparation of αS-AuNP conjugates

Pickering emulsions composed of AuNPs have been produced by using AuNPs coated with αS (αS-AuNP conjugates). αS-AuNP conjugates were prepared by incubating the mixture of αS and citrate-capped colloidal AuNPs in 20 mM Mes pH 6.5 for 12 hours at 4°C (**Figure 2A**). Successful coating of αS onto AuNP was confirmed with a red-shift of the localized surface plasmon

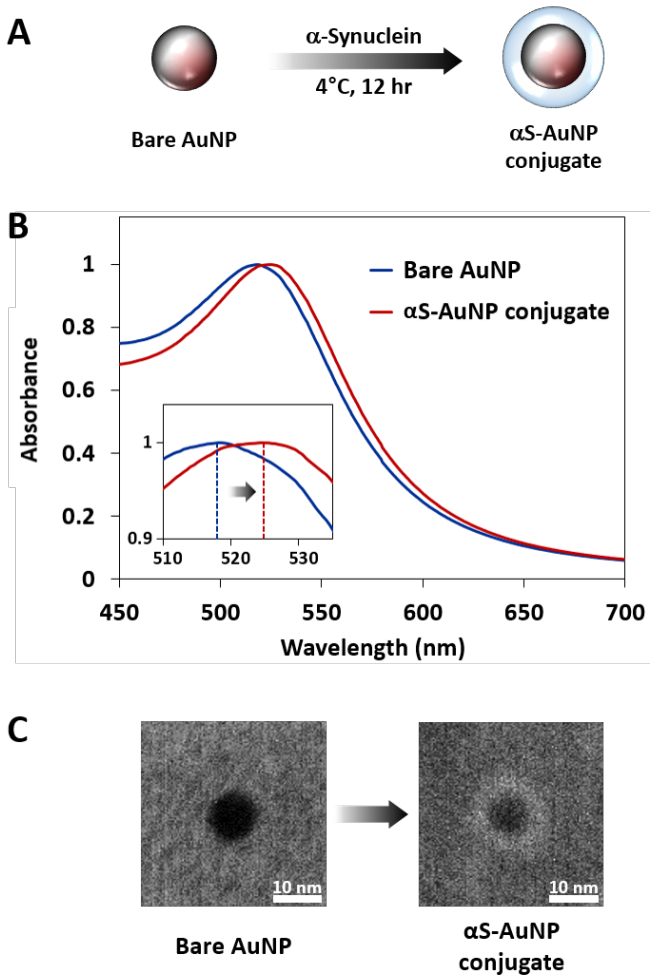

Figure 2. Coating AuNP with αS. (A) Scheme for obtaining αS-AuNP conjugate. **(B)** LSPR spectra of bare AuNPs and αS-AuNP conjugates. The spectrum of αS-AuNP conjugates was red-shifted due to an increase in the local refractive index at the AuNP surface caused by αS. **(C)** TEM images of bare AuNP and αS-AuNP conjugate.

resonance (LSPR) spectrum obtained using a UV-VIS spectrophotometer (**Figure 2B**) and observing αS represented as a white halo around the AuNP using a transmission electron microscope (TEM) (**Figure 2C**). The principle that αS binds to AuNP is thought to be an electrostatic interaction between the positively charged N-terminal (pI = 9.96) of αS consisting mainly of basic amino acids and the negatively charged citrate-capped surface of AuNP [45] (**Figure 3A** and **3B**). Evidence of the orientation of binding αS can be shown through zeta (ζ) potential measurements, as bare (citrate-capped) AuNP and αS-AuNP conjugate will have the same charges because of the negatively charged citrate and C-terminal (pI = 3.64) of αS, respectively. The ζ potential of bare AuNP was -23.6 mV (± 2.1 mV) before the αS coating and -15.6 mV (± 3.6 mV) after at 20 mM Mes (pH 6.5) (**Figure 4**). The binding of αS, therefore, is greatly affected by the surface charge and surface charge density of AuNP. The surface charge effect on the conjugate formation was confirmed by altering the citrate-coated surface charge of AuNP with pH of the solution. However, AuNPs (20 nm) became unstable and thus agglomerated at pHs lower than 5 and higher than pH 8 as shown with LSPR spectra (**Figure 5**). Therefore, the stable conjugates could be prepared only at pH 6 and pH 7. In fact, the slightly acidic pH (pH 6.5) was the condition to prepare the αS-AuNP conjugates for the Pickering emulsion formation. Moreover, the AuNP stability was also dependent on ionic strength of the solution since the particles

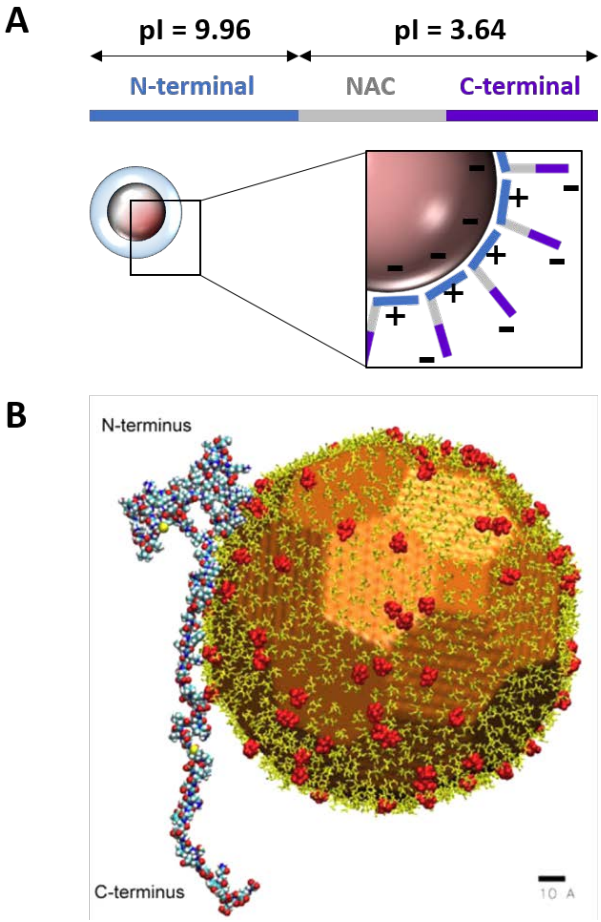

Figure 3. Interaction between αS and AuNP. (A) Scheme of αS orientation upon its binding onto AuNP **(B)** VMD rendering of αS simulated interaction with individual citrate capped AuNPs[Lin, Wayne, et al. 119(36) **2015**, 21035-21043].

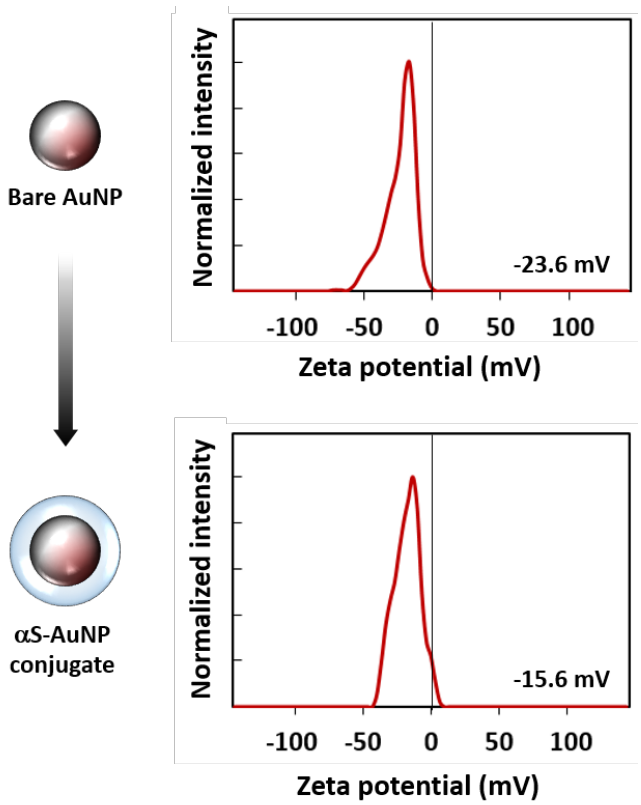

Figure 4. Zeta (ζ) potential of bare AuNP and αS-AuNP conjugate. The particles and conjugates were in 20 mM Mes pH 6.5, and the measurements were carried out at 25ºC.

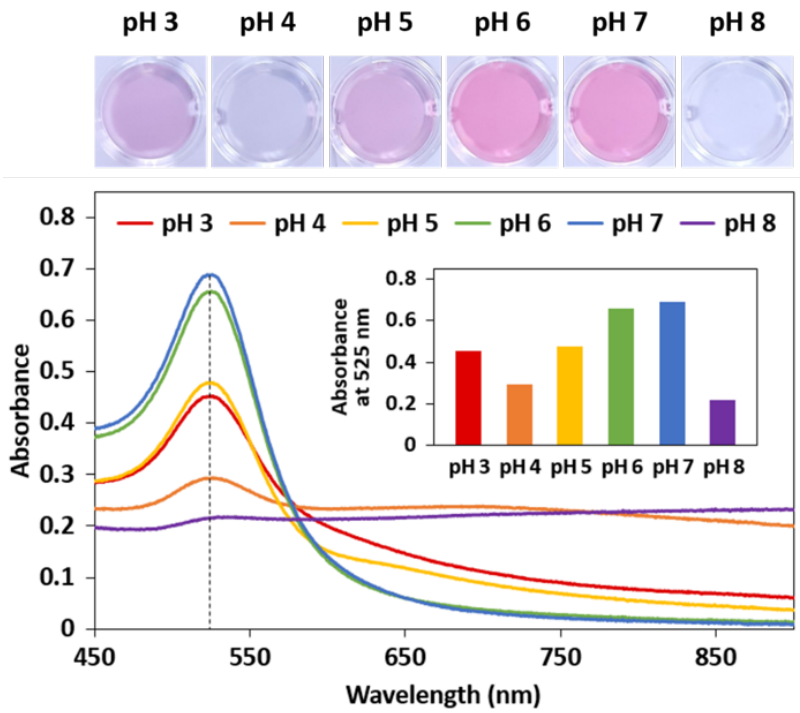

Figure 5. Colloidal stability of AuNPs in various pH condition. The inset graph shows the absorbance of each sample at wavelength of 525 nm.

became agglomerated at the high salt concentration of Mes (50 mM and 100 mM) even at the same pH of 6.5 (**Figure 6**). Therefore, the properties of AuNP such as surface charge and surface charge density definitely play an important role in producing the stable αS-AuNP conjugate and subsequent formation of Pickering emulsion.

(2) Pickering emulsion of AuNPs

The Pickering emulsions were prepared by adding a small amount (1/10 of the solution) of chloroform to the αS-AuNP conjugates solution, and then treating with a brief sonication for 5 seconds at 40 kHz and 100 W (**Figure 7A**). After sonication treatment, the red color of the water layer caused by colloidal αS-AuNP conjugates became transparent and the chloroform layer was disappeared as the αS-AuNP conjugates formed a deep red emulsion layer below the water layer (**Figure 7B** and **7C**). Because the density of chloroform is bigger than water, the formed emulsion settled in the bottom of the water layer. In the case of bare AuNPs, on the other hand, the chloroform layer remained intact even after sonication treatment, and the particles became aggregated and the color changed from red to purple (**Figure 7B**). This phenomenon could be understood by the Derjaguin-Landau-Verwey-Overbeek (DLVO) theory [46] of colloidal stability [47], suggesting that two

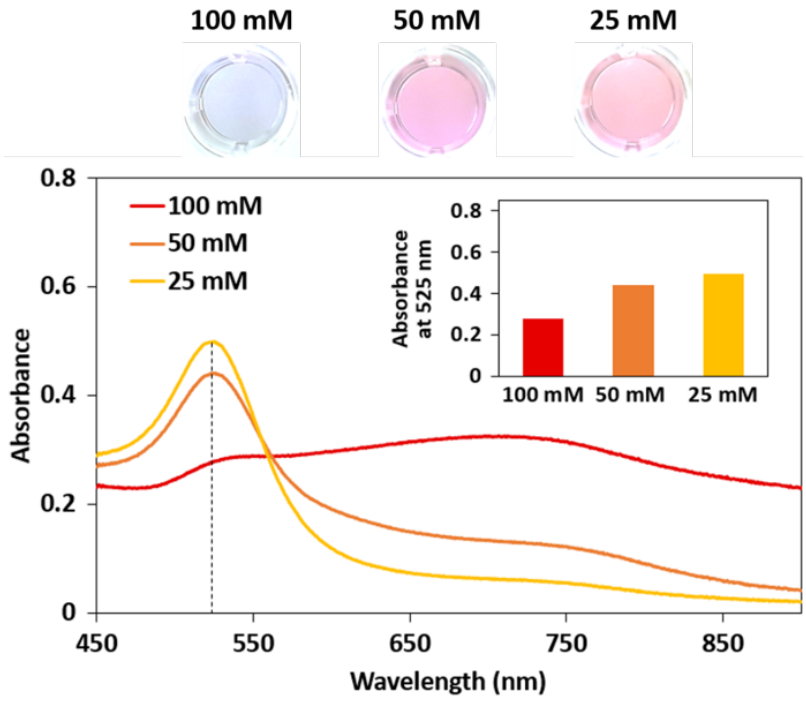

Figure 6. Colloidal stability of AuNPs in various ionic strength. The inset graph shows the absorbance of each sample at wavelength of 525 nm.

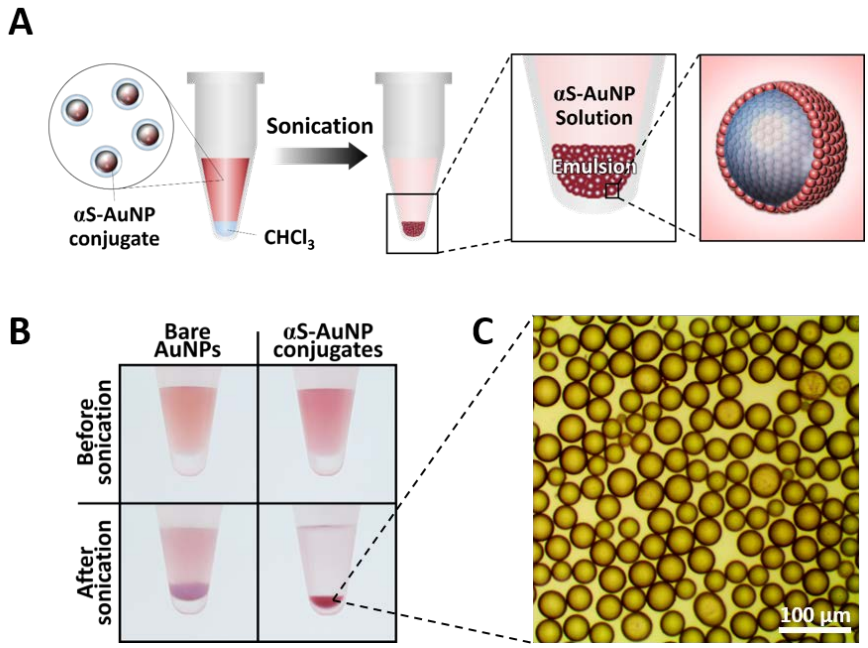

Figure 7. Pickering emulsion formation of αS-AuNP conjnugates. (A) Schematic representation of the formation process of αS-AuNP conjugate Pickering emulsions. **(B)** Agglomerate and Pickering emulsion formation of bare AuNPs and αS-AuNP conjugates obtained after sonication, respectively. **(C)** Microscopic images of Pickering emulsion composed of the αS-AuNP conjugates.

particles colloidally stable by a sufficiently high energy barrier (primary maximum) to prevent aggregation of the particles become irreversible aggregation at the primary minimum *via* high energy treatment using sonication (**Figure 8**). This irreversible aggregation is not observed in the case of αS-AuNP conjugates because the distance between the particles is maintained due to the protein coat on the particle surface. The effect of preventing the AuNP aggregation by protein coat is also confirmed during αS-AuNP conjugate preparation. The αS-AuNP conjugates did not aggregate during centrifugation at 13,200 rpm (16,100 g) and their pallets were easily resuspended, but the bare AuNPs irreversibly aggregated at the same rpm, making resuspension impossible (data not shown). As a result, in the Pickering emulsion formation, the coating of AuNPs with αS is an essential process because it plays an important role in preventing irreversible aggregation of the particles.

(3) Detachment energy

The αS-AuNP conjugates formed Pickering emulsions in all cases using 5, 10, 20 and 30 nm AuNP, and the size of the emulsions formed increased in proportion to the size of the gold nanoparticles (**Figure 9**). Average size of the Pickering emulsions prepared with αS-AuNP conjugates enclosing 5 nm, 10

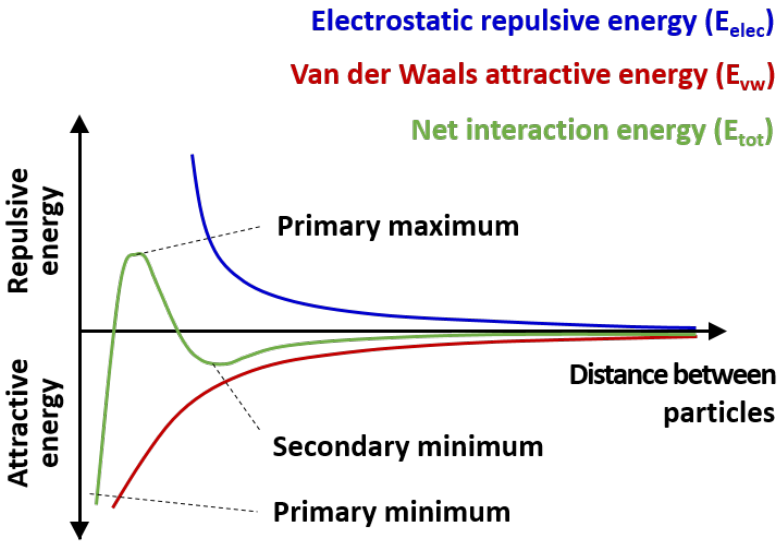

Figure 8. Schematic plots of the DLVO interaction. The plot shows how the attractive van der Waals and repulsive electrostatic double-layer forces together determine the total interaction potential.

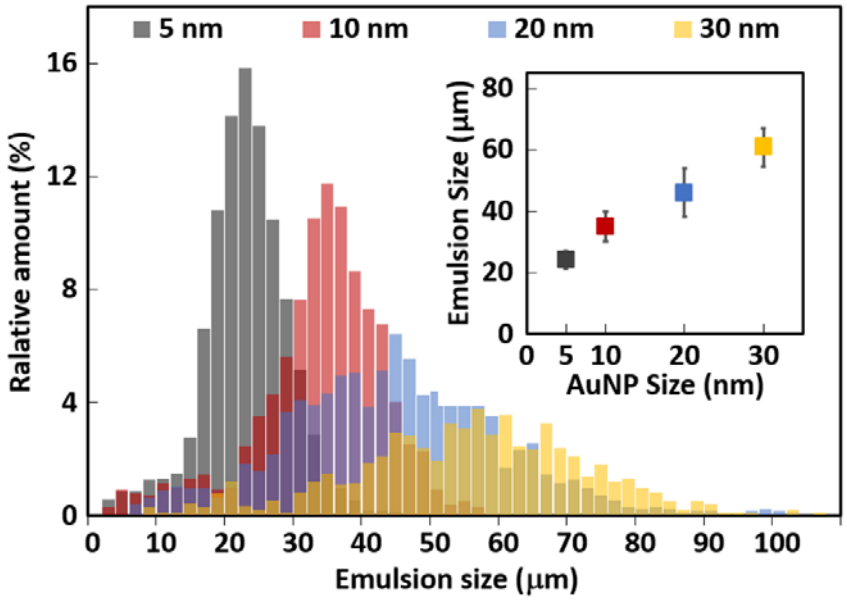

Figure 9. Size distribution of the Pickering emulsions comprised of 5, 10, 20, and 30 nm αS-AuNP conjugates. The emulsion size was obtained by measuring the individual emulsions revealed on microscopic images. The inset graph shows a linear relationship between the particle size and the average size of Pickering emulsions.

nm, 20 nm, 30 nm core AuNPs measured 24.1 μm (± 3.0 μm), 35.1 μm (± 4.7 μm), 46.0 μm (± 7.8 μm), 60.9 μm (±6.3 μm), respectively. If the contact angle depends only on the interfacial tension of the oil-water, oil-particle, and water-particle, αS-AuNP conjugate of different core sizes may be considered to have the same contact angle at the oil-water interface. From this viewpoint, it seems natural that a sphere structure formation with those different sets of conjugates would result in the larger emulsions in size for the larger conjugates. In the case of Bare AuNPs, however, Pickering emulsions were not formed even in vigorous shaking or vortexing, not sonication, at all sizes of 5 nm, 10 nm, 20 nm and 30 nm; αS-AuNP conjugates formed Pickering emulsions through vigorous shaking or vortexing (data not shown). This may be because E_d of bare AuNP is lower than that of αS-AuNP conjugate. The E_d varies greatly according to the contact angle (θ) of the particle with interface (**Figure 10**), but it is technically difficult to measure θ for the nano-sized particle. The θ of the nanoparticle, therefore, could be derived indirectly by measuring contact angle of water (θ_w) or oil (θ_w) droplet on planar bare gold plate (AuP) or αS-coated gold plate (αS-AuP) (**Figure 11A**). By joining Young's equations [48, 49] for the three contact angles (θ, θ_w and θ_o), the cosθ was obtained by

$$\cos\theta = (\gamma_{WG}\cos\theta_w - \gamma_{OG}\cos\theta_o) / \gamma_{OW} \qquad \textbf{(Equation 2)}$$

in which the θ_W and θ_O can be measured using a drop shape analyzer. Contact angles (θ_w) of 20 mM Mes (pH 6.5) droplets on bare AuP and αS-AuP were

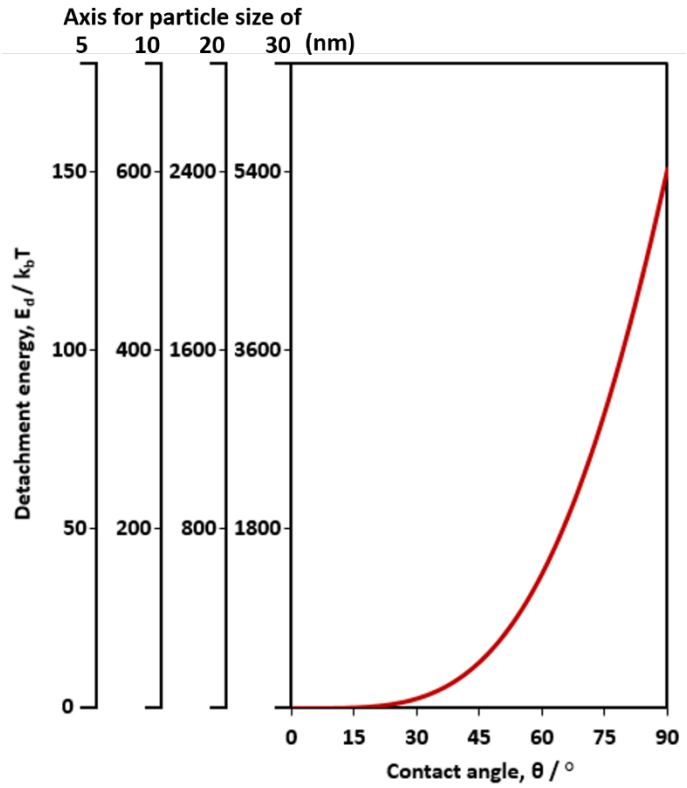

Figure 10. Detachment energy by particle size and contact angle at water-chloroform interface. The detachment energy increases exponentially as the size of the particles increases and the contact angle approaches 90°.

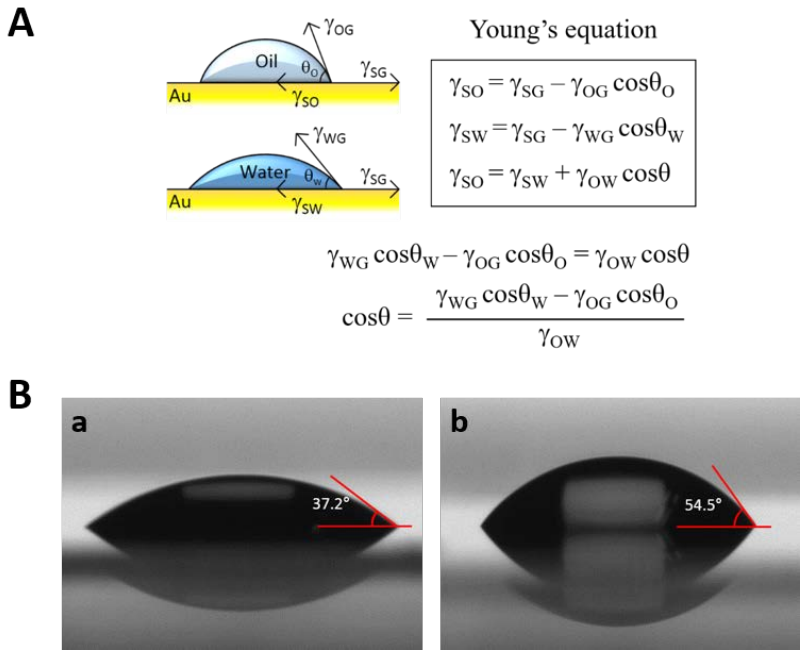

Figure 11. Measurement of contact angle on planar gold plate. (A) Schematic representation for obtaining cosθ via measuring contact angle of water (θ_w) or oil (θ_w) droplet on planar gold plate. **Equation 2** was obtained by joining three Young's equations. **(B)** Contact angles (θ_w) of 20 mM Mes (pH 6.5) droplets on bare AuP (**a**) and αS-AuP (**b**).

37.2° and 54.5°, respectively (**Figure 11B**), while contact angles (θ_o) of chloroform droplets were too low to measure using analyzer on both surfaces and therefore the $\cos\theta_o$ was approximated by 1. As a result, the E_d of αS-AuNP conjugate calculated by **Equations 1** and **2** is 41.0 k_bT, which is about 305 times higher than that of bare AuNP (0.13 k_bT). Since the surface tension of the oil phase (γ_{OG}) and the interfacial tension with water (γ_{OW}) are important factors in obtaining the E_d, Pickering emulsions were prepared using various organic solvents having different surfaces and interfacial tension values (**Figure 12**). The γ_{OG} and γ_{OW} of each organic solvent and E_d of both bare AuNP and αS-AuNP conjugate for each organic solvent are shown in **Table 1**. The bare AuNPs did not form a Pickering emulsion for all the organic solvents (data not shown), whereas the αS-AuNP conjugates formed the emulsion for *tert*-butyl acetate, chloroform, toluene, and hexane except *n*-butyl alcohol and ethyl acetate (**Figure 12**). Note that Pickering emulsions were formed even when the ethyl acetate was used as an oil phase with αS-AuNP conjugates where they have a lower E_d value than using toluene or hexane with bare AuNPs. This is thought to be due to the αS-αS interaction between particles, since αS is characterized in that unit-assembly is accelerated when it comes into contact with an organic solvent [42, 43]. In the presence of toluene, stable but polydisperse emulsions were formed, while *tert*-butyl acetate and hexane produced unstable and agglomerated emulsions (**Figure 12**). When

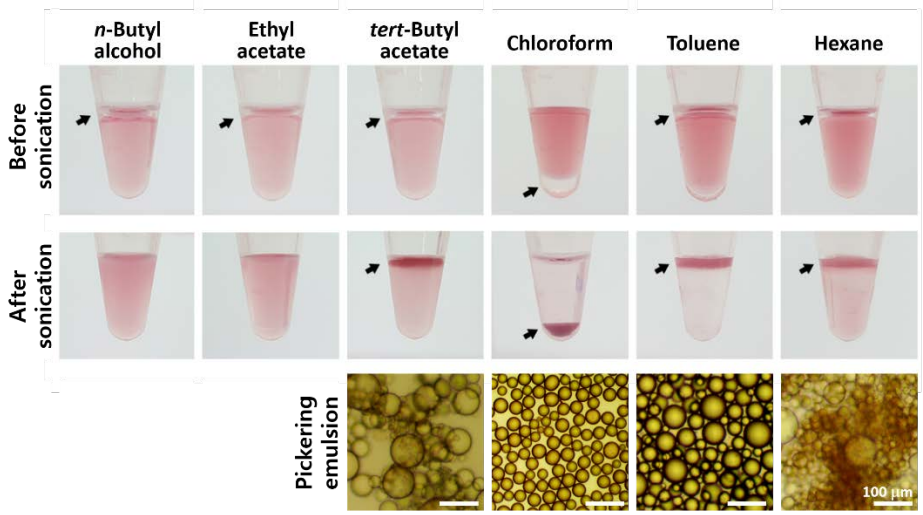

Figure 12. Pickering emulsion formation of αS-AuNP conjugates using various organic solvents with the sonication. Pickering emulsions were formed with *tert*-butyl alcohol, chloroform, toluene and hexane, but not with *n*-butyl alcohol and ethyl acetate. The Pickering emulsions with *tert*-butyl acetate or hexane were aggregated with each other, while the emulsions with chloroform or toluene did not aggregated. Optical images of the Pickering emulsions are shown. The arrow indicates the position of the organic solvent or picking emulsions.

Table 1. The surface tension, interfacial tension and detachment energy of bare AuNP and αS-AuNP conjugate for various organic solvents.

Organic solvent	*n*-Butyl alcohol	Ethyl acetate	*tert*-Butyl acetate	Chloroform	Toluene	Hexane
Surface tension* (γ_{oG})	24.2	23.3	22.0	26.7	28.4	18.4
Interfacial tension* (γ_{ow})	1.8	6.8	22.0	31.6	36.1	51.1
E_d of Bare AuNP**	N/A	N/A	N/A	0.13	5.20	7.86
E_d of αS-AuNP conjugate**	N/A	N/A	1.52	41.0	57.2	42.7

* The unit is mN / m, which is the value when the temperature is 25°C.
** The value when $\theta_o = 0$ and R = 5 nm, divided by k_bT.

chloroform was used, on the other hand, the emulsions were formed with decent monodispersity. This is because the chloroform-induced emulsion were settled on the lower side of the water layer due to the high density of chloroform, which protects the emulsions from fusion, coalescence or disruption by preventing the emulsions from air exposure and evaporation of the chloroform to the air. In addition, this positioning of the chloroform-induced Pickering emulsions make them practical for further stabilization and additional modification to the surface after loading internal materials. Taken together, the αS-AuNP conjugate has a higher detachment energy due to the protein surrounding the particle surface, and thus stably forms a Pickering emulsion. In other words, the protein coat of the particles not only prevents irreversible aggregation of the particles, but also makes the particles have a high detachment energy. Also, by using chloroform as an oil phase, a Pickering emulsion with high monodispersity was formed at the lower side of the water phase, which allows to expect additional applications such as surface modification and further stabilization.

(4) Size control of Pickering emulsion

The average size of the Pickering emulsion could be controlled by adjusting

the concentration of αS-AuNP conjugates. This is because, when the amount of αS-AuNP conjugates is insufficient in the process of adsorption of the conjugates on the surface of the oil phase which have been emulsified by the sonication, there are vacancies of the conjugates on the emulsion surface, allowing coalescence between the emulsions (**Figure 13**). On the other hand, when the amount of conjugate is sufficient, coalescence between the emulsions does not occur because the conjugate is adsorbed on the entire emulsion surface without voids (**Figure 13**). In order to confirm this, Pickering emulsions were prepared with various concentrations of αS-AuNP conjugates (0.5-fold, 1.0-fold, 2.0-fold, 3.0-fold and 5.0-fold where 1.0-fold = 5.7×10^{12} particles/ml). As expected, the resulting optical microscope images showed that the size of the Pickering emulsions decreased with the use of high concentrations of Au-AuNP conjugates (**Figure 14**). In comparison with the particle concentration of 1.0-fold which gave rise to the emulsion size of 32.2 μm (± 5.5 μm), the average capsule size decreased to 12.1 μm (± 3.7 μm), 8.1 μm (± 3.0 μm), and 4.6 μm (± 2.1 μm) as the αS-AuNP concentration increased by 2-fold, 3-fold, and 5-fold, respectively (**Figure 15**). In the presence of the lowest concentration of 0.5-fold, the average capsule size increased drastically to 106.4 μm (± 22.6 μm) with a markedly broad emulsion distribution (**Figure 15**). If all of the chloroform and αS-AuNP conjugates are involved in the formation of Pickering emulsion, sum of the surface area of

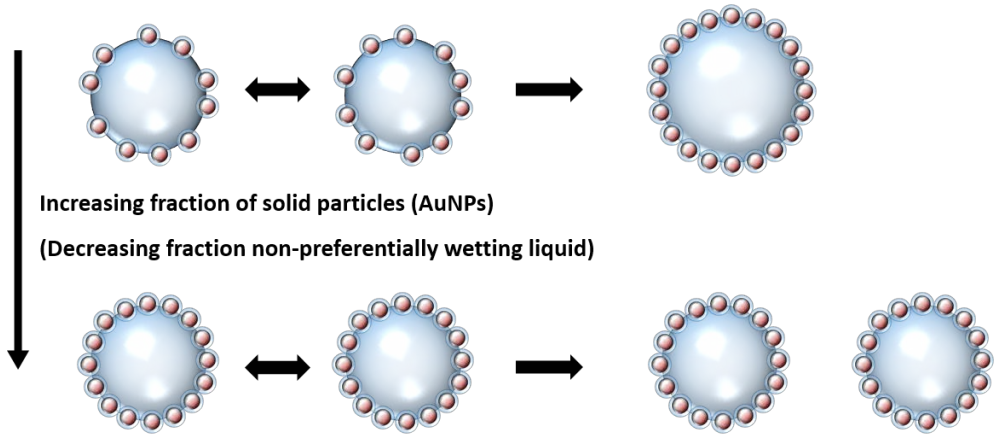

Figure 13. Schematic representation of size adjusting process of Pickering emulsion according to fraction of AuNPs.

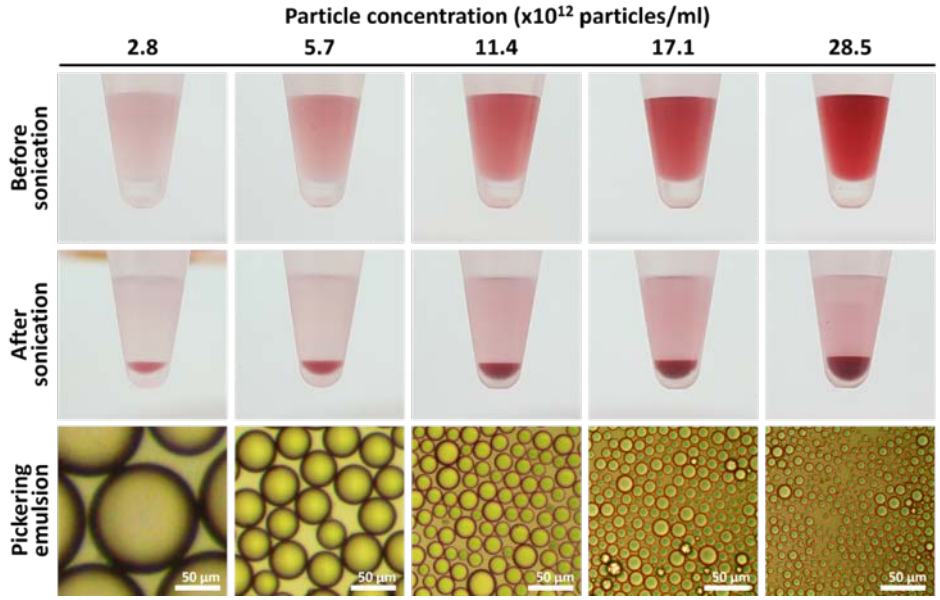

Figure 14. Optical and microscopic images of Pickering emulsions prepared with αS-AuNP conjugates at various concentrations.

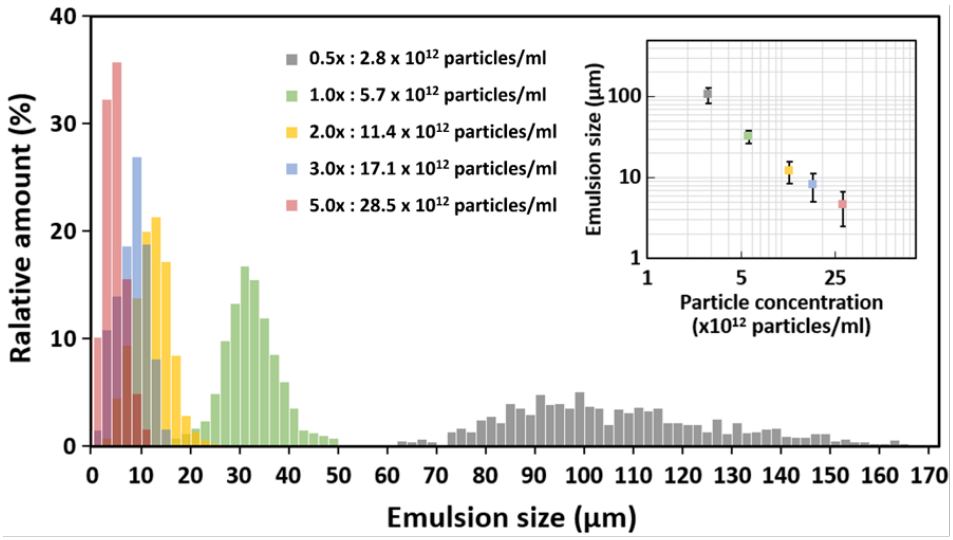

- **0.5x : 106.4 ± 22.6 µm**
- **1.0x : 32.2 ± 5.5 µm**
- **2.0x : 12.1 ± 3.7 µm**
- **3.0x : 8.1 ± 3.0 µm**
- **5.0x : 4.6 ± 2.1 µm**

Figure 15. Size distribution of the Pickering emulsions prepared with αS-AuNP conjugates at various concentration. The inset graph shows an inverse proportional relationship between the particle concentration and the average size of Pickering emulsions.

the emulsions would be equal to sum of the cross-sectional areas occupied by the conjugates on the surface of the emulsions. If the amount of chloroform used is constant, therefore, the number of particles used would be inversely proportional to the average size of emulsions. The inset graph in **Figure 15** shows the inverse proportion relationship between the particle concentration and the average size of Pickering emulsions. These data may indicate that the Pickering emulsions could be kept small by stabilizing the oil phase (chloroform) droplets with a sufficient amount of the particles, which would prevent the emulsions from coalesce with each other. As a results, by adjusting the concentration and/or the particle size of αS-AuNPs, the size of microcapsules could be readily controlled.

(5) General strategy for Pickering emulsion formation

In forming the Pickering emulsion of αS-AuNP conjugates, after determination of the oil phase, an important factor is the surface properties of the particle reflected by the surrounded αS shell. Therefore, it could be expected that Pickering emulsions would be formed even when using other nano-sized particles which are conjugated with αS. In order to conform this, fabrication of Pickering emulsions was evaluated with silver nanoparticles

(AgNPs), quantum dots (QDs), and magnetic nanoparticles (MNPs). Following by incubating the mixture of αS with 20 nm AgNPs or 77 nm MNPs, fresh conjugates of αS-AgNP or αS-MNP conjugates were obtained by centrifugation, respectively. αS-QD conjugates were isolated from the mixture of αS and 8 nm QDs by dialysis. Successful coating of αS onto AgNP was assessed with a red-shift of the LSPR spectrum (**Figure 16A**). After sonication, Pickering emulsions which showed high monodispersity were formed with average size of 51.1 μm (±7.4 μm) when the αS-AgNP conjugates were used while no emulsions were formed with bare AgNPs (**Figure 16B** and **16C**). For the αS-QD conjugates, the increased absorbance at around 280 nm indicates a successful coating by the αS (**Figure 17A**). With sonication treatment, like other nanoparticles, Pickering emulsions were formed only with αS-QD conjugates and were not formed with bare QDs (**Figure 17B**). Observation of the formed emulsions with an optical microscope revealed polydispersity in their size (**Figure 17C**) compared to emulsions composed of αS-AuNP conjugates or αS-AgNP conjugates. When electricity or light is applied, QD emits light of specific frequencies which could be tuned by the size, shape and material of the QD [50, 51]. After excitation of αS-QD_{525} and αS-QD_{625} conjugates (subscripts indicate the emission peak positions of each bare QD) with UV light, their emission was scanned using a luminescence spectrophotometer (**Figure 18A**). The emission peak positions of the two

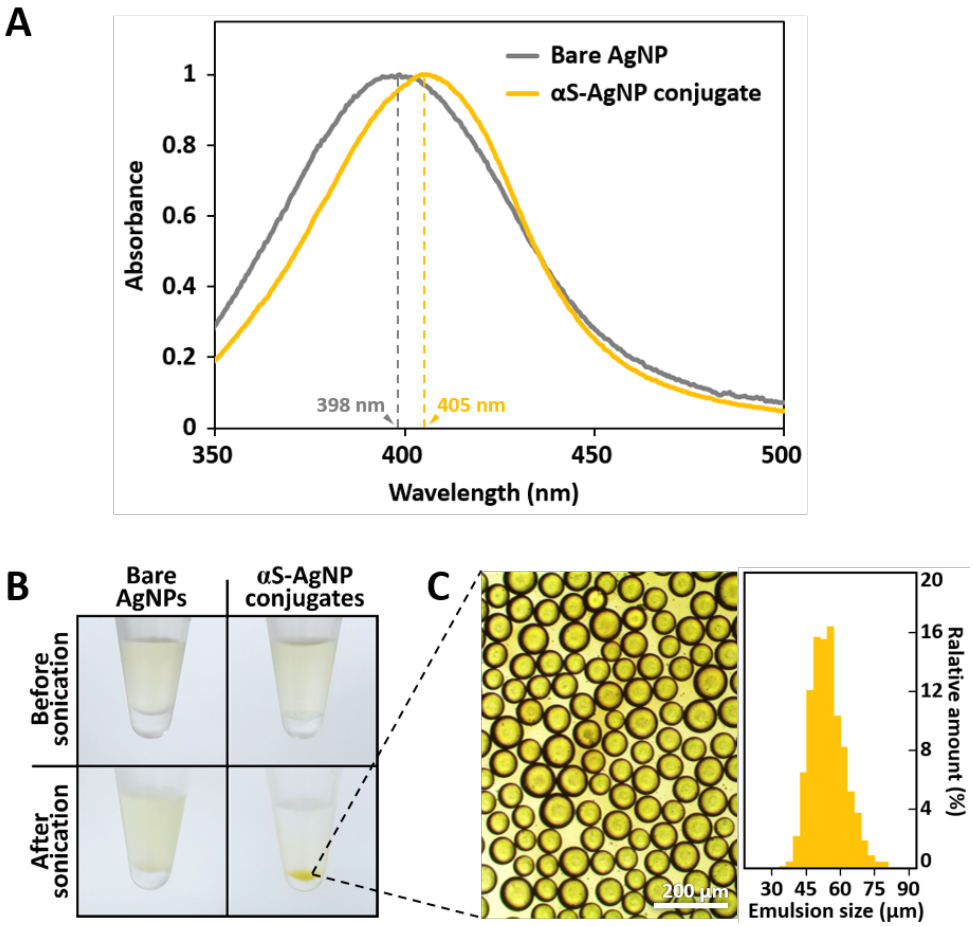

Figure 16. Pickering emulsion formation of αS-AgNP conjugates. (A) LSPR spectra of bare AgNPs and αS-AgNP conjugates. The core particle size is 20 nm. **(B)** Pickering emulsion formation of αS-AgNP conjugates obtained after sonication. Bare AgNPs did not form Pickering emulsions. **(C)** Microscopic image and size distribution of Pickering emulsions composed of the αS-AgNP conjugates.

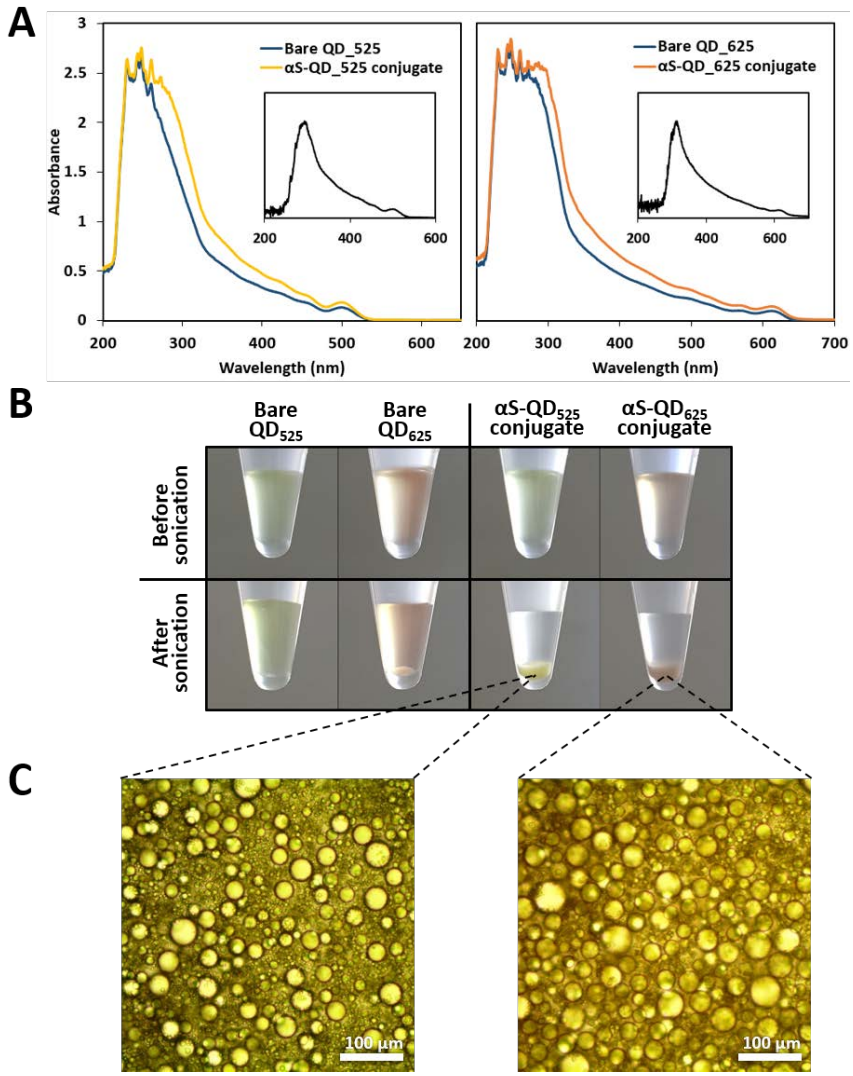

Figure 17. Pickering emulsion formation of αS-QD conjugates. (A) Absorption spectra of bare QDs and αS-QD conjugates. The inset graph represents the difference between the two spectra. **(B)** Pickering emulsion formation of αS-QD conjugates obtained after sonication. Bare QDs did not form Pickering emulsions. **(C)** Microscopic images of Pickering emulsion composed of αS-QD_{525} conjugates (left) and αS-QD_{625} conjugates (right).

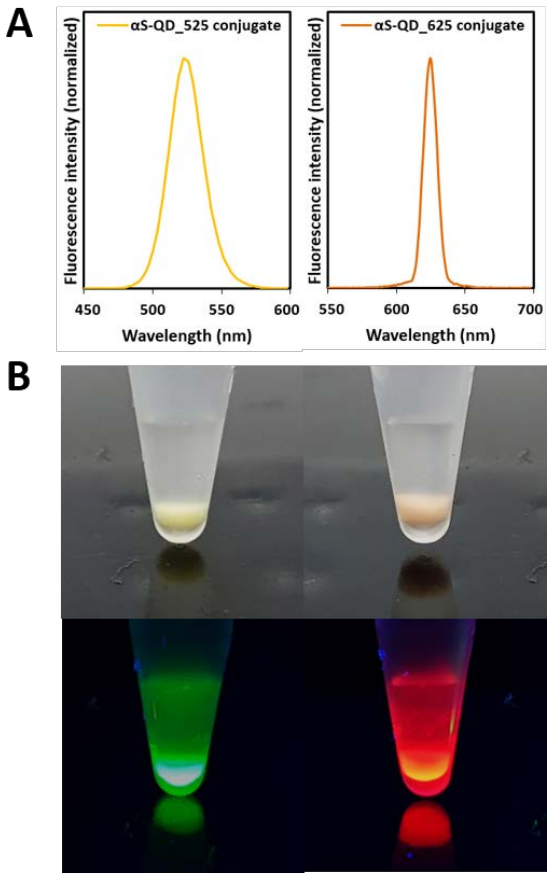

Figure 18. Pickering emulsions of αS-QD conjugates. (A) Photo-luminescence spectra of αS-QD_{525} conjugates (left) and αS-QD_{625} conjugates (right). **(B)** Optical images of αS-QD conjugates microcapsules under visible light (top) and UV light (312 nm) (bottom).

conjugates were identical to the respective bare QDs, which indicating that the coating with αS did not inhibit the photoluminescent characteristics of the QD. Under UV light, therefore, the Pickering emulsions composed of each αS-QD conjugates also emitted light with wavelength that corresponding to their luminescent property (**Figure 18B**), which could be further applicable for *in vivo* imaging or biosensing. In the case of the αS-MNP conjugates, however, the aggregation of the conjugates occurred in the 20 mM Mes pH 6.5 (**Figure 19A**). Thus the Pickering emulsions were formed using the distilled water (DW) as water phase. The microscopic images show that a small amount of polydisperse emulsions were formed with the αS-MNP conjugates, while the emulsions were not formed with bare MNPs (**Figure 19B**). The reason why the Pickering emulsion composed of αS-MNP conjugates was unstably formed is thought to be due to the orientation of αS bound to the MNP surface. That is, the binding orientation of αS conjugated to the MNP might have been changed due to the basic pH condition of the solution when preparing αS-MNP conjugate. When measuring the ζ potential of each NPs, all of the NPs showed negative charge before coating with αS (-23.6 ± 2.1 mV, -23.4 ± 1.8 mV, -22.0 ± 1.6 mV, -21.6 ± 1.9 mV, and -39.4 ± 0.8 mV for AuNP, AgNP, QD_{525}, QD_{625}, and MNP, respectively) (**Figure 20**). After coating each NPs with αS, all NPs except MNP still showed negative charge (-15.6 ± 3.6 mV, -13.7 ± 2.7 mV, -19.2 ± 1.1 mV, and -20.2 ± 0.4 mV for conjugates of αS-AuNP, αS-AgNP, αS-

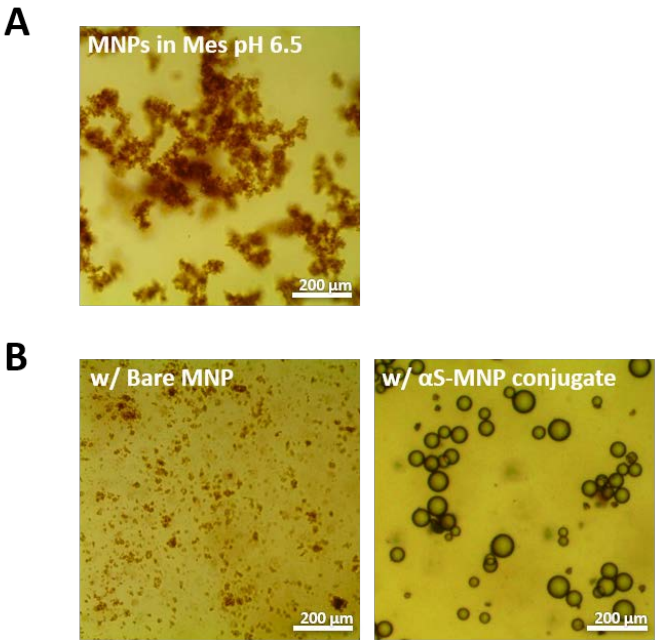

Figure 19. Pickering emulsions of αS-MNP conjugates. (A) Microscopic image of aggregation of bare MNPs in 20 mM Mes pH 6.5. **(B)** Microscopic images of Pickering emulsion formation with bare MNPs (left) and αS-MNP conjugates (right). Bare MNPs did not form Pickering emulsion.

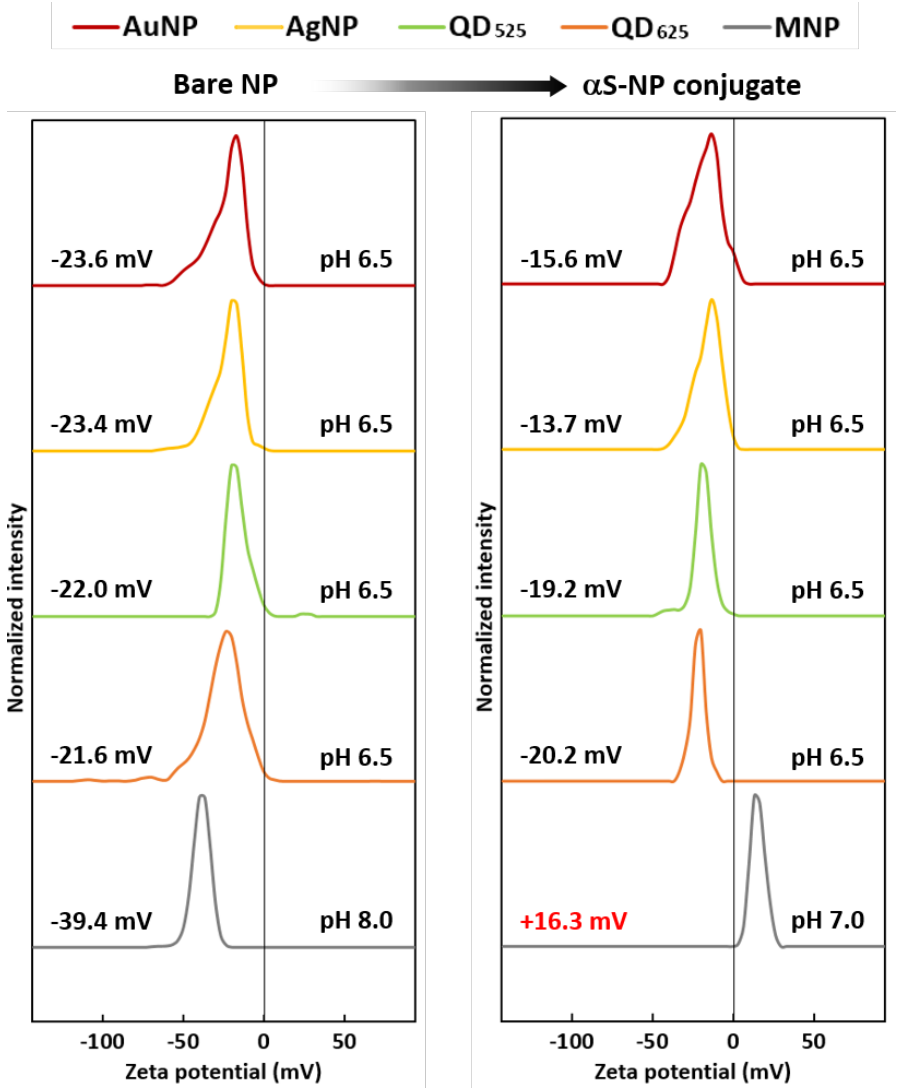

Figure 20. Zeta (ζ) potential of bare NPs and αS-NP conjugates. Only MNP showed positive charge after conjugation with αS.

$QD_{525,}$ and αS-QD_{625}, respectively), but the charge of MNP changed to positive (16.3 ± 0.3 mV) (**Figure 20**). This suggests that the αS-MNP conjugate exposes a positively charged N-terminal instead of a negatively charged C-terminal. The binding orientation of αS on a particle could be changed using cystein mutant of αS *via* gold-thiol bond. Therefore, αS-AuNP conjugates with different orientation of αS achieved by using αS mutants of S9C, A53C and Y136C were prepared, and Pickering emulsions were formed using each $αS_{mutant}$-AuNP conjugates (**Figure 21**). As a result, a stable Pickering emulsions were prepared using $αS_{S9C}$-AuNP conjugates, whereas a film-like structure was observed in a case of using $αS_{A53C}$-AuNP conjugates (**Figure 21**). In addition, Pickering emulsions composed of the $αS_{Y136C}$-AuNP conjugate were well formed, but the remaining structures after chloroform evaporation were found to be aggregated (**Figure 21**). This suggests that exposure of C-terminal of αS on Pickering emulsion plays an important role in preventing emulsion aggregation. In the self-assembly of αS, the C-terminal blocks the rapid assembly of αS [52], which means that the C-terminal of αS prevent Pickering emulsions from aggregation due to its electrostatic repulsion as well as structural hindrance. Taken together, a variety of NPs including AuNP, AgNP, QD, and MNP were coated with αS to prepare αS-NP conjugates, and Pickering emulsions composed of each αS-NP conjugates were formed. However, there were differences in average size and size dispersity of the

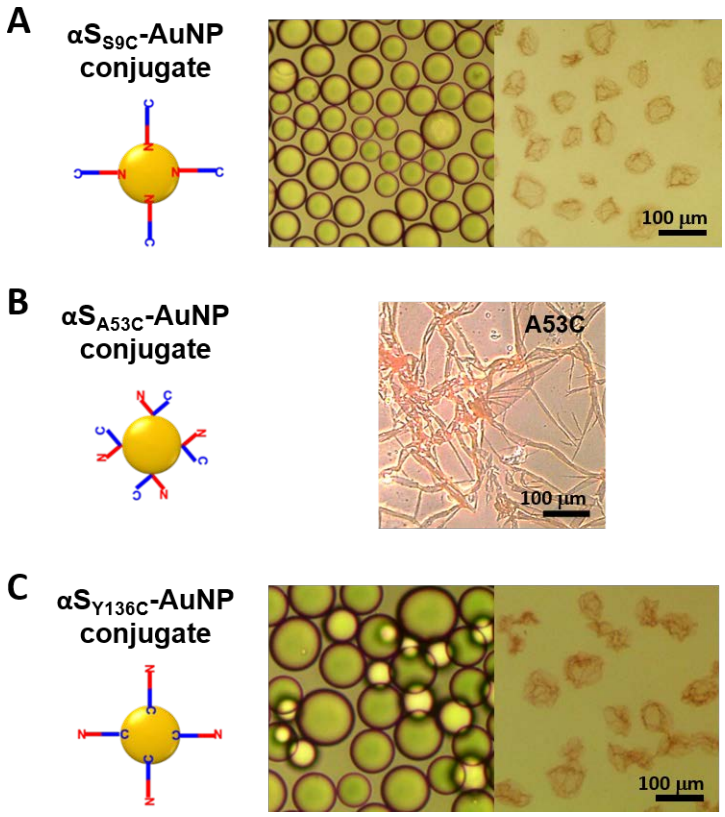

Figure 21. Pickering emulsion formation according to the binding orientation of αS onto AuNP. Microscopic images of Pickering emulsion formation of C-terminal exposed conjugates **(A)**, both C- and N-terminal exposed conjugates **(B)**, and N-terminal exposed conjugate **(C)**.

emulsions depending on the surface characteristics of each αS-NP conjugates such as particle size, surface charge of the particle, and bonding orientation of surface protein.

I-3. Conclusions

Here, Pickering emulsion formation have been presented as a method of producing microencapsulation using nanoparticles as a coating material. AuNPs were formed conjugates with αS proteins, which not only prevented the irreversible aggregation of the particles but also significantly increased the E_d of the particle at the water-oil interface. Following by sonication treatment, the αS-AuNP conjugates were assembled into Pickering emulsions with high monodispersity and stability when chloroform was used as an oil phase. The resulting emulsions were formed at the bottom of the water layer due to the high density of the internal chloroform, suggesting the possibility of further modification such as additional stabilization process or localization of antibodies on the surface. In addition, the size of the Pickering emulsion could be controlled by adjusting the concentration and size of the αS-AuNP conjugates used to form the Pickering emulsion.

Since the formation of these Pickering emulsions are considered to depend on the water, oil, and particle surface characteristics, AgNPs, QDs, and MNPs

are coated with αS protein in the same manner as AuNPs, in order to produce Pickering emulsions composed of AgNPs, QDs, and MNPs, respectively. As a result, monodispersed Pickering emulsions composed of AgNP conjugates or QD conjugates were also prepared by sonication. A small amount of Pickering emulsions composed of MNPs was also formed but did not seem to have a stable structure. This was thought to result from the orientation of αS bound to the MNP surface. However, since the binding of αS to particles is due to electrostatic interactions, it has been reported that the orientation of αS bound to the particles can be changed as the particle surface is modified [45]. Therefore, this problem could be overcome through additional surface modification of the particles or changing the pH of the reaction solution. From these results, it could be suggested that one of the strategies for fabrication of microcapsules composed of nanoparticles is to prepare αS-NP conjugates and use them in the production of Pickering emulsions.

Part II

Microcapsule composed of Gold Nanoparticles *via* Self-assembly of α-Synuclein

II-1. Introduction

(1) Pickering emulsion: stabilization

Pickering emulsions need to be further stabilized and transformed into robust structure for application in cargo delivery system by overcome the thermal energy (Brownian motion) of nanoparticles that could disrupt their weak assemblies at the interface [53]. Several stabilization strategies have been introduced [54, 55], which include thermal annealing [56, 57], gel trapping [58, 59], polyelectrolytes adsorption [56, 60, 61], polymerization [62, 63], and covalent cross-linking [10, 64-67], but these procedures require multiple steps or harsh conditions. Here, therefore, a simple method for stabilization of Pickering emulsion by molecular self-assembly of αS under mild condition is introduced. When αS-NP conjugates form a Pickering emulsion, it is inevitable that the αS toward the oil side meets the organic

solvent and thus αS-αS assembly would be accelerated primarily at the oil/water interface. As the particles are locked by self-assembly of αS, the emulsion gains a larger stability in addition to E_d of the particles. This had been already inferred from the fact that the αS-AuNP conjugates forms Pickering emulsions with *tert*-butyl acetate despite having a very low E_d (**Figure 12** and **Table 1**). This means that formation and stabilization of the emulsion occur simultaneously due to αS conjugated onto nanoparticle without any additional process or additives. If the stability due to the protein self-assembly is high enough, the emulsion will retain its structure even in the absence of organic solvent (there will be no effect of E_d because the interface is not present) and the structure can be utilized as a microcapsule.

(2) Microcapsule for cargo delivery system

The nanoparticle microcapsule derived from Pickering emulsion, called colloidosome, could be utilized in cargo delivery system if it satisfies the following conditions: (1) cargoes are easily loaded in a microcapsule; (2) the resulting microcapsules are physically and chemically stable; and (3) the release of cargo is controlled by physiological/pathological agents. Microcapsules exhibiting specific targeting and triggered cargo release in the cargo delivery system are further developed to be useful in the areas of drug

delivery system [68-71], sensor development [2, 71], and self-healing process [72, 73]. Following by loading a cargo while forming the Pickering emulsion, the resulting microcapsule of αS-AuNP conjugates are expected to be mechanically stable since by the αS-αS interaction of β-sheet formation. In addition, this facile αS-mediated assembly would allow controlled cargo release by responding to protease or specific ligands of αS. Furthermore, the additional functionalization by immobilizing functional materials such as antibodies for sensing or targeting could be also allowed using chemical modification sites provided by protein (αS) surrounding the microcapsule.

(3) AuNP for bio-application

The AuNPs that make up the microcapsule for cargo delivery also have various bio-applicable properties. In cancer research, AuNPs coated with polyethylene glycol (PEG) and conjugated with antibody for targeting tumor cell could be used as a targeting material for tumors using surface enhanced Raman spectroscopy (SERS) [74-77]. In addition, AuNPs are being investigated for photothermal therapy (PTT), which is a treatment that selectively eradicates abnormal cells, especially cancer cells, in the affected areas using heat converted from light [78-83]. Therefore, in biological application, the microcapsules composed of the αS-AuNPs conjugate could

release the cargoes include drugs, imaging agents, or chemicals as the αS-αS bond is eliminated by protease, and the αS-AuNP conjugates forming a shell of the microcapsule could work themselves using their own therapeutic properties. Taken together, the αS-mediated AuNP hybrid microcapsules could serve as a framework to develop multi-functional cargo carriers exhibiting photo-responsive and protease-sensitive properties for biological application.

II-2. Results and Discussion

(1) Fabrication of microcapsule

If Pickering emulsions composed of αS-AuNP conjugates were exposed to air or incubated at room temperature (RT) for more than 2 days, the chloroform inside would be evaporated and the shell structures of the emulsions, αS-AuNP conjugates microcapsules, would be left (**Figure 21** and **22**). The optical image of the capsule presented wrinkled surface which reflects sufficiently stabilized microcapsule formation. In this process of microcapsule formation, the αS-αS interaction is considered to be essential for the microcapsule stabilization since Pickering emulsions composed of AuNPs conjugated with either bovine serum albumin (BSA) (**Figure 23A**, green line) or lysozyme (LYZ) (**Figure 23A**, orange line) are disintegrated as the chloroform

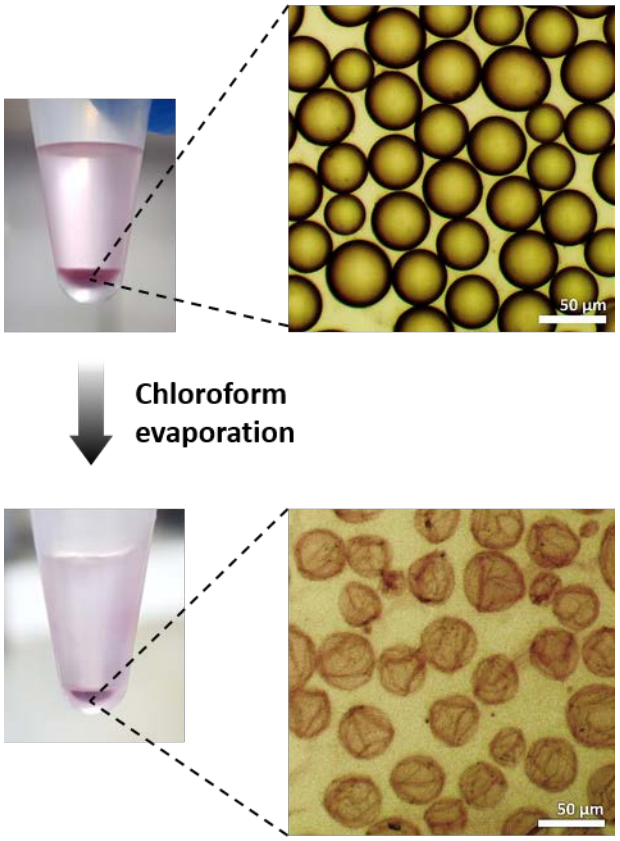

Figure 22. Microcapsule formation of αS-AuNP Pickering emulsion. Optical and microscopic images of the αS-AuNP conjugate microcapsules before (top) and after (bottom) chloroform evaporation.

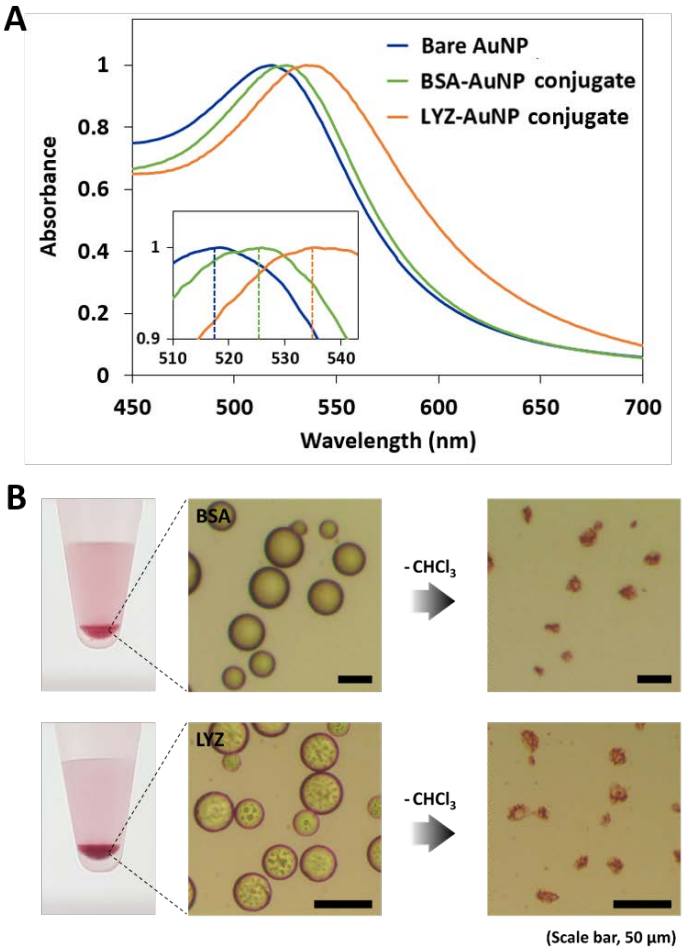

Figure 23. Pickering emulsion and microcapsule formation of BSA-AuNP conjugates and LYZ-AuNP conjugates. (A) LSPR spectra of bare AuNPs, BSA-AuNP conjugates and LYZ-AuNP conjugates. The core particle size is 10 nm. **(B)** Microcapsule formation from Pickering emulsions composed of either BSA-AuNP conjugates or LYZ-AuNP conjugates. Both conjugates did not form microcapsules.

evaporated (**Figure 23B**). In addition, the microcapsule formation was also dependent upon pH of aqueous phase. Uniform and stable microcapsules were formed in a buffer solution of pH 6 or higher, presumably due to isoelectric point (pI) of the αS bound to the AuNP (**Figure 24**). The pI of the αS is 4.4 [84], but the positively charged N-terminal region was demonstrated to be responsible for the αS binding to negatively charged AuNP [85] to form αS-AuNP conjugate, thus the pI of αS bound to AuNP would be close to 3.64, which is pI of αS except the N-terminal region [44]. As a result, in the acidic solutions near the changed pI of αS (pH 3.0 and pH 4.0), αS-AuNP conjugates hardly produced the microcapsules due to either aggregation into a film-like structure or adhesion to the surface of the tube before the assembly into Pickering emulsion (**Figure 24**). Even though capsules were formed at pH 5.0, the size distribution was heterogeneous. Therefore, the charged state of αS conjugated to AuNPs is considered to be critical to the formation of microcapsules with high monodispersity.

(2) β-sheet formation within microcapsule

αS which is comprised the shell of the microcapsule was confirmed by immunostaining with anti-αS antibody tagged with fluorescent dye, Alexa Fluor 488 (AF488) (**Figure 25A**). The high intensity of green fluorescence of

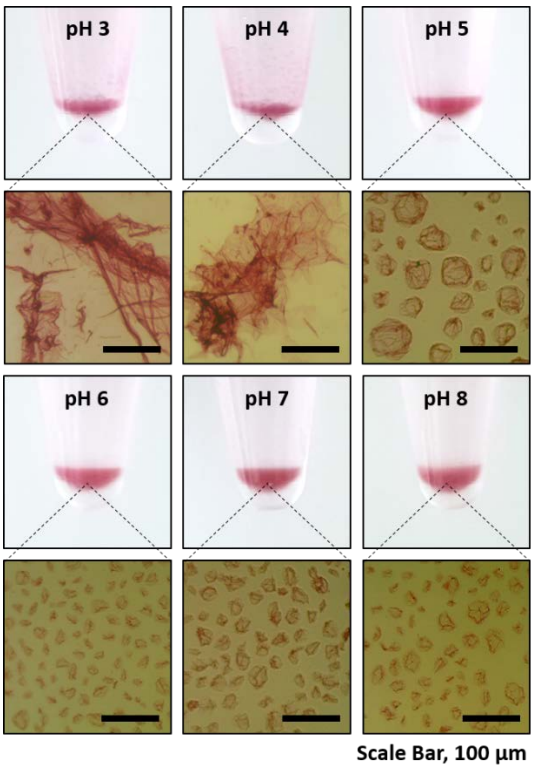

Figure 24. Preparation of AuNP microcapsules at various pH. Microscopic images of microcapsules obtained by preparing Pickering emulsion at various pH and evaporating chloroform inside are shown. A film-like structures were formed instead of microcapsules at pH 3 and pH 4, and heterogeneous microcapsules were formed at pH 5.

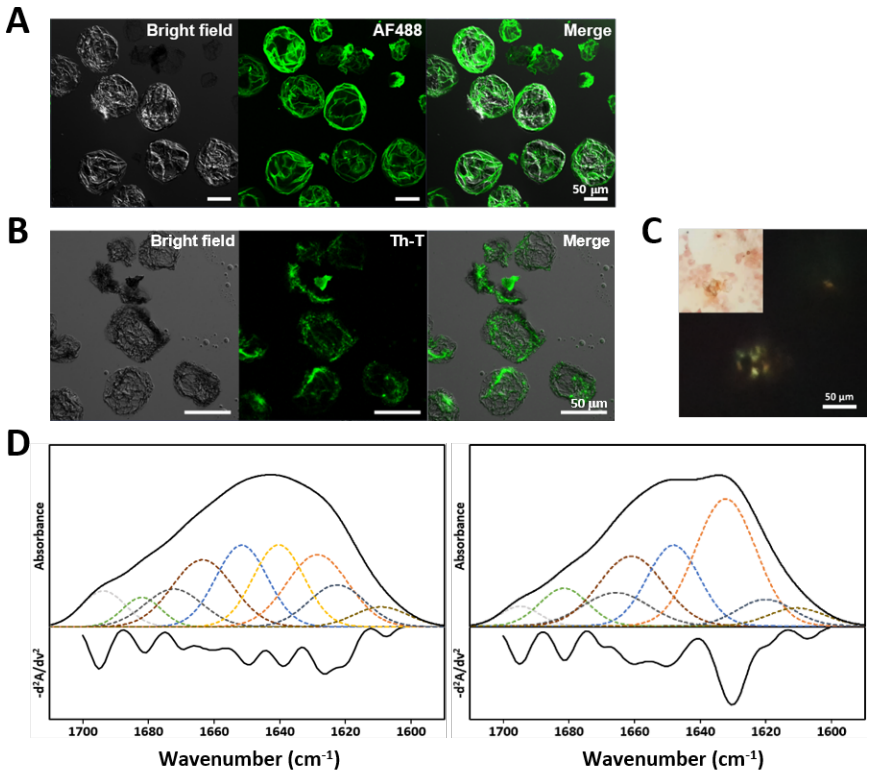

Figure 25. β-Sheet formation within microcapsules. (A) Fluorescent microscopic image of the microcapsules immunostained with mouse monoclonal anti-αS antibody and a secondary antibody of goat anti-mouse IgG labeled with a fluorescent dye of AF488. **(B)** Fluorescent microscopic image of the microcapsules stained with Th-T. **(C)** Congo red birefringence of the AuNP microcapsule (inset) revealed with a polarization microscope. (**D**) FT-IR spectra of the αS-AuNP conjugates (left) and the αS-AuNP microcapsules (right). Both second-derivative and deconvolved spectrum are also shown for each spectrum.

AF488, which was found in a shell shape including the wrinkled structure of microcapsules, indicated that αS conjugated with particles could be interacted with adjacent αS by forming β-sheet structures within the microcapsule. The β-sheet formation between the αS molecules was confirmed by not only the Thioflavin-T (Th-T) binding fluorescence of the microcapsules (**Figure 25B**), but also apple-green birefringence of Congo red staining [86] on the microcapsules (**Figure 25C**) and an amide I band in Fourier transform infrared (FT-IR) spectrum of αS-AuNP conjugates before and after the formation of the Pickering emulsion (**Figure 25D**). Secondary derivatives of the amide I band region of the FT-IR spectra were obtained and then the secondary structure of the protein was analyzed using deconvolved spectra based on the peak positions of the derivatives [87]. Significant increase was confirmed in the two components which exhibit β-sheet formation (1632 and 1681 cm^{-1}) in the deconvolved spectrum [88] of the αS-AuNP conjugates after the emulsion formation compared to the spectrum of the control (before the emulsion formation). In fact, chloroform-induced β-sheet formation of the αS conjugated with AuNPs was previously demonstrated when the free-standing monolayer film of AuNPs was prepared from the polycarbonate substrate pre-coated with αS-AuNPs with chloroform [43]. As a result, the stable αS-mediated AuNP microcapsules have been fabricated using αS-AuNP conjugates by producing oil-in-water Pickering emulsions with chloroform

inside and subsequent molecular interaction between the outlying αS molecules leading to robust β-sheet formation induced by chloroform. The importance of β-sheet formation of intra-microcapsule was confirmed by microcapsule fabrication using amyloid β (Aβ) peptide (1-42). Like αS, Aβ is an intrinsically disordered protein (IDP) and has amyloidogenic properties to form β-sheet formation. Aβ-AuNP conjugates were prepared by the same method as that for producing αS-AuNP conjugates. Their successful coating with αS was assessed with a red-shift of the LSPR spectrum (**Figure 26A**). Microscopic image shows that Pickering emulsions composed of Aβ-AuNP conjugates were formed after sonication treatment (**Figure 26B**, a). Interestingly, fusion or coalescence was observed among these Pickering emulsions (**Figure 26B**, b). In addition, as the internal chloroform evaporated, the resulting microcapsules were aggregated each other (**Figure 27A** and **27B**). This aggregation of microcapsule was also observed in the Pickering emulsion prepared using the Y136C mutant of αS in the previous experiment (**Figure 21**), which has already been explained by the absence of exposed C-terminal region that blocks rapid assembly of αS. In the result using the Aβ-AuNP conjugate, the coalescence of the Pickering emulsion or the aggregation of the microcapsule is thought to be the result from the absence of the moiety blocking the β-sheet formation of inter-emulsion or inter-capsule. Taken together, in the Pickering emulsion formation and subsequent microcapsule

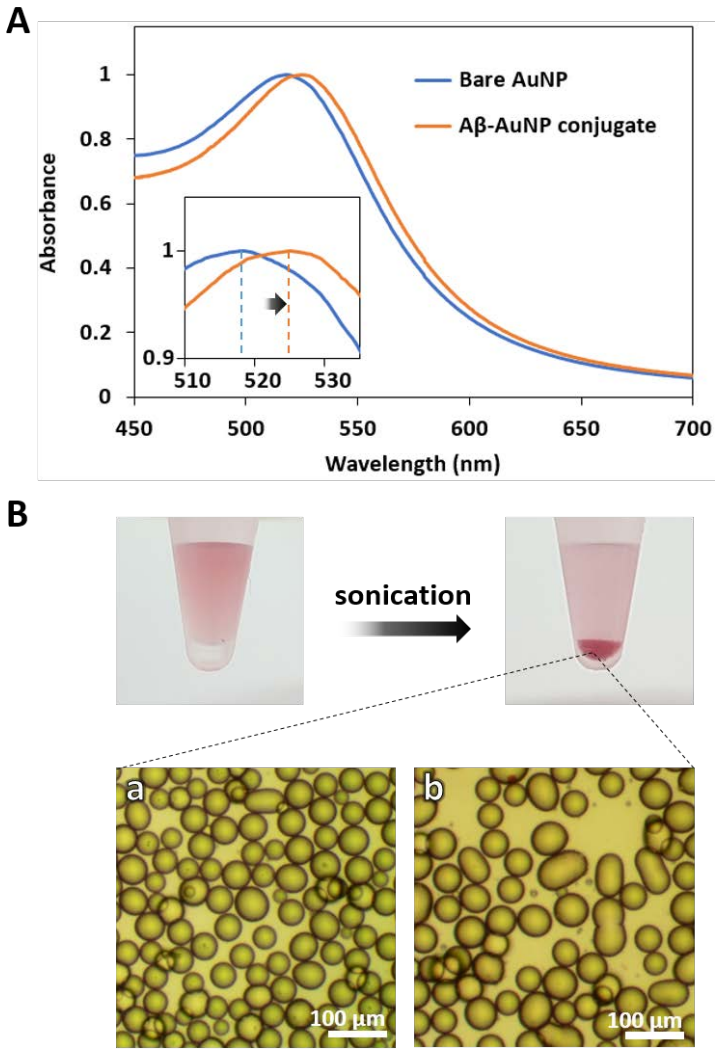

Figure 26. Pickering emulsion formation of Aβ-AuNP conjugates. (A) LSPR spectra of bare AuNPs and Aβ-AuNP conjugates. **(B)** Pickering emulsion formation of Aβ-AuNP conjugates obtained after sonication and their microscopic images.

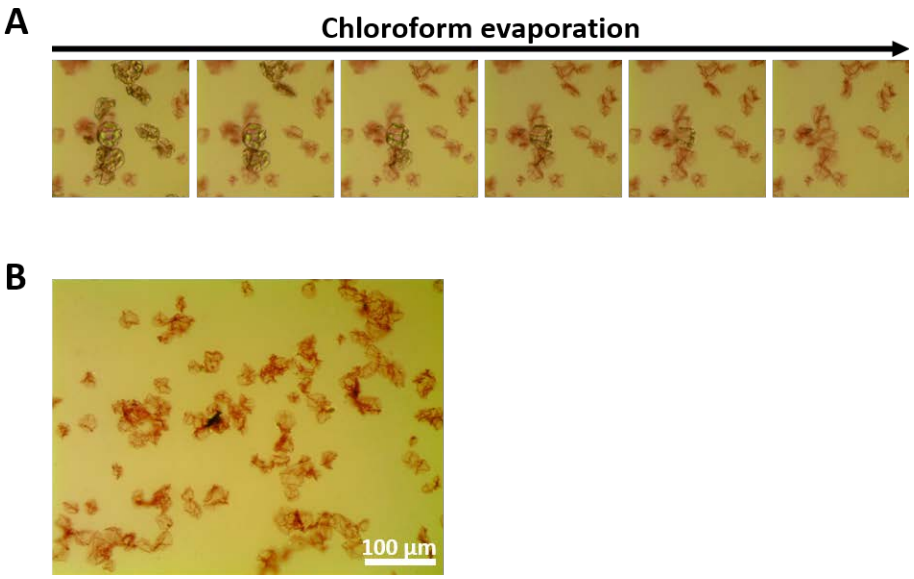

Figure 27. Microcapsules formation of Aβ-AuNP conjugates. (A) Microscopic images of Pickering emulsions composed of Aβ-AuNP conjugates during chloroform evaporation. **(B)** Microscopic images of aggregated Pickering emulsions composed of Aβ-AuNP conjugates.

fabrication, not only intra-emulsion β-sheet formation induced by chloroform, but also blocking of the inter-emulsion or inter-capsule β-sheet formation is an important factor in the production of individually stable microcapsule structures.

(3) Chloroform-mediated stabilization of microcapsule

It has already been confirmed that the αS-AuNP conjugate forms a Pickering emulsion in all cases where the core particle size is 5, 10, 20 and 30 nm (**Figure 9**). As the internal chloroform evaporates, however, the Pickering emulsions composed of larger conjugates (20 and 30 nm AuNPs) failed to maintain their structure of microcapsules and burst, while the emulsions with small conjugates (5 and 10 nm AuNPs) remained intact and formed microcapsules (**Figure 28**). Interestingly, this structural degradation represents a significant volumetric shrinkage just prior to capsule bursting due to complete evaporation of chloroform. First, as the chloroform evaporates in the shrinkage step, the fraction of the preferentially wetting liquid (water) increases and therefore the Pickering emulsion becomes capillary state (**Figure 29**) [89]. It has been reported that the capillary force (F_c) for a finite particles separation of two spheres of equal size connected by a fluid bridge is given by

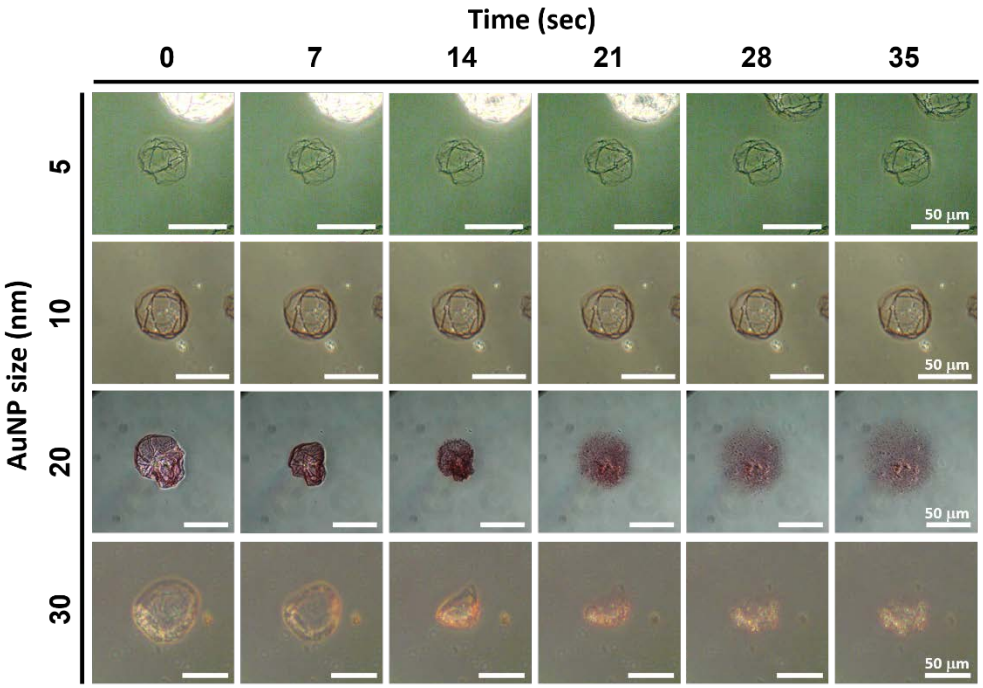

Figure 28. Microcapsules formation from Pickering emulsion without pre-incubation. Microscopic images of Pickering emulsions during chloroform evaporation. The emulsions were obtained without any pre-incubation. The Pickering emulsions comprised of the smaller conjugates (5 and 10 nm core) maintained their structures whereas the emulsions of the larger conjugates (20 and 30 nm core) burst within the time period in seconds.

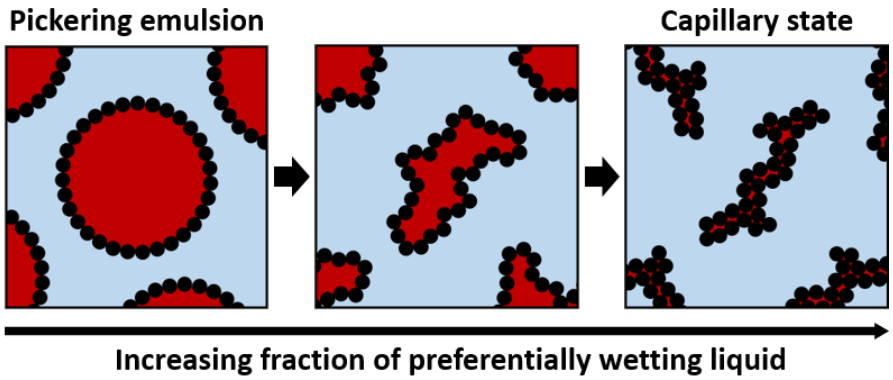

Figure 29. Schematic representation of transition from Pickering emulsion to capillary state by chloroform evaporation. As the fraction of the preferentially wetting liquid (water) increases, the Pickering emulsion becomes capillary state.

$$F_c = \frac{2\pi r\,\gamma_{OG}\cos\theta}{1 + 1.05\hat{s} + 2.5\hat{s}^2}, \quad \text{with } \hat{s} = s\sqrt{\frac{r}{V_l}} \qquad \textbf{(Equation 3)}$$

where s is their separation distance and V_l is the volume of the liquid bridge. The **Equation 3** is simplified to the well-known expression $F_c = 2\pi r\gamma_{OG}\cos\theta$ for spheres that are in contact [89, 90]. As the chloroform continues to evaporate, the capillary force sharply increases according to **Equation 3**, resulting in shrinkage of the microcapsules as the particles gather along the chloroform. In the second step, when the chloroform is completely evaporated, the F_c disappears and bursting of the microcapsule occurs due to repulsive force induced by negatively charged αS-AuNP conjugates. This bursting phenomenon could be understood with the DLVO theory [46], suggesting that two particles become repulsive as they approach one another before forming irreversible aggregates at the primary minimum. Failure of microcapsule fabrication using larger conjugates is due to the fact that the αS-αS interaction was not enough to withstand shrinkage or bursting. However, by simply incubating for 8 hours at 37°C underneath the aqueous phase, the microcapsules with 20 and 30 nm cored αS-AuNP conjugates retained their structure without disruption (**Figure 30**). This is attributable to induction of additional interaction between the αS molecules through the incubation. As a results, all the Pickering emulsions were eventually stabilized into microcapsules by the αS-AuNP conjugates regardless of their core sizes. For

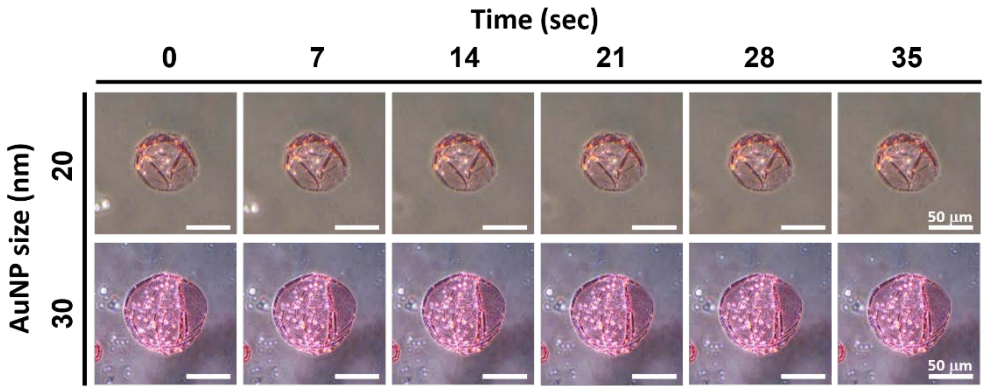

Figure 30. Microcapsules formation from Pickering emulsion with pre-incubation. Microscopic images of the stable microcapsule made of the larger conjugates (20 and 30 nm core) after 8 hours prior incubation before the chloroform evaporation.

the larger particles, the more stabilization energy was required, which indicates that the αS-mediated particle-particle interaction(s) would be essential for the microcapsule fabrication.

(4) Structural characteristics of microcapsule

The structure of the microcapsule shell composed of homogeneous AuNPs was visualized with transmission electron microscope (TEM) (**Figure 31A**). The wrinkled structure with increased density of particles, which reflects folded area of the shell due to its robustness, was also shown in TEM image. The shell of the microcapsule, which appears as a TEM image, seems to have a large gap between particles, but the spatial gap between the AuNPs appeared to be stuffed with αS molecules conjugated on the particles as shown in the images obtained using field emission scanning electron microscope (FE-SEM) (**Figure 31B**). Therefore, after loading cargo inside the capsule, it seems to be possible to control premature cargo leakage. In addition, the height of the collapsed microcapsule made of the αS-AuNP conjugates was measured to be around 22 nm using an atomic force microscope (AFM) (**Figure 31C**). Considering that the core size of the αS-AuNP conjugate used was 10 nm, this indicates that the shell of the microcapsule consists of conjugates in a single layer. This would be a natural result considering that the microcapsule is

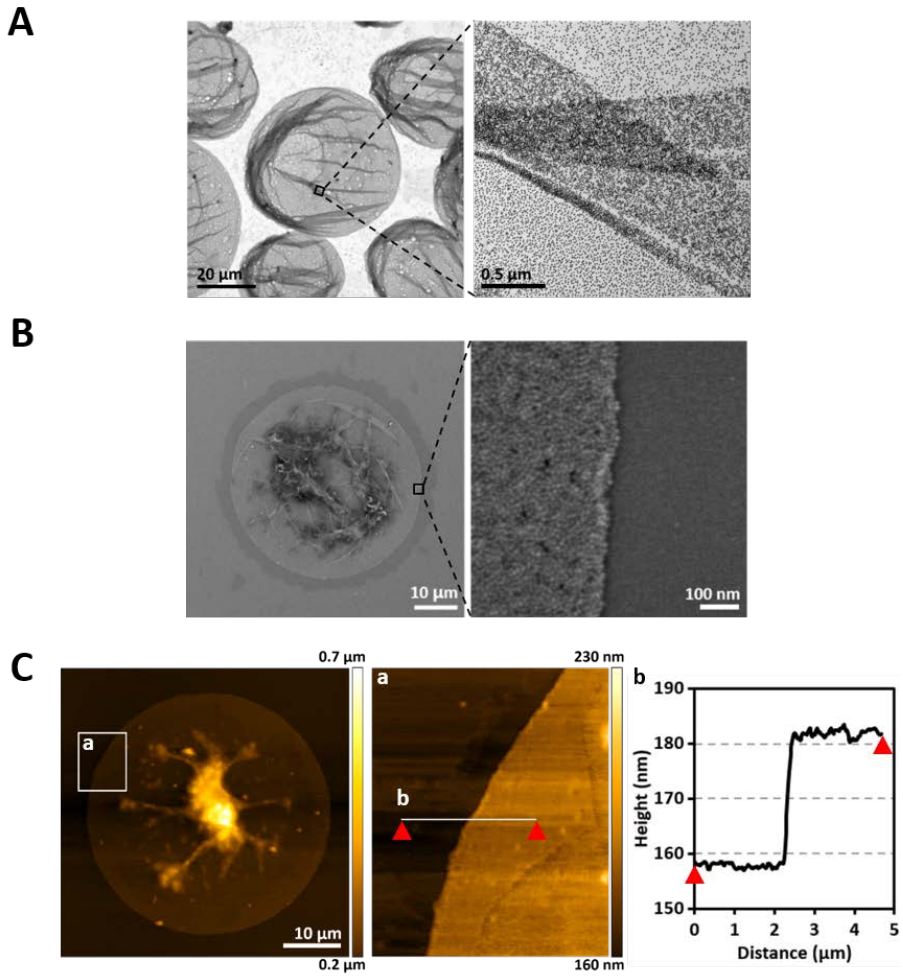

Figure 31. Structural characteristics of microcapsules. (A) TEM image of the microcapsules and an enlarged image of the shell layer comprising αS-AuNPs. **(B)** SEM image of the αS-AuNP microcapsule and an enlarged image of the region indicated on the shell. (**C**) AFM images of the αS-AuNP microcapsule. The y-profile of the enlarged region of the capsule is shown.

derived from Pickering emulsion which is comprised with the particles aligned at the oil-water interface. Taken together, investigation of the structural characteristics of the microcapsule revealed that a stable capsule composed of a single layer of αS-AuNP conjugates was obtained, which could be further applied as a cargo carrier due to the αS molecules stuffing voids between the particles.

(5) Cargo release from microcapsule

Since the microcapsules are stabilized by forming β-sheets between the αS, the protease would work as a trigger of disintegrating the capsules and releasing the cargo inside through hydrolysis of the αS and removal of the interaction between the particles. To confirm this, Rhodamine 6G (R6G) were loaded into the microcapsule at a concentration of 10 μg/ml in the presence of chloroform inside. The fluorescence images obtained using confocal laser scanning microscope (CLSM) show that R6G, which represents red fluorescence, is located inside the shell of the microcapsule labeled with AF488-conjugated anti-αS antibody (**Figure 32**). Note that R6G is still retained inside while the chloroform inside the capsule evaporates (**Figure 32**, white arrow). Protease-induced cargo (R6G) release was investigated with trypsin, a serine protease found in the digestive system of many vertebrates

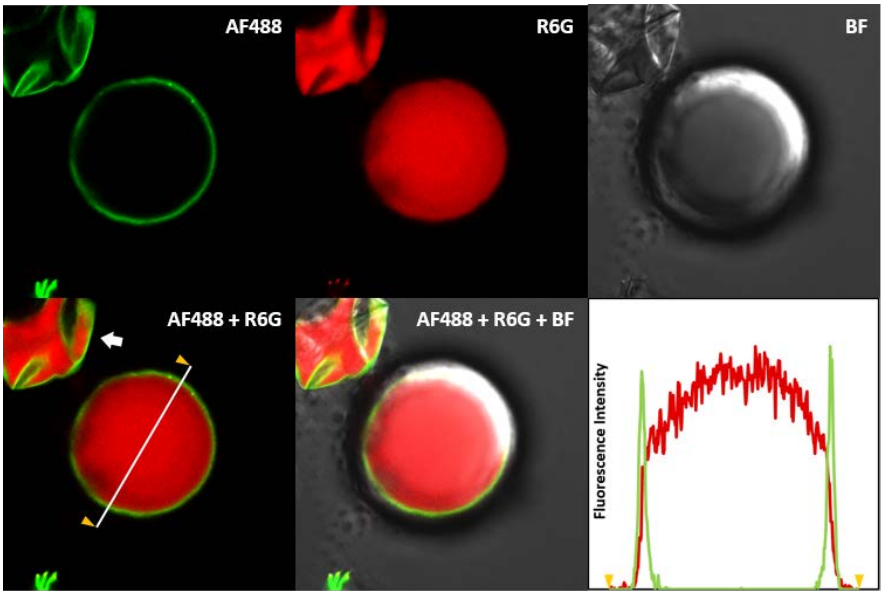

Figure 32. Loading of R6G into microcapsule. Fluorescence image of the microcapsules containing R6G (red). The protein of αS present on the microcapsule shell was also immunostained with a primary antibody raised against αS and a secondary antibody labeled with a fluorescent dye of AF488 (green). The fluorescence intensity profile shows that R6G is present only inside the microcapsule. White arrow indicated that R6G is still retained inside while the chloroform inside the capsule evaporates.

[91], at the concentration of 50 μg/ml. As a result, the release of R6G by trypsin treatment was observed and saturated at 30 minutes of reaction time (**Figure 33**). Degradation of the emulsions and microcapsules by trypsin was observed under an optical microscope. Treatment of excess amount of trypsin (100 μg/ml) caused the emulsion to be degraded by bursting itself or by fusion with the nearby emulsion (**Figure 34A**), and in the case of microcapsules, fragments were produced by degradation of the protein (**Figure 34B**). The cargo release could be selectively controlled by digesting proteins and disrupting αS-αS interactions through other proteases including thrombin, cathepsin-B, calpain-1, and matrix metalloproteinases (MMPs) (**Figure 35**). The microcapsules were incubated with one of the proteases in phosphate-buffered saline (PBS) for 1 hour at 37ºC. As a results, the release of R6G by all proteases was observed with slight differences, showing the lowest value from serine proteases of thrombin and the highest value from lysosomal cysteine protease of cathepsin-B in comparison with the trypsin-induced cargo release (81.2 % and 109.6 %, respectively). The MMPs showed similar cargo release to trypsin in both MMP-2 (97.0 %) and MMP-9 (100.2 %), and calpain-1, the calcium-dependent intracellular cysteine protease, unleashed the cargo by 102.7 % in comparison with the trypsin. Since the extracellular activities of thrombin and MMPs would rapidly increase under pathological conditions such as blood clotting, inflammation, and metastasis of cancer cells,

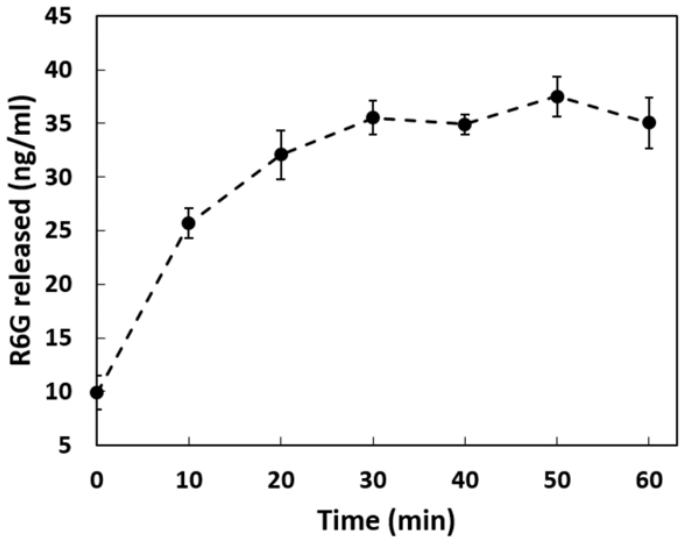

Figure 33. Release of R6G from microcapsules by trypsin treatment. Cargo (R6G) release from the microcapsules treated with trypsin at 50 μg/ml for 1 hour at 25°C. Error bars represent standard deviation (n=3).

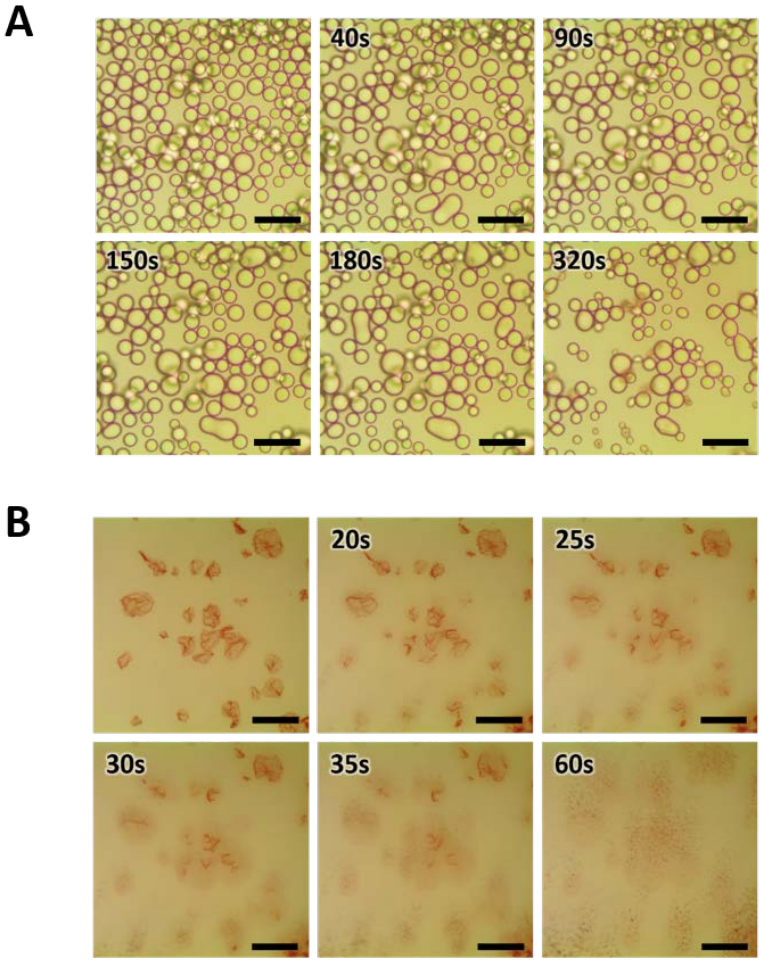

Figure 34. Degradation of Pickering emulsions and microcapsules under trypsin treatment. Microscopic images of degradation process of the Pickering emulsions (**A**) and the microcapsules (**B**) upon trypsin treatment at 100 μg/ml over time. The scale bars represent 100 μm.

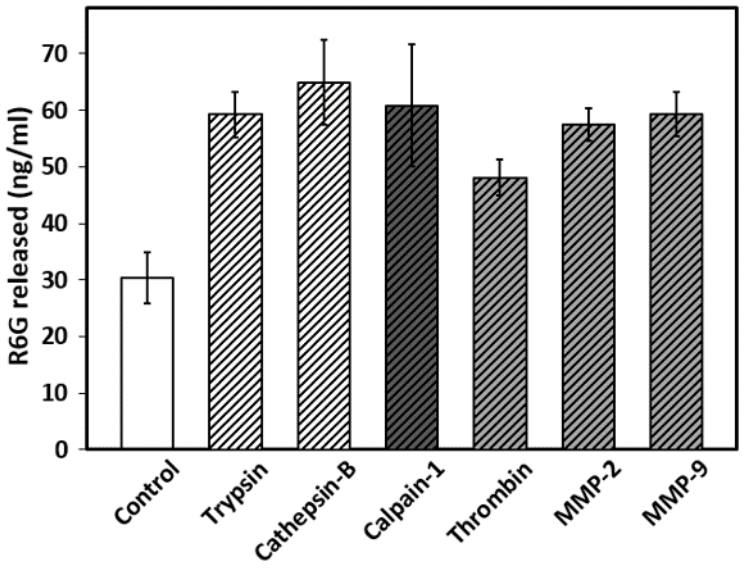

Figure 35. Cargo release from microcapsules by various proteases. Protease-induced cargo (R6G) release from the microcapsules treated with various proteases at 10 μg/ml for 1 hour at 37°C. Error bars represent standard deviation (n=3).

the αS-AuNP conjugate microcapsules could be employed to carry biologically active cargoes including drugs to the pathologically affected areas where the proteases are activated extracellularly. Interestingly, in addition to the protease, the cargo of R6G was readily released in the presence of 5 mM Cu^{2+} in particular, and Ca^{2+} and Mg^{2+} exhibited moderate levels of the R6G release among various metal ions tested (**Figure 36**). Despite the copper-dependent cargo release, however, most of the copper ions inside the human body are sequestered and the concentration of free copper ion in the blood is maintained below 20 μM [92]. In addition, free ion concentrations of Ca^{2+} and Mg^{2+} in the body are also suggested to be relatively low since they are mostly sequestered within various intracellular organelles like ER and mitochondria inside the cell or by being complexed with biological molecules like proteins, nucleic acids, and ATP/ADP. In fact, free Ca^{2+} level in blood is estimated 1.1 to 1.3 mM at most and free Mg^{2+} level is 0.4 to 0.6 mM [93]. Therefore, the effect of copper-dependent cargo release might be insignificant for the microcapsules to perform cargo delivery *in vivo*. The copper-dependent cargo release might be due to a specific interaction between αS and copper ion as reported in previous studies [20, 94]. In these studies, the copper ion was demonstrated to affect the amyloidogenesis of αS through specific molecular interaction. In particular, copper ion exhibits high affinity (K_d ~ 0.1 μM) with a specific amino acids sequences (^{1}MDVFMKGLS^{9} and ^{48}VAHGV^{52}) located

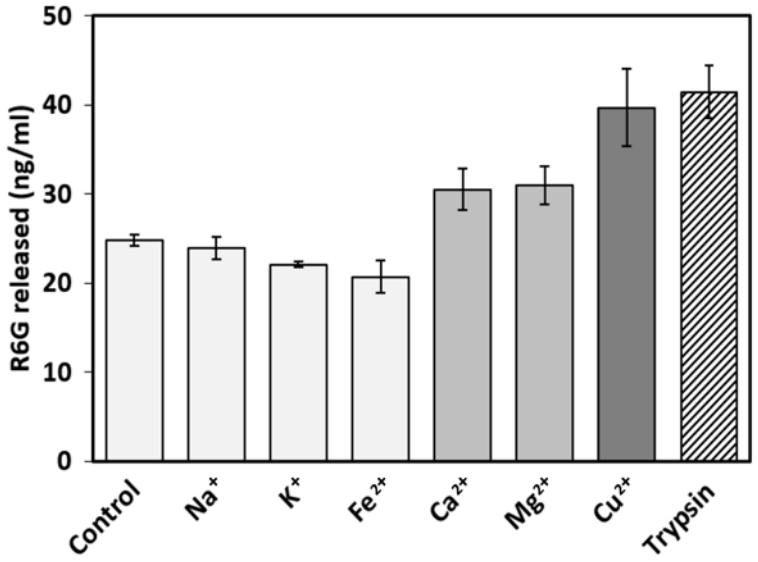

Figure 36. Cargo release from microcapsules by various metal ions. R6G release from the microcapsules incubated with various cations at 5 mM. Error bars indicate standard deviation (n=3).

at the N-terminal domain of αS [94], which might interfere with the electrical interaction between AuNP and αS. Taken together, in addition to the cargo release by the protease, this copper-dependent release indicates that αS plays a critical role in controlling the cargo release from the αS-AuNP conjugate microcapsules.

(6) Mechanical and chemical stability of microcapsule

Structural robustness of microcapsules was evaluated by loading R6G into microcapsules and comparing R6G release under various mechanical and chemical conditions with trypsin-induced cargo release. The mechanical stability was confirmed with their rheological response in a syringe pump-driven fluidic system. The microcapsules loaded with 10 μg/ml of R6G in the presence of chloroform inside (**Figure 32**) were flowed through a Teflon tube with an inner diameter of 1.0 mm at various flow rates of 10 cm/s, 30 cm/s, 50 cm/s, and 70 cm/s for a total flow distance of 1.0 m (**Figure 37**). The aortic blood flow is laminar and the average velocity is about 40 cm/s within the blood vessels' total cross-sectional area of 3-5 cm [95]. The flow velocity of 70 cm/s in the experiment therefore exceeds the peak blood flow velocity of 58.2 cm/s in the ascending aorta [96]. The results indicate that the microcapsules were not disintegrated and keep their structure even at a flow

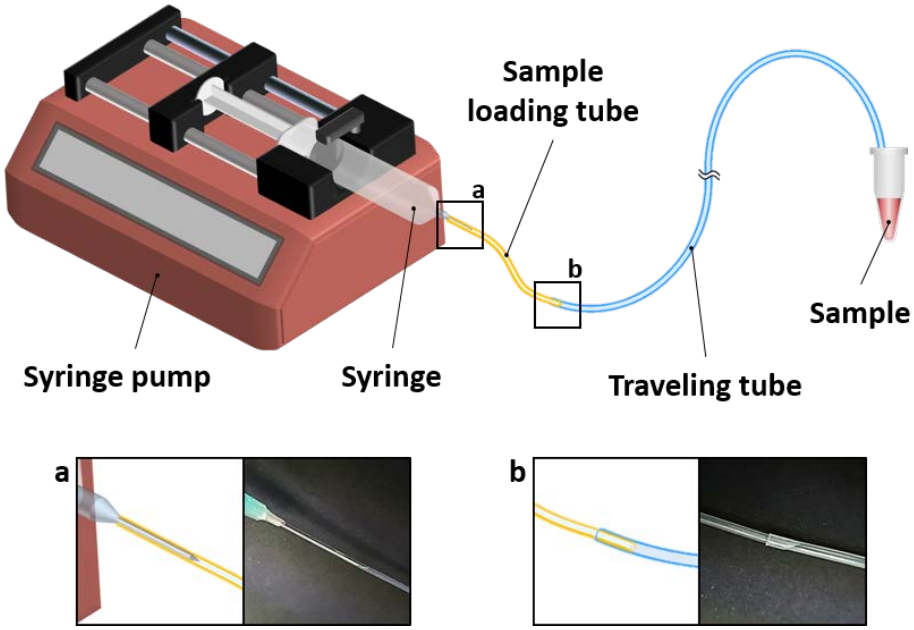

Figure 37. Schematic representation of fluidic system. A fluidic system was assembled with a syringe pump, a 50ml syringe, and Teflon tubes (sample loading tube and traveling tube). The inner diameter of the sample loading tube and the traveling tube were 0.8 mm and 1.0 mm, respectively. Samples were collected after flowing in a 1.0 m long traveling tube at flow rates of 10, 30, 50 and 70 cm/s.

velocity of 70 cm/s (**Figure 38A**) and the enclosed R6G was also well retained, which was confirmed through trypsin-induced cargo release. Upon the trypsin treatment, the microcapsules experiencing the flow were found to release similar amount of R6G as the microcapsules without flow in both levels of pre-mature diffusive release and trypsin-induced burst release (**Figure 38B**). This indicates the mechanical stability of microcapsules sufficiently sustainable in the physiological circulatory system. Not only the mechanical stability, but also the chemical stability of the microcapsules was investigated with pH change and ionic strength. The microcapsules prepared in 20 mM Mes buffer at pH 6.5 were buffer-changed with 10 times diluted McIlvaine buffer (citrate-phosphate buffer) from pH 3 to pH 8 and the changes were observed. The microcapsules were stable at pH 5 and above without any structural changes, whereas at acidic condition of pH 4 and below, the emulsions are fused and internal R6G was released (**Figure 39**). Especially at pH 3, the microcapsules formed large agglomerates (**Figure 39A**) and showed R6G release comparable to trypsin-induced cargo release (**Figure 39B**). This phenomenon is also affected by the pI value of αS surrounding the microcapsule as previously described in the experiment of forming the Pickering emulsion according to the pH of the aqueous phase. In addition, the microcapsules retained the internal cargo stably even in solutions with high ionic strength up to 1.0 M, adjusted by NaCl (**Figure 40**). Note that although

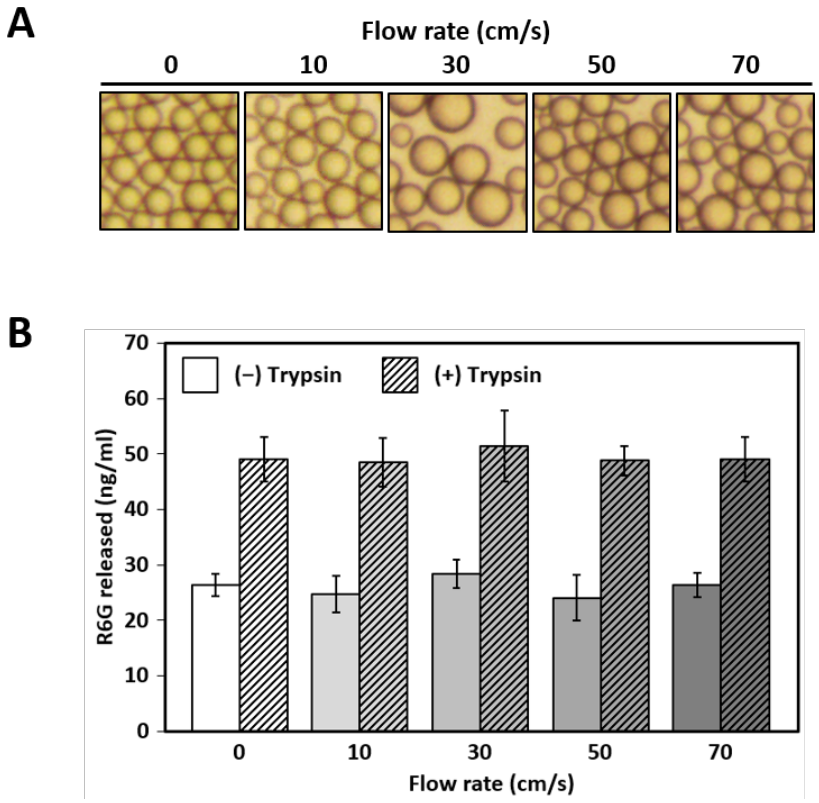

Figure 38. Microcapsules in fluidic system. (**A**) Optical images of the microcapsules prior to the trypsin treatment. The capsules experienced an enforced flow of the syringe-based fluidic system at the flow rates indicated. (**B**) The cargo retained within the capsules after the experience of enforced flow. Trypsin-induced cargo release also presented under a trypsin treatment at 50 µg/ml for 30 min at room temperature. Error bars indicate standard deviation (n=3).

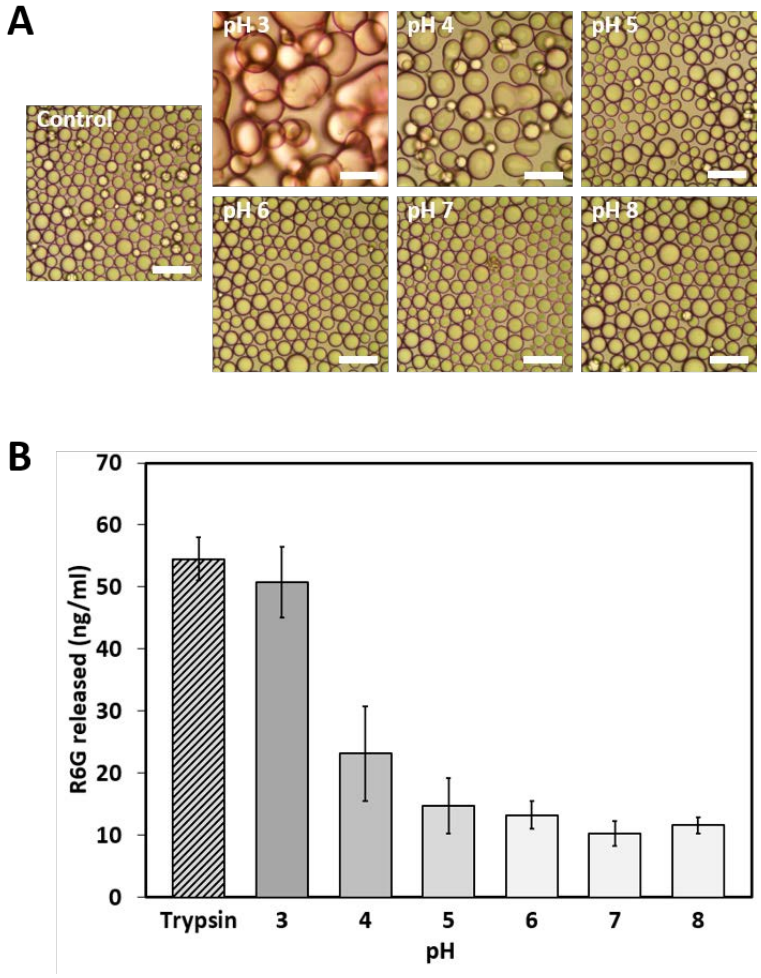

Figure 39. Stability of microcapsules in various pH conditions. (**A**) Microscopic images of the microcapsules incubated for 5 minutes at various pH conditions indicated. The scale bars represent 100 μm. (**B**) R6G release from the microcapsules at various pH conditions. Error bars indicate standard deviation (n=3).

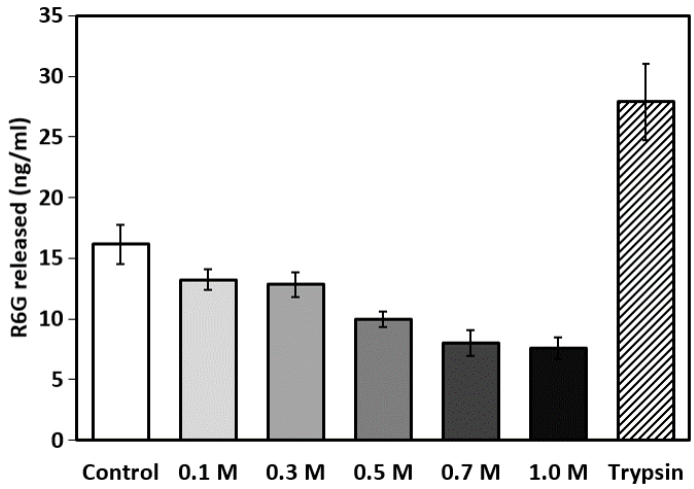

Figure 40. Cargo (R6G) release from microcapsules under various ionic strength. R6G release from the microcapsules in the high ionic strength solution of NaCl. The trypsin-induced R6G release was also examined as a positive control. Error bars indicate standard deviation (n=3).

the microcapsules were stable at such high ionic strengths, the copper-dependent cargo release observed in the previous was occurred at only presence of 5 mM Cu^{2+}. The low diffusive release of R6G at high ionic strength was consider to be simply due to reduced partitioning of R6G into the solution by high ionic strength. Taken together, the microcapsules made with αS-AuNP conjugates assembled *via* αS-αS interaction have been demonstrated to be stable against the physical and chemical influences, such as rheological behavior, pH change, and ionic strength, which the capsules would encounter with in biological condition during the cargo delivery.

(7) Light-responsivity of microcapsule

AuNPs exhibit a photothermal effect that absorbs light at a specific wavelength and converts it to heat, and it has been confirmed that αS-AuNP conjugates still have this effect at various concentrations. In the LSPR spectrum of the αS-AuNP conjugates (**Figure 2B**), the conjugates had the highest absorbance at about 525 nm, thus confirming the photothermal effect using a green laser at 532 nm. Thermal stability of the protein-AuNP composites and the Pickering emulsion composed of them was investigated for the heat generated by photothermal effects. After 30 minutes of laser irradiation, the highest temperature of each protein-AuNP conjugate solutions

obtained by infrared (IR) thermographic image (data not shown) was reached about 50 °C (**Figure 41A**). The αS-, Aβ-, and BSA-AuNP conjugate solutions showed no significant change in appearance, whereas the LYZ-AuNP conjugates were aggregated and sedimented at the bottom of the water layer (**Figure 41B**, a). After the sonication treatment, all the protein-AuNP conjugates formed Pickering emulsions even in the case of the LYZ-AuNP conjugates (**Figure 41B**, b), which was probably because the aggregates of LYZ-AuNP conjugates were resuspended by sonication. After the additional 15 minutes of laser irradiation, the Pickering emulsions were well retain their structure except for the emulsion composed of the LYZ-AuNP conjugates(**Figure 41B**, c and **41C**). In the case of the LYZ-mediated AuNP Pickering emulsion, the structure was completely collapsed and irregular emulsions and the aggregations were observed (**Figure 41C**). As a result, the αS-, Aβ-, and BSA-AuNP conjugates and the microcapsules made therefrom were thermally stable from about 50 °C (or locally higher) heat generated from their photothermal effects, which suggests the availability of AuNP microcapsule as a photothermal agent for PTT. Several experiments were conducted to confirm the possibility. First, IR thermographic images of solutions containing various concentrations of AuNP were obtained while the laser beam was irradiated for 3 minutes to check the dependence of photothermal effect on the particle concentration (**Figure 42**). During

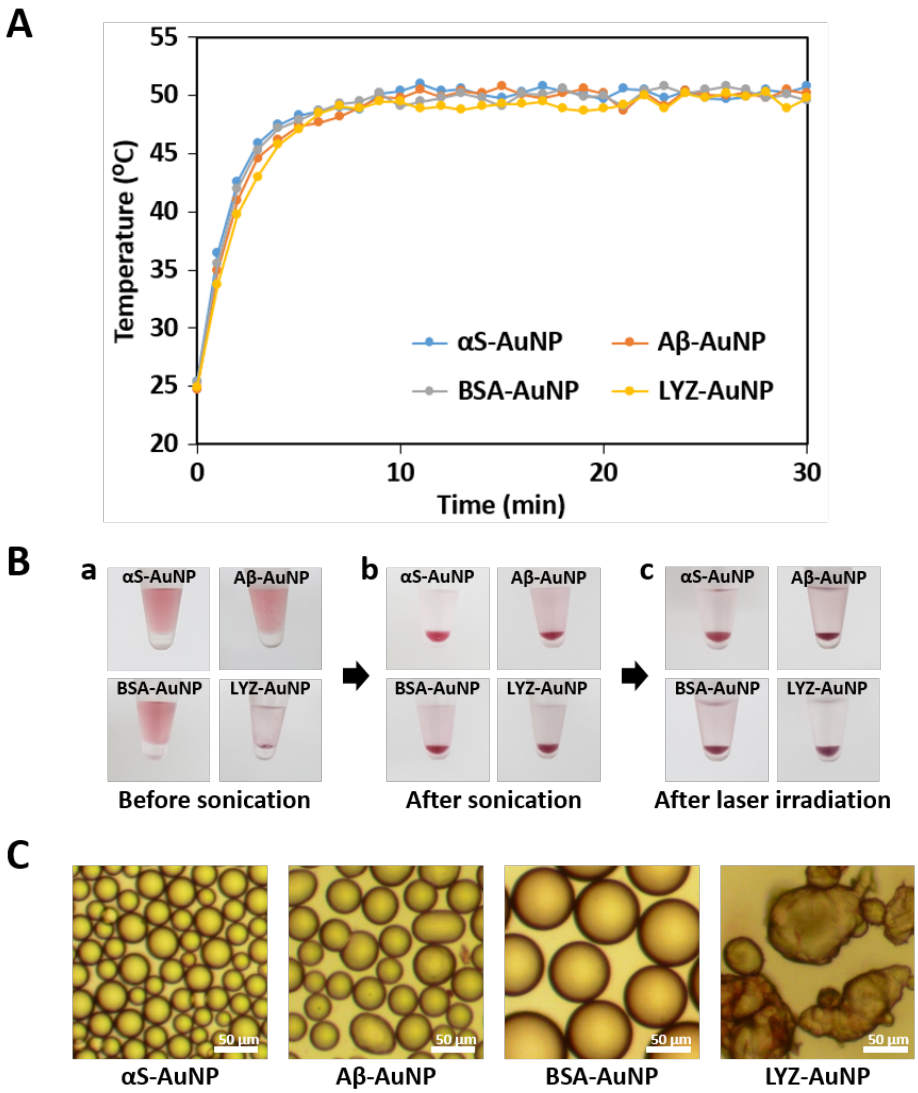

Figure 41. Thermal stability of protein-AuNP conjugates. (A) Photothermal effect of the protein-AuNP-containing solutions. **(B)** Pickering emulsion formation of various protein-AuNP conjugates after laser irradiation for 30 minutes. **(C)** The Pickering emulsions which composed of various protein-AuNP conjugates after laser irradiation for 15 minutes.

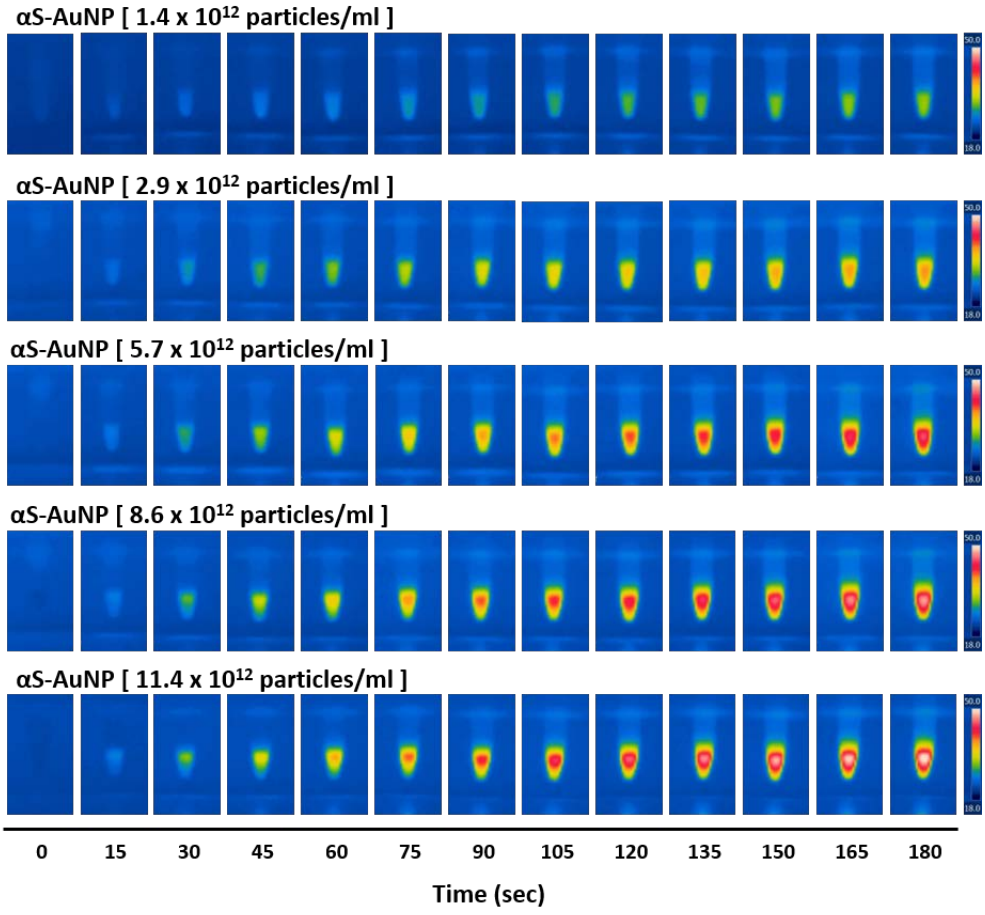

Figure 42. IR thermographic images of the solutions containing various amounts of αS-AuNPs. The images were obtained during 3 min irradiation of a laser beam at 532 nm.

irradiation of the laser, as the concentration of the conjugates elevated, both the initial temperature increase rate and the final temperature were augmented (**Figure 43**). This means that the higher the density of the particles, the faster the rate of temperature increase, so that if the particles are assembled in the microcapsule form, they could expect to exhibit the rapid photothermal effect. This is confirmed by comparing the photothermal effects of the un-assembled αS-AuNP conjugates with the microcapsules at the same particle concentration (1.14 x 10^{12} particles/ml) (**Figure 44**). It turned out that as individual αS-AuNP conjugates were assembled into microcapsules, the initial heat generation rate during the first 15 seconds was found to increase by about 2.5 times from 0.21°C/s to 0.53°C/s (**Figure 44A**, inset). After 8 minutes of laser irradiation, the temperature of the solution in both cases was shown to be similar to about 49°C (**Figure 44**). However, it was confirmed in the IR thermographic images obtained using the thermographic camera (**Figure 44B**) that the heat was generated overall the solution in the dispersed αS-AuNP conjugates, whereas localized heat generation occurred at the lower part of the tube in the microcapsule (**Figure 44B**, white arrows). Therefore, this localized heat generation of the microcapsule could be applied to PTT which is a treatment that selectively eradicates abnormal cells in the affected areas using heat converted from light. Actually, PTT could be performed in the temperature range of about 42-47°C for tens of minutes [97], where the

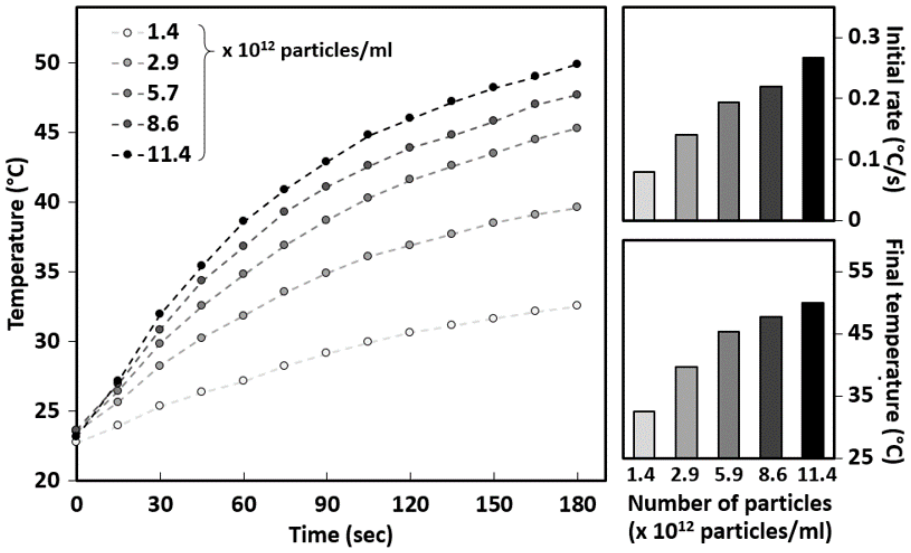

Figure 43. Photothermal effect of αS-AuNP conjugates. Photothermal effect of the αS-AuNP-containing solutions at various particle concentrations as indicated (left). The initial rates of heat generation and the final temperatures of the αS-AuNP solutions (right). The light-induced temperature increase was monitored with a thermographic camera (FLIR Systems) after an exposure of 10 nm αS-AuNPs to a laser beam at 532 nm for 3 min.

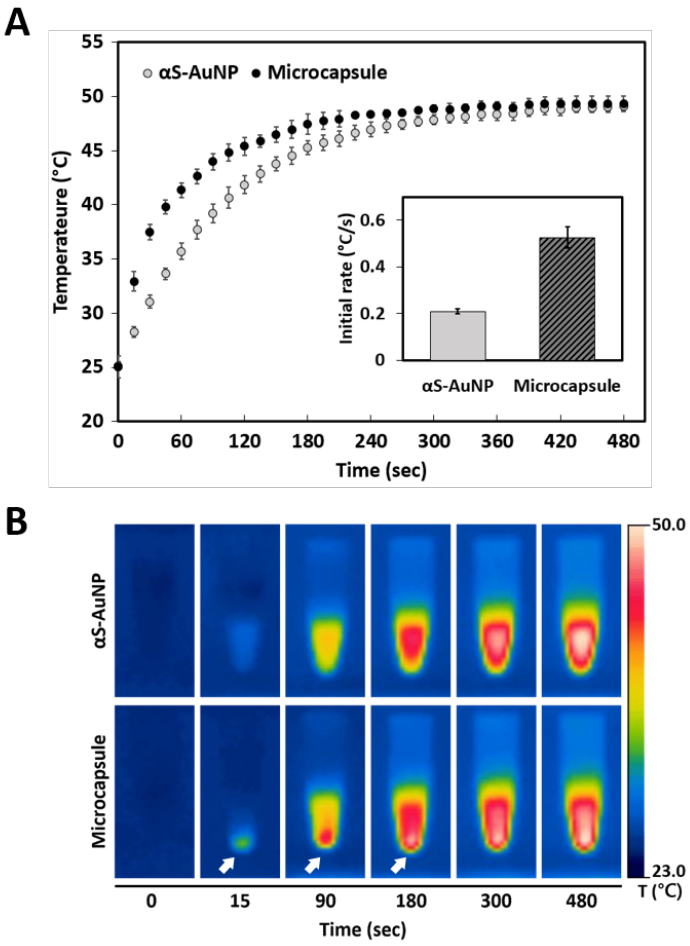

Figure 44. Photothermal effect of microcapsules. (**A**)Photothermal effect of αS-AuNPs before and after the microcapsule assembly as they were irradiated with the laser beam for 8 min. The initial rates of heat generation are shown (inset). Error bars indicate standard deviation (n=3). (**B**) IR thermographic images of the solutions containing dispersed αS-AuNP conjugates and microcapsules. The images were obtained during 8 min irradiation of a laser beam at 532 nm. White arrows indicate that localized heat generation.

membrane of the tumor cells is loosened and the internal protein is denatured [80]. Therefore, it was expected that PTT could be performed on cancer cells using microcapsules composed of αS-AuNP conjugates through laser irradiation.

(8) Bio-application of microcapsule

Based on the previous series of experiments, it is expected that the microcapsules would show therapeutic effects *in vivo* through the following process: (1) fragmentation and drug release by MMPs in cancerous lesions (**Figure 45A**), (2) cancer cell death caused by cellular uptake of drugs (and microcapsule fragments) (**Figure 45B**), and (3) cancer cell death caused by photothermal effects by the uptaked microcapsule fragments (**Figure 45C**). This process was confirmed by *in vitro* test using HeLa (**Figure 46A**), the oldest and most commonly used human cell line [98] derived from cervical cancer [99]. First, the microcapsules containing honokiol [100] (**Figure 46B**), a poorly water-soluble drug exhibiting anti-tumor properties [101], were prepared to investigate the drug delivery and release of the microcapsules. Briefly, the honokiol was dissolved in chloroform in a concentration of 10 μg/ml, and αS-AuNP Pickering emulsions were prepared and washed with fresh Mes buffer (20 mM, pH 6.5) twice to remove free αS-AuNPs. With

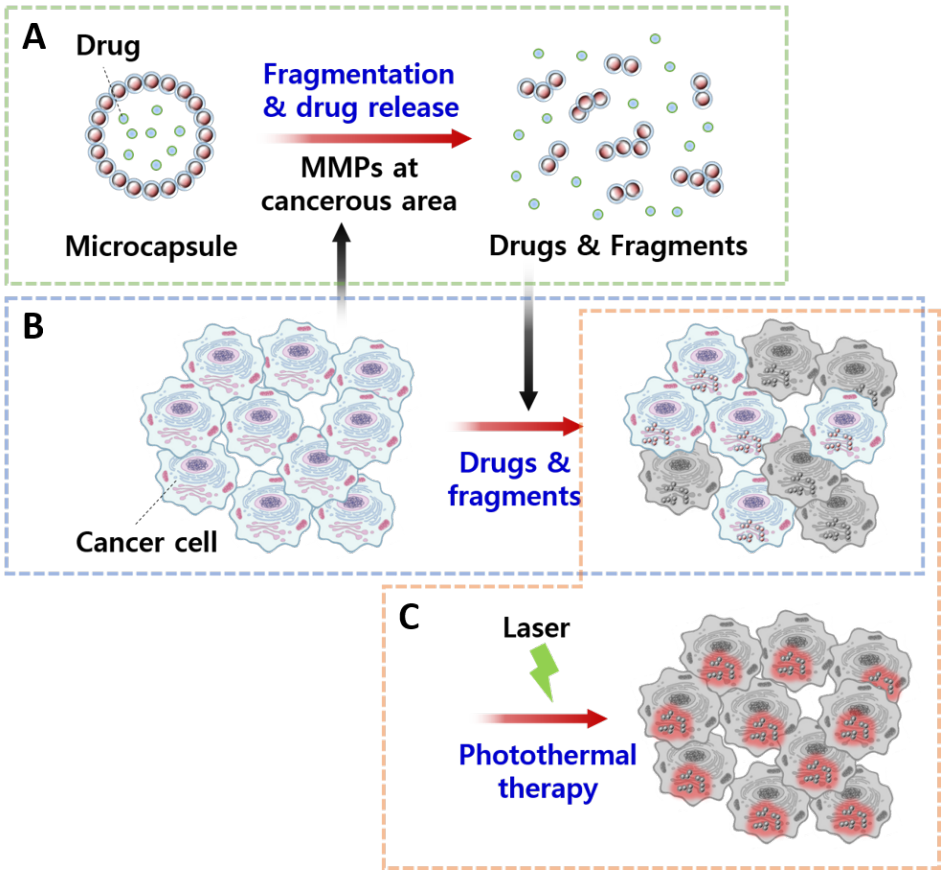

Figure 45. Schematic representation of *in vivo* application process of AuNP microcapsule for cancer therapy. (A) Fragmentation and drug release by MMPs in cancerous lesions. **(B)** Cell death caused by cellular uptake of drugs. **(C)** Cell death caused by photothermal effects by the uptaked microcapsule fragments.

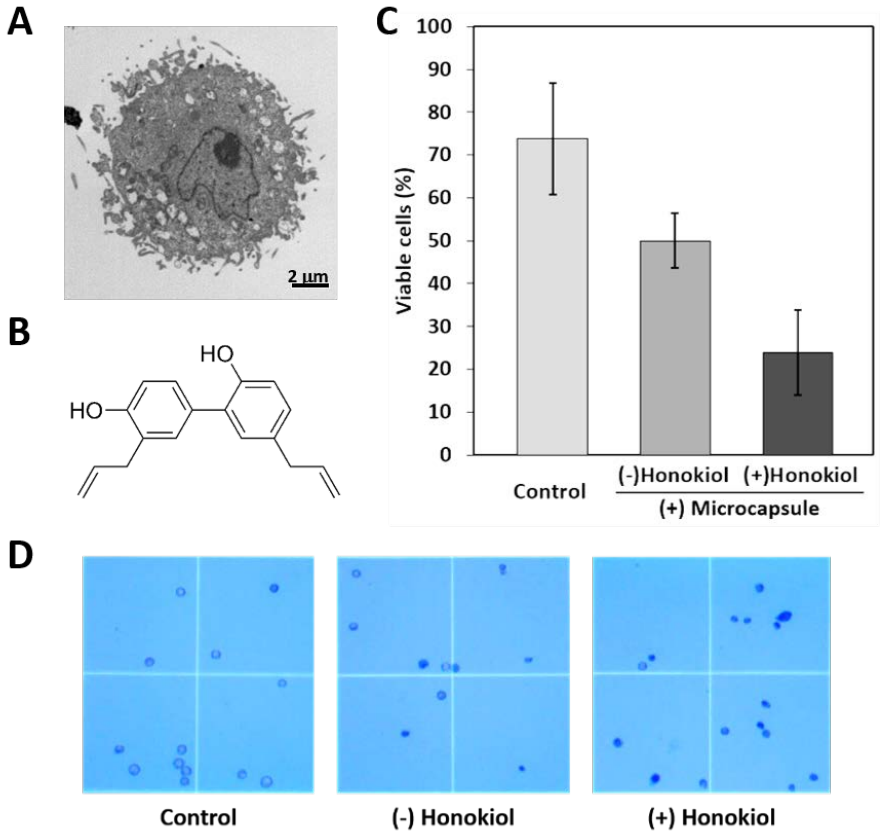

Figure 46. Drug release from microcapsule and its affect to HaLa. (A) TEM image of HeLa cell. **(B)** Structure of honokiol. **(C)** Drug- and microcapsule-induced cell death of HeLa. Error bars indicate standard deviation (n=4). **(D)** Microscopic images of the trypan blue-treated HeLa cells after the drug release from microcapsules.

incubation at 37°C for two days, the honokiol-containing microcapsules were obtained in which chloroform inside was evaporated. The microcapsules (1.14 x 10^{12} particles/30 µl) with or without honokiol were added to HeLa cells (5.7 x 10^{5} cells) in 450 µl of DMEM containing 5% dimethyl sulfoxide (DMSO). Following the trypsin-treatment with 10 µg, the cells were continuously incubated for 6 hours at 37°C (5 % CO_2). Cell viability (**Figure 46C**) was evaluated with trypan blue exclusion assay (**Figure 46D**). The result show that the cell death became augmented considerably to 76.2% from 50.0% in the presence and absence of honokiol delivered inside the microcapsules (**Figure 46C** and **46D)**. This data clearly indicates that the microcapsules could be used to deliver a drug to control the cancer cells. In addition to the cell death by the drug, the photothermal effect on the cancer cells by the microcapsule fragments was also evaluated. The microcapsule fragments were prepared by trypsin treatment (**Figure 47**) and challenged to the HeLa cells in order to examine the effect of light-induced rapid localized heat generation on cell viability *in vitro*. The use of fragments was due to the expectation that the microcapsules would be disintegrated by the protease, as described above, in actual biological lesions (**Figure 45**). After incubation for 3 hours with the microcapsules fragments, HeLa cells immunostained with anti-αS antibody showed high fluorescence intensity which represents microcapsule fragments (**Figure 48A**) comparing to fragment-untreated control cells (**Figure 48B**).

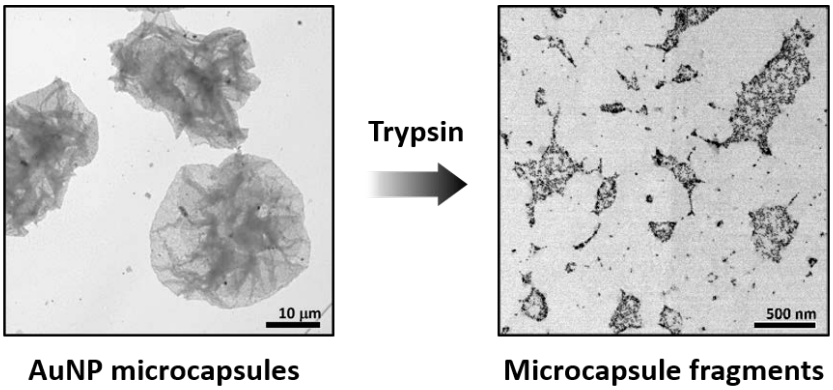

Figure 47. Preparation of microcapsule fragments. TEM images of intact microcapsules (left) and microcapsule fragments.

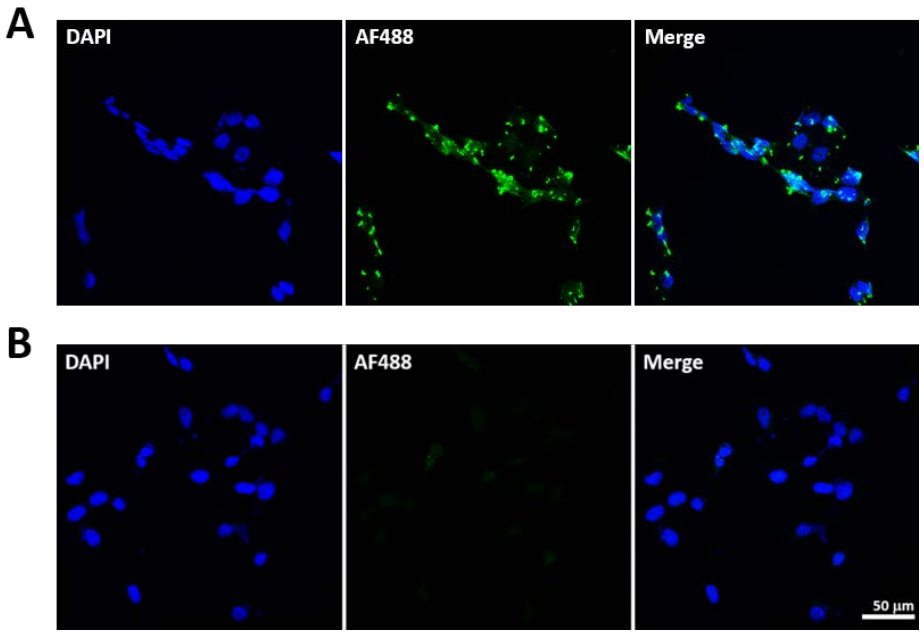

Figure 48. Confocal images of HeLa cells with or without microcapsule fragments. (**A**) Cellular localization of the trypsin-digested fragments of microcapsules. The microcapsule fragments were visualized with CLSM after being immunostained for αS with a primary antibody of mouse anti-αS IgG and a secondary antibody of goat anti-mouse IgG antibody labeled with AF488. (**B**) Confocal images of fragment-untreated HeLa cells.

The fluorescence image shows that the fragments are readily found both inside and on the surface of the cells. A TEM image of the fragment-treated cell showed that the fragments made of αS-AuNP conjugates is engulfed into the cell (**Figure 49**). However, the fragments attached to the cell surface were not present in the TEM image, which is considered to have been removed by pretreatment process for TEM observation. The viability of HeLa cells (3.6 x 10^6 cells/ml) treated with microcapsule fragments composed of 2.28 x 10^{12} αS-AuNP conjugates was investigated under laser irradiation for 3 hours in order to confirm the photothermal effect of the microcapsules for therapeutic application. Trypan blue exclusion assay showed that most of the fragment-challenged cells were eradicated during the 3 hours of laser irradiation whereas most of the control cells remained alive (**Figure 50**). In detail, the cells with fragments exhibited two phases in cell eradication rate with the first death rate of 11.0%/hour for initial 1 hour and the second death rate of 39.6%/hour for next 2 hours of irradiation, while the cells without the fragments inside hardly responded to the irradiation with a negligible cell death rate of 0.8%/hour (**Figure 51**). As a result, *in vitro* PPT experiments on cancer cells by the photothermal effect of microcapsules composed of αS-AuNP conjugates suggested the possibility of using microcapsules for pathological purposes. With not only this photothermal effect but also the fact that drugs could be loaded into the capsules, the αS-AuNP conjugate microcapsules could be

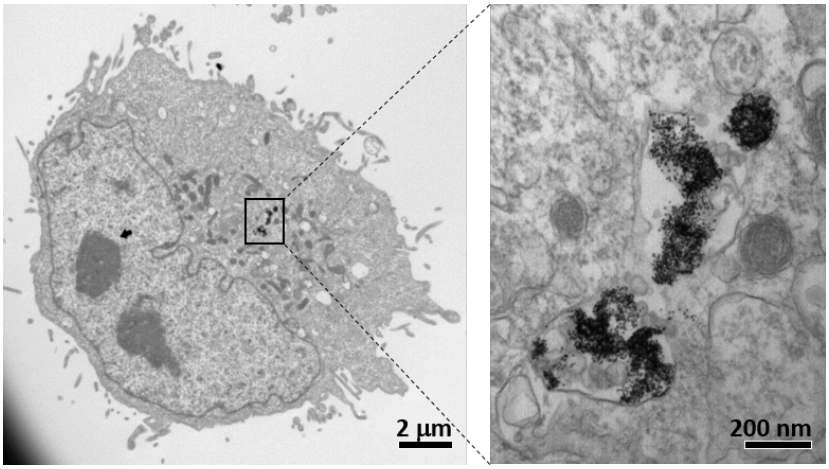

Figure 49. TEM images of cellular uptake of the microcapsule fragments. The trypsin-digested fragments of microcapsules taken up into HeLa cells were revealed with TEM.

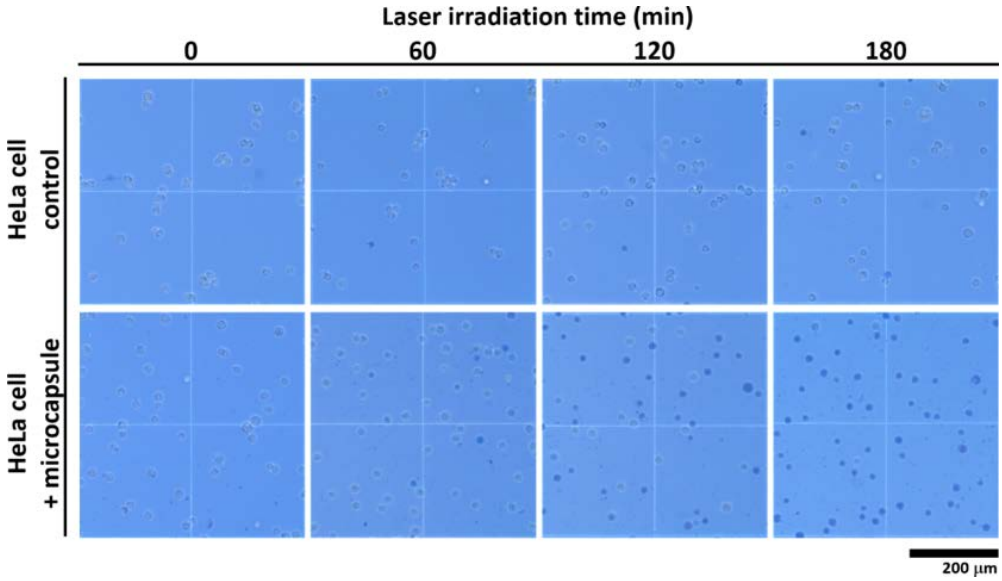

Figure 50. Microscopic images of the trypan blue-treated HeLa cells after the laser irradiation during the time indicated. The cells were prepared in the absence (top) or presence (bottom) of the microcapsule fragments.

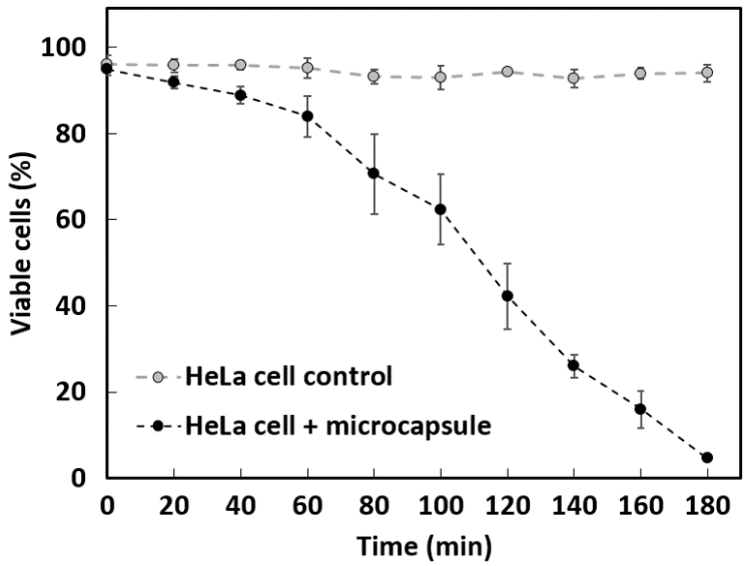

Figure 51. Light-induced cell death of HeLa cells. The death of the cells was monitored via trypan-blue exclusion assay. The cells with and without the trypsin-digested fragments inside were exposed to a laser beam at 532 nm for 3 hours. Error bars indicate standard deviation (n=4).

applied in therapeutic applications as a functional cargo carrier.

(9) Functionalization of microcapsule

AuNP microcapsules with capable of not only controlled release of cargo by protease but also photothermal property have been prepared by Pickering emulsion formation with self-assembly of αS conjugated with AuNP. However, since Pickering emulsion prepared for microcapsule fabrication is an oil-in-water emulsion, there was a limitation that it could loaded only hydrophobic materials. In order to solve this problem, inverted micelles fabricated using 1,2-dioleoyl-sn-glycero-3-phosphocholine (DOPC) were introduced (**Figure 52A**). Since the inverted micelles were also generated by ultrasonication, AuNP microcapsules should be prepared by vortexing or vigorous shaking instead of the sonication (**Figure 52A**). After the shaking, orthogonal cargo loading could be achieved by entrapping both hydrophobic substances pre-dissolved in chloroform and hydrophilic agents pre-packed within the inverted micelles made of DOPC (**Figure 52B**). In addition, other nanoparticles such as AgNPs, QDs and MNPs which have their own function could be loaded in the carrier or incorporated into the shell of the capsule in order to impart their functionality to the microcapsule. Microcapsules containing QDs which could be utilized for *in vivo* optical imaging were prepared and the presence of QDs

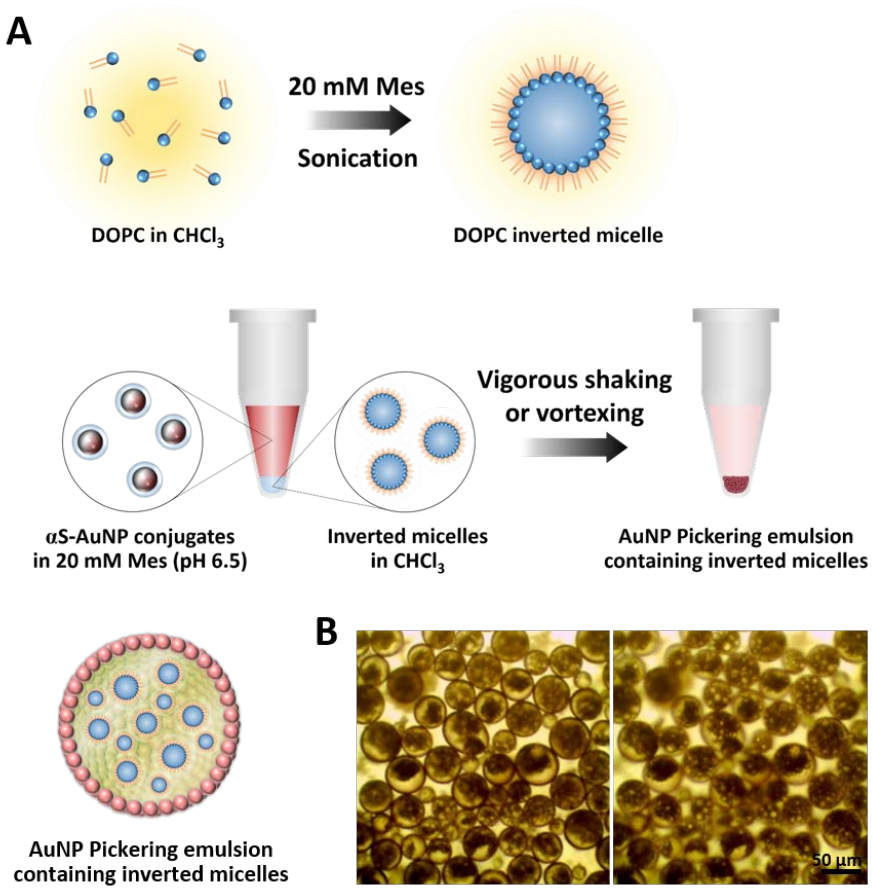

Figure 52. Preparation of inverted micelle-containing Pickering emulsion. **(A)** Schematic representation of preparation of inverted micelles and Pickering emulsion containing inverted micelles. **(B)** Microscopic images of different focuses of Pickering emulsions containing inverted micelles.

was confirmed by fluorescence image (**Figure 53A**). In addition, a microcapsule of which shell is composed of αS-QD conjugate alone (**Figure 53B**) or mixed conjugates of αS-QD and αS-AuNP (**Figure 53C**) was also prepared. If the QD's emission wavelength region and the AuNP's absorption wavelength region are close to each other, a wide absorption region of the QD could be transferred to the AuNPs, which is also used for the biosensing strategies based on quenching effect [102]. AuNP microcapsules containing MNPs could be also widely utilized using such diverse techniques of the MNPs as targeted drug delivery, electromagnetic hyperthermia, or magnetic resonance imaging (MRI) [103]. The resulting MNP-containing microcapsules (**Figure 54A**) exhibited magnet-induced motion (**Figure 54B**), which could be employed to localizes the capsules to the target sites with magnetic field. Further, the protein surrounding the surface of the microcapsule provides a site capable of attaching various functional materials. Especially for the targeting purpose, antibodies were immobilized onto the outlying αS modified using a photoactivatable heterobifunctional crosslinker, Sulfo-SANPAH. Briefly, after photolabeling of the αS on the microcapsule using a nitrophenyl azide group of the crosslinker, antibodies were attached to the capsule surface using chemical crosslinking with an amine-reactive N-hydroxysuccinimide ester. The antibodies bound to the microcapsules before and after evaporation of the internal chloroform were confirmed by

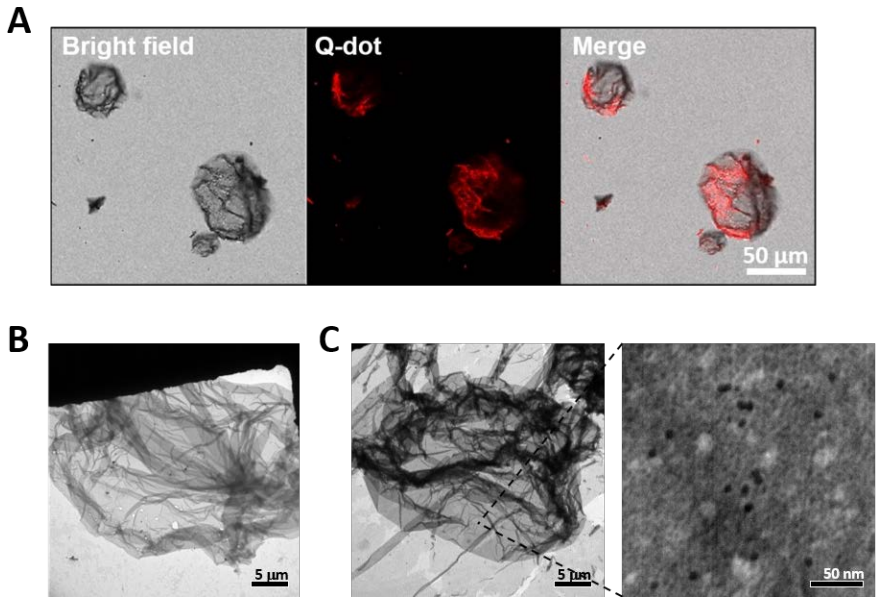

Figure 53. Microcapsules with QDs. (A) Fluorescence microscopic image of the microcapsules containing QDs inside. **(B)** TEM image of microcapsule composed of αS-QD conjugates only. **(C)** TEM images of microcapsule composed of both conjugates of αS-AuNP and αS-QD. Dark black dots are AuNPs.

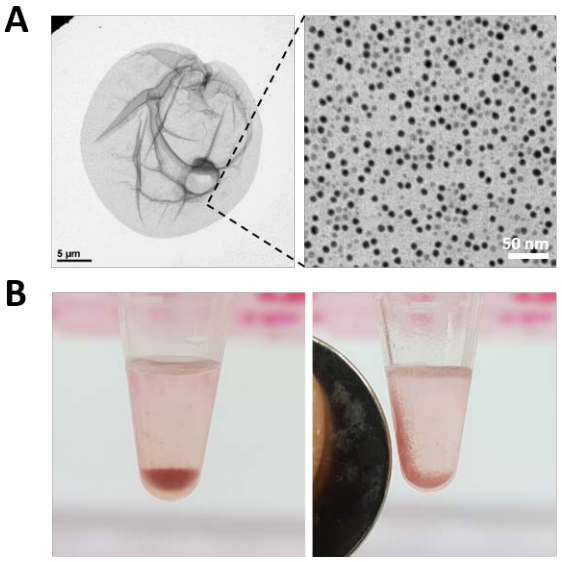

Figure 54. The microcapsules containing MNPs. (A) TEM images of MNP-containing AuNP microcapsule. Dark black dots are AuNPs. **(B)** Movement of the MNP-contaning microcapsule by external neodymium magnet.

fluorescence images (**Figure 55**). Thus, this two-step photo-activatable cross-linking strategy could be used to conjugate various chemical and biological agents to the capsule surface as well as antibodies by using coat protein of αS as a chemical anchor to diversify the molecular function of AuNP microcapsule. In summary, a multifunctional AuNP microcapsule fabrication process that provides orthogonal cargo loading, targeting property and imaging characteristics for cargo delivery system was introduced, and the resulting capsules could be equipped with additional functional agents including antibodies by crosslinking with surface protein.

II-3. Conclusions

Here, the fabrication of AuNP microcapsules accomplished by self-assembly of αS and their functionalization and application have been introduced. As αS conjugated onto AuNP was contacted with chloroform in the process of Pickering emulsion formation, robust β-sheet formation between protein molecules was produced resulting in the fabrication of microcapsule composed of single layer of compact AuNPs. These αS-αS interactions are thought to proceed only in the capsules due to the blocking effect of the inter-capsule interaction by the C-terminal of αS. The microcapsules could be further stabilized through chloroform-induced stabilization *via* additional

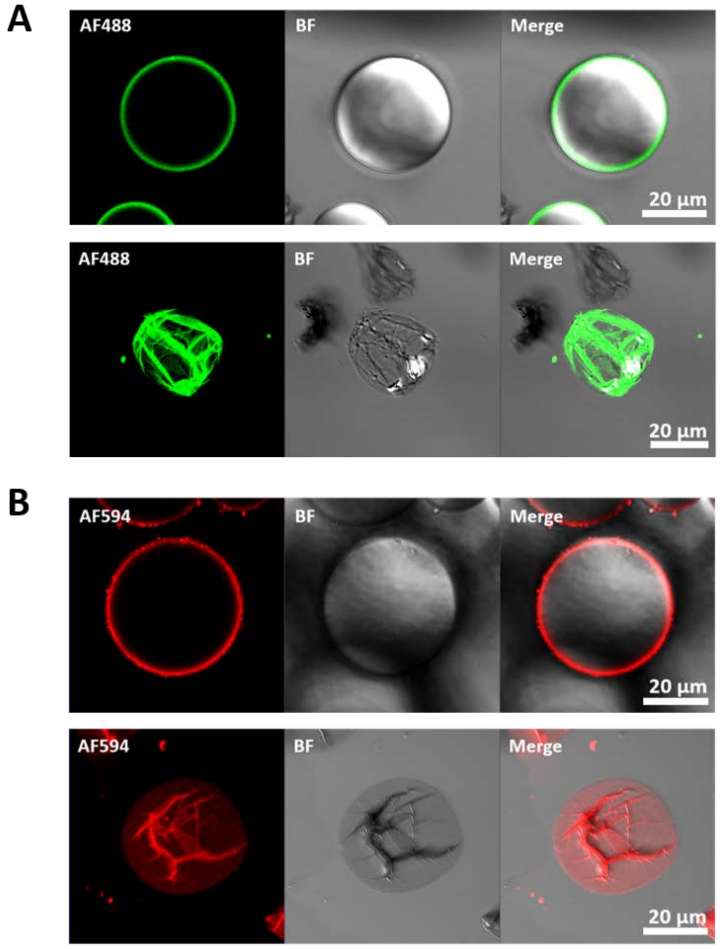

Figure 55. Fluorescence microscopic images of the Pickering emulsions and microcapsules. The emulsions and microcapsules decorated with the antibodies tagged with two separate fluorescent dyes of AF488 (**A**) and AF594 (**B**) by employing a photoactivatable crosslinking agent of Sulfo-SANPAH.

incubation, and mechanically and chemically stable even in the fluidic system, high ionic strength and broad pH range. The degradation of microcapsules and consequent cargo release could be achieved by undermining the protein-protein interactions *via* cleavage the protein with protease, which had been shown to be effective as cancer therapy using real drug (honokiol) and cancer cells (HeLa) *in vitro*. The microcapsules also present a photothermal property for more effective cancer cell death due to the AuNPs forming the shell. Considering the synergistic effect of both drug and PTT, αS-AuNP microcapsule is expected to act as an ideal carrier in drug delivery system. In addition, the microcapsule could be additional functionalized by introducing other nanoparticles or inverted micelles and conjugating antibodies by crosslinker using surface proteins as an anchor. Therefore, this multimodal microcapsule of which cargo release is controllable as a bio-applicable cargo carrier has a high possibility to be applied in the development of controllable soft materials or sensors as well as drug delivery systems. Furthermore, since the frame for fabrication of the microcapsule and its maintain force are based on Pickering emulsion formation and αS-αS interactions respectively, it is expected that the microcapsules could be composed and fabricated with not only AuNPs but also various nanoparticles present their individual optical and electromagnetic properties including AgNPs, QDs or MNPs by forming conjugation with αS (**Figure 56**). Taken together, the αS-mediated multimodal

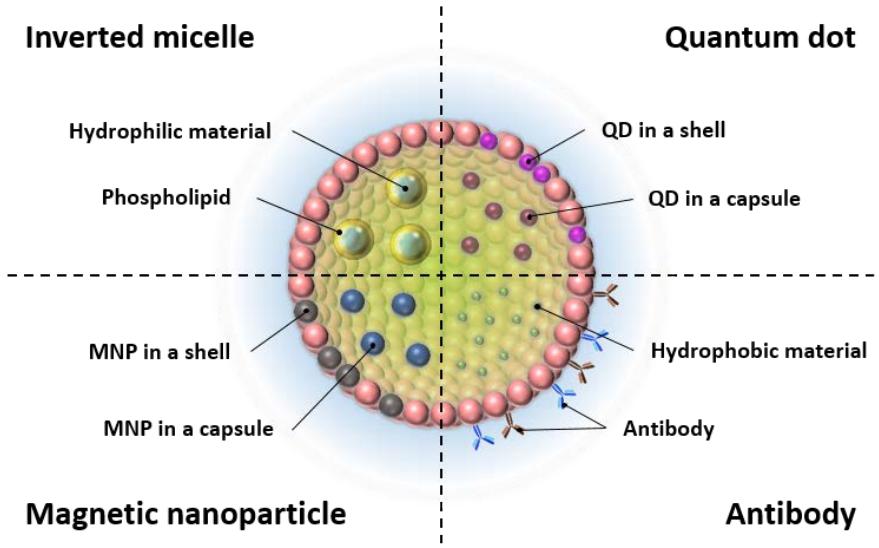

Figure 56. Schematic representation of multi-functional AuNP microcapsule.

AuNP microcapsules that exhibit structural robustness, specific targeting, triggered release, and photothermal activity are suggested to be served as a framework to develop a multifunctional cargo carrier system which would be useful in diverse area including biomedical science, and sensor development technology.

Experimental Section

(1) Expression and purification of recombinant αS

Human recombinant αS gene cloned in pRK172 was overexpressed in *Escherichia coli* **(***E. coli*, BL21-DE3). The cells were grown in Luria-Bertani medium (Becton**,** Dickinson and Company, Sparks, MD) in the presence of ampicillin (0.1 mg/ml). After the induction with 0.5 mM IPTG for 4 hours at 37°C, the cells were harvested by a centrifugation at 3,000 g for 20 minutes at 4°C (Vision Scientific, Daejeon, Korea). The resulting cell pellet was resuspended with a lysis buffer (20 mM Tris-Cl, pH 7.5, containing 0.1 M NaCl, 0.1 mM PMSF, 1 μg/ml leupeptin, and 2 mM EDTA). Then, lysozyme and DNase were added to the concentrations of 0.1 mg/ml and 10 units/ml, respectively, and mixed gently. Following 2 hours of incubation at 37°C, the cell lysate was boiled for 20 minutes and cooled down promptly on ice, then centrifuged at 6,000 g for 20 minutes at 4°C. After a filtration through 0.22 μm Millex-GV syringe filter (Merck Millipore, Darmstadt, Germany), the supernatant was applied onto DEAE-anion exchange column pre-equilibrated with 20 mM Tris-Cl, pH 7.5. The bound αS was eluted isocratically with 0.4 M NaCl. Fractions containing αS were combined and concentrated, which was

further purified with S-200 gel filtration chromatography by using 20 mM 2-(N-morpholino)-ethanesulfonic acid (Mes), pH 6.5. The purified protein was aliquoted into 1.0 ml at 1 mg/ml and stored at -80 °C until being used.

(2) Preparation of αS-AuNP conjugates

αS-AuNP conjugates were prepared by simple co-incubation between AuNP and αS. αS monomers (1 mg/ml) stored in 20 mM Mes at pH 6.5 and AuNPs provided in water at the concentrations of 5 x 10^{13} particles/ml for 5 nm, 5.7 x 10^{12} particles/ml for 10 nm, 7 x 10^{11} particles/ml for 20 nm, and 2 x 10^{11} particles/ml for 30 nm (BBI Solutions, Cardiff, UK) were mixed at a volume ratio of 1:4 and incubated for 12 hours at 4°C to encapsulate the particles with αS. The unbound αS monomers were removed by precipitation-resuspension procedure for three times with centrifugation (Eppendorf Centrifuge 5415R, Eppendorf AG, Hamburg, Germany) at 13,200 rpm for durations different for each type of AuNPs (90 minutes for 5 nm, 60 minutes for 10 nm, 10 minutes for 20 nm, and 7 minutes for 30 nm). After resuspending the final precipitates with fresh 20 mM Mes (pH 6.5), the localized surface plasmon resonance (LSPR) spectrum of AuNPs was monitored with UV-VIS spectrophotometer (Ultrospec 2100 pro, Amersham Bioscience, Cambridge, UK) between 450 nm and 700 nm to confirm successful αS-AuNP conjugate

formation which gave a red-shift of the maximum peak. The resuspended conjugates were stored at 4°C. The storage period did not exceed one week. For the assessment of pH-dependent microcapsule formation, the final precipitates were resuspended in a 10-fold diluted McIlvaine (0.1 M citrate - 0.2 M phosphate) buffer adjusted from pH 3 to 8.

(3) Preparation of αS-AgNP conjugates

αS-AgNP conjugates were prepared in the same manner as αS-AuNP conjugates. Briefly, αS monomers (1 mg/ml at 20 mM Mes at pH 6.5) and 20 nm colloidal AgNPs (7.0×10^{10} particles/ml in water, BBI Solutions) were mixed at a volume ratio of 1:4 and incubated at 4°C for 12 hours. Unbound αS monomers were removed by centrifugation (Eppendorf Centrifuge 5415R, Eppendorf AG) three times for 10 minutes at 13,200 rpm. The precipitate was then resuspended in 20 mM Mes (pH 6.5) at the concentration of 3.5×10^{11} particles/ml to obtain fresh αS-AgNP conjugates. The LSPR spectrum of AgNP was also monitored with a UV-VIS spectrophotometer (Ultrospec 2100 pro, Amersham Bioscience).

(4) Preparation of αS-QD conjugates

αS monomers (1 mg/ml at 20 mM Mes, pH 6.5) and 2.5 mg/ml Cd:S:Se/ZnS Core/shell QDs (Crystalplex, Pittsburgh, PA) in water were mixed at a volume ratio of 1:1 and incubated at 4°C for 12 hours. The sample was then dialyzed in a Slide-A-Lyzer 20K MWCO dialysis cassette (Thermo Scientific, Rockford, IL) against 20 mM Mes (pH 6.5) to remove unbound αS. After dialysis, the αS-QD conjugates are collected and diluted 10-fold with 20 mM Mes (pH 6.5) and stored until use. The final concentration of the Cd:S:Se/ZnS Core/shell QDs without considering protein is 0.25 mg / ml. The absorption spectra and photo-luminescence spectra of αS-QD conjugates were obtained using a UV-VIS spectrophotometer (Ultrospec 2100 pro, Amersham Bioscience) and a luminescence spectrophotometer (LS-55, Perkin Elmer, Fremont, CA), respectively.

(5) Synthesis of MNPs

The MNPs (Fe_3O_4 nanoparticles) were prepared by coprecipitation of Fe(II) and Fe(III) chlorides (Fe^{II}/Fe^{III} ratio = 0.5) [104]. 5.4 g (20 mmol) of $FeCl_3 \cdot 6H_2O$ and 2.0 g (10 mmol) of $FeCl_2 \cdot 4H_2O$ were dissolved in 25 ml of 0.4 M HCl. The resulting solution was added dropwise into 250 ml of 1.5 M NaOH solution under stirring. After 40-minute-reaction, black precipitate (MNPs) was collected using a magnet, washed twice with DW and twice with

0.1 M tetramethylammonium hydroxide (TMAOH), and stored in 250 ml of 0.1 M TMAOH [105].

(6) Preparation of αS-MNP conjugates

αS monomers (0.1 mg/ml at 20 mM Mes, pH 6.5) and MNPs (7 mg/ml) in 0.1 M TMAOH were mixed at a volume ratio 19:1 and incubated at 4 ℃ for 30 minutes. The sample was placed in Eppendorf tubes in 1 ml aliquots, and then the unbound αS monomers were removed by precipitation-resuspension procedure for three times with centrifugation (Eppendorf Centrifuge 5415R) at 10,000 rpm for 10 minutes. The first resuspension step was carried out using 1 ml of 5 mM TMAOH and the second and third resuspension steps were carried out using 1 ml of DW.

(7) Pickering emulsion formation of αS-NPs

Add 1/10 volume of chloroform to the αS-NP (AuNP, AgNP, and QD) conjugate solution, and briefly shaken to form a bulky emulsion. Ultrasound (40 kHz, 100W) was then applied to the mixture with WUC-A03H ultrasonic cleaner (DAIHAN Scientific) for 5 seconds, and briefly vortexed to obtain Pickering emulsions with high monodispersity. Size distribution of the

emulsion droplets was evaluated with optical microscope (CKX41, Olympus, Tokyo, Japan) and an image analyzer of ImageJ software (developed at the National Institutes of Health). The photoluminescence of the Pickering emulsions composed of αS-QD conjugates was observed using a UV transilluminator at a wavelength of 312 nm (100W) (ETX-20M, Vilber Lourmat, Torcy, France).

(8) Contact angle measurements

5 ml of αS solution (0.2 mg / ml in Mes pH 6.5) was placed on a planar bare gold plate and reacted for 12 hours at 4°C in a humid chamber to obtain αS-coated gold plate. The contact angles and the images of droplets were monitored by using a drop shape analyzer (DSA100, Kruss, Germany).

(9) Zeta (ζ) potential measurements

The ζ potential of the NPs and αS-NP conjugates were measured by Zetasizer Nano ZS90 (Malvern instruments Ltd., Worcestershire, UK) at a temperature of 25 °C. The samples were filled in folded capillary cells (zeta cells) and measured with the applied voltage of 150 V. ζ potential values were calculated and converted from electrophoretic mobility, which was carried

out by the Zetasizer software 7.12 (Malvern instruments Ltd.). Data represent the mean ± standard deviation obtained for three measurements.

(10) Transmission electron microscope (TEM)

An aliquot of the sample was dropped onto a 200-mesh copper grid (Electron Microscopy Sciences, Hatfield, PA) and dried in the air. The resulting grids were examined with TEM of JEM1010 (JEOL, Tokyo, Japan). When required, 2% uranyl acetate (20 μl) was used for negative staining of protein. The staining was carried out in a darkroom to prevent any degradation of uranyl acetate.

(11) Atomic force microscope (AFM)

Following a transfer of the AuNP microcapsules onto a silicon wafer, the sample was air-dried. The microcapsule surface was examined with AFM (Dimension 3100, Veeco Instruments Inc., Woodbury, NY) in tapping mode using PPP-NCHR cantilever (Nanosensors, Neuchatel, Swiss) with 285 kHz resonant frequency. All images obtained were analyzed with Gwyddion software (Department of Nanometrology, Czech Metrology Institute, Czech).

(12) Field emission scanning electron microscope (FE-SEM)

The microcapsule-containing solution was dropped onto a silicon wafer and air-dried, which was then coated with platinum in a vacuum sputter coater (EM ACE200, Leica, Wetzlar, Germany). The sample was examined with FE-SEM (SUPRA 55VP, Carl Zeiss, Oberkochen, Germany) at 2.0 kV.

(13) Confocal laser scanning microscope (CLSM)

The αS-AuNP microcapsules were prepared with chloroform in the presence or absence of Rhodamine 6G (R6G). The microcapsules prepared with 10 nm AuNPs at 5.7 x 10^{12} particles/ml were treated with mouse monoclonal anti-αS IgG (sc-12767, Santa Cruz Biotechnology, Santa Cruz, CA) at 1:50 dilution, and incubated for 2 hours at 37°C. After three consecutive washing steps for the settling microcapsules by replacing the supernatant with fresh 20 mM Mes (pH 6.5) to remove unbound antibodies, the microcapsules were tagged with a secondary antibody of goat anti-mouse IgG antibody labeled with Alexa Fluor 488 (AF488; A11001, Invitrogen, Carlsbad, CA) at 1:200 dilution for 1 hour at 37°C. Following removal of the free secondary antibody, the fluorescent microcapsules were examined with CLSM (LSM710, Carl Zeiss, Jena, Germany). The obtained images were

processed with ZEN imaging software (ZEN 2.3 blue edition, Carl Zeiss, Jena, Germany).

(14) Thioflavin-T (Th-T) binding fluorescence assay

20 µl of αS-AuNP Pickering emulsions (1.14 x10^{12} particles / 20 µl) in 20 mM Mes (pH 6.5) was mixed with 180 µl of 50 µM Th-T in 50 mM glycine (pH 8.5). Following 30 minutes of incubation under dark at room temperature, the Th-T binding was monitored with CLSM (Carl Zeiss). The wavelength of excitation and emission of Th-T was 450 nm and 485 nm, respectively.

(15) Congo red staining

To monitor the Congo red birefringence, an aliquot containing the microcapsules was air-dried on a glass slide. The sample was then stained with a saturated Congo red solution, and reacted at room temperature for 30 minutes before being examined with an optical microscope equipped with crossed polarizers.

(16) Fourier transform infrared (FT-IR) spectroscopy

FT-IR spectrophotometer (Nicolet 6700, Thermo Scientific, Madison, WI) was used to analyze the secondary structure of the αS attached onto AuNPs before and after the assembly of microcapsules from αS-AuNP conjugates. The solutions containing either αS-AuNP conjugates or the microcapsules were rapidly frozen in liquid nitrogen and lyophilized with a freeze-dryer (EYELA FDU-2200, Tokyo Rikakikai, Tokyo, Japan). FT-IR spectra were obtained at a resolution of 4 cm^{-1} by using the spectrophotometer equipped with a deuterated triglycine sulfate (DTGS) KBr detector. For analysis, the second-derivative spectra were obtained by smoothing and normalizing the amide I band region (1700 to 1600 cm^{-1}) with a baseline subtraction. The frequencies of the peaks found in the second-derivative spectra were used as initial peak points for curve fitting. In the curve fitting, each deconvolved curve was fitted to Gaussian curve using Origin Pro 2015 software (OriginLab Corporation, Northampton, MA).

(17) Rhodamine 6G (R6G) release assay

The αS-AuNP microcapsules were prepared as described above by using chloroform in which R6G was dissolved at 10 μg/ml. After an additional standing incubation of the emulsions for either 10 minutes or 30 minutes at 37°C, the chloroform present underneath the emulsion layer was removed with

a pipette, and the emulsions were washed twice with 20 mM Mes at pH 6.5 by replacing top aqueous layer. The R6G release was then examined with the microcapsules after being incubated for 30 minutes at room temperature under various conditions including pH change from pH 3 to pH 8 adjusted with a 10-fold diluted McIlvaine buffer (0.1 M citrate - 0.2 M phosphate), ionic strength of the solution adjusted with NaCl, and cations such as Na^{+}, K^{+}, Fe^{2+}, Ca^{2+}, Mg^{2+} and Cu^{2+} at the final concentration of 5 mM. To assess proteolytic susceptibility of the microcapsules, the R6G release assay was performed with various proteases such as trypsin, cathepsin-B, calpain-1, thrombin, MMP-2, and MMP-9 at the final concentration of 10 μg/ml. The microcapsules were incubated with one of the proteases in phosphate-buffered saline (PBS) for 1 hours at 37°C. The amount of R6G released was determined by measuring the fluorescence of R6G dissolved in the aqueous layer at 552 nm with an excitation at 520 nm by using a luminescence spectrophotometer (LS-55, Perkin Elmer).

(18) Flow-induced R6G release

A fluidic system was assembled with a syringe pump (NE-1000, New Era Pump Systems Inc., Farmingdale, NY) and a 50 ml syringe connected to a sample loading tube with an inner diameter of 0.8 mm followed by a traveling

tube with total length of 1.0 m and inner diameter of 1.0 mm. The R6G-containing microcapsules were loaded into the sample loading tube and allowed to experience the flow at several constant rates of 10 cm/s, 30 cm/s, 50 cm/s, and 70 cm/s driven by the syringe pump. The release of R6G was monitored by collecting the microcapsules that had passed through the traveling tube.

(19) Photothermal effect of αS-AuNP microcapsules

To monitor the photothermal effect of αS-AuNPs before and after their assembly into the microcapsules, a 2000 mW 532 nm Diode Pumped Solid State (DPSS) green laser (CST-H-532-2000, Ultralasers, Toronto, Canada) and a thermographic camera (i2, FLIR Infrared Systems Ltd., North Billerica, MA) were used. A 10x beam expander (BEX-10X, Ultralasers, Toronto, Canada) was mounted on the aperture and the samples were placed 30 cm away from the aperture. The laser was irradiated from the top of the sample kept in Eppendorf tube without a cap. Heat generation of the samples were monitored with the thermographic camera during either 3 or 8 minutes of the laser irradiation. The IR thermographic images were acquired in every 15 seconds and the images were analyzed with FLIR tools software (FLIR Infrared Systems Ltd., North Billerica, MA). The maximum temperature of

the samples obtained at the area showing maximum heat generation in the thermographic images was plotted over time, in which the initial rate was measured with the temperature change during an initial 15 seconds of irradiation.

(20) Drug release assay

Honokiol purchased from Merck was dissolved in chloroform at 10 μg/ml, and the αS-AuNP Pickering emulsions were prepared and washed with fresh 20 mM Mes (pH 6.5) twice to remove free αS-AuNPs. Following a two day incubation at 37ºC, the honokiol-containing microcapsules were obtained with chloroform inside evaporated. The microcapsules (1.14×10^{12} particles/30 μl) with or without honokiol were added to HeLa cells (5.7×10^5 cells) in 450 μl of DMEM containing 5% dimethyl sulfoxide (DMSO). Following the trypsin-treatment with 10 μg, the cells were continuously incubated for 6 hours at 37°C (5 % CO_2). Cell viability was evaluated with trypan blue exclusion assay.

(21) Trypan blue exclusion assay

HeLa cells were seeded onto a petri dish at 3.6×10^6 cells/ml within Dulbecco's modified eagle medium (DMEM, Hyclone Laboratories, Logan,

UT) containing 10% fetal bovine serum (FBS, Gibco BRL, Grand Island, NY) and 50 units/ml of penicillin-streptomycin (Gibco BRL, Grand Island, NY). After the confluency of the cells reached about 90%, the cells were harvested using 2 ml of HyClone™ Trypsin (Hyclone Laboratories) diluted with 2 ml of DMEM. The harvested cells in 200 μl were placed in an Eppendorf tube and centrifuged at 1000 rpm for 3 minutes. Subsequently, the supernatant was changed with 200 μl of fresh DMEM, and then 50 μl of the microcapsule fragments (1.1×10^{13} particles/ml) were added thereto. The mixture was gently mixed and reacted for 3 hours in a shaking incubator (NB-205, BioTek Instruments, Seoul, Korea) at 37°C. The medium was replaced with 200 μl of PBS through centrifugation (1000 rpm, 3 minutes) and the plate was irradiated with a laser beam (532 nm, 2000 mW) for 180 minutes. In the meantime, 10 μl samples were taken every 20 minutes, mixed with 10 μl of 0.4% trypan blue (Gibco BRL) in PBS, and allowed to react for 1 minute. Then, the total number of cells and the number of stained cells were counted by using a hemocytometer and an optical microscope.

(22) Fabrication of the αS-AuNP microcapsules containing inverted micelles

Add 1/10 volume of 20 mM Mes (pH 6.5) to the chloroform containing 1,2-dioleoyl-sn-glycero-3-phospocholine (DOPC) at 10 mg/ml. Ultrasound (40 kHz, 100W) was then applied for 5 seconds with a bath-type sonicator of WUC-A03H ultrasonic cleaner (DAIHAN Scientific, Wonju, Korea) to obtain inverted micelles. The chloroform solution containing inverted micelles (20 μl) was added to 200 μl of αS-AuNP solution, and shaken vigorously to form the αS-AuNP Pickering emulsions loaded with the inverted micelles.

(23) Fabrication of the αS-AuNP microcapsules loaded with QDs or MNPs.

CdSe quantum dots (Q-dots) with average size of 5 nm stored in toluene and magnetic nanoparticles (MNPs) comprising iron oxide (II, III) with particle size of 10 nm provided in chloroform were purchased from Merck. The toluene of the Q-dot solution was replaced with chloroform *via* solvent evaporation. The chloroform solution containing either Q-dots or MNPs (20 μl) was added to 200 μl of αS-AuNP solution, and subjected to the ultrasound (40 kHz, 100W) for 5 seconds to prepare the αS-AuNP Pickering emulsions containing either Q-dots or MNPs.

(24) Conjugation of antibody onto the αS-AuNP microcapsules

Following the microcapsule preparation, the upper aqueous layer was replaced with 20 mM Mes, pH 6.5, containing a photoactivatable crosslinking agent of sulfosuccinimidyl 6-(4′-azido-2′-nitrophenyl-amino) hexanoate (Sulfo-SANPAH; Thermo Scientific, Rockford, IL) at 1 mM after washing the microcapsules gently with the Mes twice. The sample was then exposed to UV light (200 mJ at 302 nm) for 10 minutes with UV crosslinker (CL-1000M, UVP, Cambridge, UK). The microcapsules were washed three times with the fresh Mes to remove the unbound Sulfo-SANPAH. Antibody solution (20 μg) containing either goat anti-mouse IgG1 labeled with AF594 (A21125, Invitrogen, Carlsbad, CA) or goat anti-mouse IgG with AF488 (A11001, Invitrogen) was added and allowed to react with the microcapsules overnight at 4°C. After washing three times with the fresh Mes, the antibody-labeled microcapsules were examined with CLSM.

References

[1] A. Gharsallaoui, G. Roudaut, O. Chambin, A. Voilley, R. Saurel, Applications of Spray-Drying in Microencapsulation of Food Ingredients: an Overview, Food Res Int 40(9) (2007) 1107-1121.

[2] S.H. Kim, J.G. Park, T.M. Choi, V.N. Manoharan, D.A. Weitz, Osmotic-Pressure-Controlled Concentration of Colloidal Particles in Thin-Shelled Capsules, Nat Commun 5 (2014).

[3] A. Abbaspourrad, N.J. Carroll, S.H. Kim, D.A. Weitz, Polymer Microcapsules with Programmable Active Release, J Am Chem Soc 135(20) (2013) 7744-7750.

[4] B.M. Discher, Y.Y. Won, D.S. Ege, J.C.M. Lee, F.S. Bates, D.E. Discher, D.A. Hammer, Polymersomes: Tough Vesicles Made from Diblock Copolymers, Science 284(5417) (1999) 1143-1146.

[5] E. Amstad, S.H. Kim, D.A. Weitz, Photo- and Thermoresponsive Polymersomes for Triggered Release, Angew Chem Int Edit 51(50) (2012) 12499-12503.

[6] D.D. Lasic, Liposomes: From Physics to Applications, Elsevier Science Ltd (1993).

[7] G.V. Betageri, D.L. Parsons, Drug Encapsulation and Release from Multilamellar and Unilamellar Liposomes, Int J Pharm 81(2-3) (1992) 235-241.

[8] W. Hackl, M. Barmann, E. Sackmann, Shape Changes of Self-Assembled Actin Bilayer Composite Membranes, Phys Rev Lett 80(8) (1998) 1786-1789.

[9] M. Morikawa, M. Yoshihara, T. Endo, N. Kimizuka, α-Helical Polypeptide Microcapsules Formed by Emulsion-Templated Self-Assembly, Chem-Eur J 11(5) (2005) 1574-1578.

[10] M.C. Levy, M.C. Andry, Microcapsules Prepared through Interfacial Cross-Linking of Starch Derivatives, Int J Pharm 62(1) (1990) 27-35.

[11] S.U. Pickering, Emulsions, J Chem Soc 91 (1907) 2001-2021.

[12] Y. Chevalier, M.A. Bolzinger, Emulsions Stabilized with Solid Nanoparticles: Pickering Emulsions, Colloid Surface A 439 (2013) 23-34.

[13] B.P. Binks, Particles as Surfactants - Similarities and Differences, Curr Opin Colloid In 7(1-2) (2002) 21-41.

[14] S. Tsuji, H. Kawaguchi, Thermosensitive Pickering Emulsion Stabilized by Poly(N-isopropylacrylamide)-Carrying Particles, Langmuir 24(7) (2008) 3300-3305.

[15] T. Saigal, H.C. Dong, K. Matyjaszewski, R.D. Tilton, Pickering Emulsions Stabilized by Nanoparticles with Thermally Responsive Grafted Polymer Brushes, Langmuir 26(19) (2010) 15200-15209.

[16] M.M. Zhang, T.H. Ngo, N.I. Rabiah, T.P. Otanicar, P.E. Phelan, R. Swaminathan, L.L. Dai, Core-Shell and Asymmetric Polystyrene-Gold Composite Particles via One-Step Pickering Emulsion Polymerization, Langmuir 30(1) (2014) 75-82.

[17] Q. Lan, C. Liu, F. Yang, S.Y. Liu, J. Xu, D.J. Sun, Synthesis of Bilayer Oleic Acid-Coated Fe3O4 Nanoparticles and Their Application in pH-Responsive Pickering Emulsions, J Colloid Interf Sci 310(1) (2007) 260-269.

[18] Y. Tan, K. Xu, C. Liu, Y.L. Li, C.G. Lua, P.X. Wang, Fabrication of Starch-Based Nanospheres to Stabilize Pickering Emulsion, Carbohyd Polym 88(4) (2012) 1358-1363.

[19] T.C. Zhou, K. Zhang, T. Kamra, L. Bulow, L. Ye, Preparation of Protein Imprinted Polymer Beads by Pickering Emulsion Polymerization, J Mater Chem B 3(7) (2015) 1254-1260.

[20] R.M. Rasia, C.W. Bertoncini, D. Marsh, W. Hoyer, D. Cherny, M. Zweckstetter, C. Griesinger, T.M. Jovin, C.O. Fernandez, Structural Characterization of Copper(II) Binding to α-synuclein: Insights into the

Bioinorganic Chemistry of Parkinson's Disease, P Natl Acad Sci USA 102(12) (2005) 4294-4299.

[21] A.K. Dunker, J.D. Lawson, C.J. Brown, R.M. Williams, P. Romero, J.S. Oh, C.J. Oldfield, A.M. Campen, C.R. Ratliff, K.W. Hipps, J. Ausio, M.S. Nissen, R. Reeves, C.H. Kang, C.R. Kissinger, R.W. Bailey, M.D. Griswold, M. Chiu, E.C. Garner, Z. Obradovic, Intrinsically Disordered Protein, J Mol Graph Model 19(1) (2001) 26-59.

[22] H.J. Dyson, P.E. Wright, Intrinsically Unstructured Proteins and Their Functions, Nat Rev Mol Cell Bio 6(3) (2005) 197-208.

[23] A.K. Dunker, I. Silman, V.N. Uversky, J.L. Sussman, Function and Structure of Inherently Disordered Proteins, Curr Opin Struc Biol 18(6) (2008) 756-764.

[24] A.C.M. Ferreon, Y. Gambin, E.A. Lemke, A.A. Deniz, Interplay of α-Synuclein Binding and Conformational Switching Probed by Single-Molecule Fluorescence, P Natl Acad Sci USA 106(14) (2009) 5645-5650.

[25] O. Ullman, C.K. Fisher, C.M. Stultz, Explaining the Structural Plasticity of α-Synuclein, J Am Chem Soc 133(48) (2011) 19536-19546.

[26] R. van der Lee, M. Buljan, B. Lang, R.J. Weatheritt, G.W. Daughdrill, A.K. Dunker, M. Fuxreiter, J. Gough, J. Gsponer, D.T. Jones, P.M. Kim, R.W. Kriwacki, C.J. Oldfield, R.V. Pappu, P. Tompa, V.N. Uversky, P.E.

Wright, M.M. Babu, Classification of Intrinsically Disordered Regions and Proteins, Chem Rev 114(13) (2014) 6589-6631.

[27] E.J. Jo, J. McLaurin, C.M. Yip, P. St George-Hyslop, P.E. Fraser, α-Synuclein Membrane Interactions and Lipid Specificity, J Biol Chem 275(44) (2000) 34328-34334.

[28] W.S. Davidson, A. Jonas, D.F. Clayton, J.M. George, Stabilization of α-Synuclein Secondary Structure Upon Binding to Synthetic Membranes, J Biol Chem 273(16) (1998) 9443-9449.

[29] C.C. Jao, A. Der-Sarkissian, J. Chen, R. Langen, Structure of Membrane-Bound α-Synuclein Studied by Site-Directed Spin Labeling, P Natl Acad Sci USA 101(22) (2004) 8331-8336.

[30] T. Bartels, L.S. Ahlstrom, A. Leftin, F. Kamp, C. Haass, M.F. Brown, K. Beyer, The N-Terminus of the Intrinsically Disordered Protein α-Synuclein Triggers Membrane Binding and Helix Folding, Biophys J 99(7) (2010) 2116-2124.

[31] K. Vamvaca, M.J. Volles, P.T. Lansbury, The First N-terminal Amino Acids of α-Synuclein Are Essential for α-Helical Structure Formation In Vitro and Membrane Binding in Yeast, J Mol Biol 389(2) (2009) 413-424.

[32] D.F. Clayton, J.M. George, The Synucleins: a Family of Proteins Involved in Synaptic Function, Plasticity, Neurodegeneration and Disease, Trends Neurosci 21(6) (1998) 249-254.

[33] J.H. Lee, C.S. Hong, S. Lee, J.E. Yang, Y.I. Park, D. Lee, T. Hyeon, S. Jung, S.R. Paik, Radiating Amyloid Fibril Formation on the Surface of Lipid Membranes through Unit-Assembly of Oligomeric Species of α-Synuclein, Plos One 7(10) (2012) e47580.

[34] H.T. Li, H.N. Du, L. Tang, J. Hu, H.Y. Hu, Structural Transformation and Aggregation of Human α-Synuclein in Trifluoroethanol: Non-Amyloid Component Sequence is Essential and β-Sheet Formation is Prerequisite to Aggregation, Biopolymers 64(4) (2002) 221-226.

[35] H.Y. Kim, H. Heise, C.O. Fernandez, M. Baldus, M. Zweckstetter, Correlation of Amyloid Fibril β-Structure with the Unfolded State of α-Synuclein, Chembiochem 8(14) (2007) 1671-1674.

[36] F. Chiti, C.M. Dobson, Protein misfolding, functional amyloid, and human disease, Annu Rev Biochem 75 (2006) 333-366.

[37] S.J. Wood, J. Wypych, S. Steavenson, J.C. Louis, M. Citron, A.L. Biere, α-Synuclein Fibrillogenesis is Nucleation-Dependent - Implications for the Pathogenesis of Parkinson's Disease, J Biol Chem 274(28) (1999) 19509-19512.

[38] P.H. Nguyen, M.S. Li, G. Stock, J.E. Straub, D. Thirumalai, Monomer Adds to Preformed Structured Oligomers of Aβ-Peptides by a Two-Stage Dock-Lock Mechanism, P Natl Acad Sci USA 104(1) (2007) 111-116.

[39] J.H. Lee, G. Bhak, S.G. Lee, S.R. Paik, Instantaneous Amyloid Fibril Formation of α-Synuclein from the Oligomeric Granular Structures in the Presence of Hexane, Biophys J 95(2) (2008) L16-L18.

[40] G. Bhak, J.H. Lee, J.S. Hahn, S.R. Paik, Granular Assembly of α-Synuclein Leading to the Accelerated Amyloid Fibril Formation with Shear Stress, Plos One 4(1) (2009) e4177.

[41] G. Bhak, Y.J. Choe, S.R. Paik, Mechanism of Amyloidogenesis: Nucleation-Dependent Fibrillation versus Double-Concerted Fibrillation, Bmb Rep 42(9) (2009) 541-551.

[42] D. Lee, Y.J. Choe, Y.S. Choi, G. Bhak, J. Lee, S.R. Paik, Photoconductivity of Pea-Pod-Type Chains of Gold Nanoparticles Encapsulated within Dielectric Amyloid Protein Nanofibrils of α-Synuclein, Angew Chem Int Edit 50(6) (2011) 1332-1337.

[43] J. Lee, G. Bhak, J.H. Lee, W. Park, M. Lee, D. Lee, N.L. Jeon, D.H. Jeong, K. Char, S.R. Paik, Free-Standing Gold-Nanoparticle Monolayer Film Fabricated by Protein Self-Assembly of α-Synuclein, Angew Chem Int Edit 54(15) (2015) 4571-4576.

[44] G. Bhak, J. Lee, C.H. Kim, D.Y. Chung, J.H. Kang, S. Oh, J. Lee, J.S. Kang, J.M. Yoo, J.E. Yang, K.Y. Rhoo, S. Park, S. Lee, K.T. Nam, N.L. Jeon, J. Jang, B.H. Hong, Y.E. Sung, M.H. Yoon, S.R. Paik, High-Density Single-Layer Coating of Gold Nanoparticles onto Multiple Substrates by

Using an Intrinsically Disordered Protein of α-Synuclein for Nanoapplications, Acs Appl Mater Inter 9(10) (2017) 8519-8532.

[45] W. Lin, T. Insley, M.D. Tuttle, L.Y. Zhu, D.A. Berthold, P. Kral, C.M. Rienstra, C.J. Murphy, Control of Protein Orientation on Gold Nanoparticles, J Phys Chem C 119(36) (2015) 21035-21043.

[46] K. Marshall, R. STOUT, R. Mitchell, Mechanism of the Initial Events in the Sorption of Marine Bacteria to Surfaces, Microbiology 68(3) (1971) 337-348.

[47] S. Usui, DLVO Theory of Colloid Stability, in: H. Ohshima, K. Furusawa (Eds.), Electrical phenomena at interfaces: fundamentals, measurements, and applications, Marcel Dekker Inc (1998) 101-118.

[48] T. Young, III. An essay on the cohesion of fluids, Philosophical transactions of the royal society of London 95 (1805) 65-87.

[49] R.N. Wenzel, Resistance of solid surfaces to wetting by water, Industrial & Engineering Chemistry 28(8) (1936) 988-994.

[50] M. Sabaeian, A. Khaledi-Nasab, Size-Dependent Intersubband Optical Properties of Dome-Shaped InAs/GaAs Quantum Dots with Wetting Layer, Appl Optics 51(18) (2012) 4176-4185.

[51] A. Khaledi-Nasab, M. Sabaeian, M. Sahrai, V. Fallahi, Kerr Nonlinearity Due to Intersubband Transitions in a Three-Level InAs/GaAs Quantum

Dot: the Impact of a Wetting Layer on Dispersion Curves, J Optics-Uk 16(5) (2014) 055004.

[52] W. Hoyer, D. Cherny, V. Subramaniam, T.M. Jovin, Impact of The Acidic C-Terminal Region Comprising Amino Acids 109-140 on α-Synuclein Aggregation in vitro, Biochemistry-Us 43(51) (2004) 16233-16242.

[53] E. Glogowski, R. Tangirala, J.B. He, T.P. Russell, T. Emrick, Microcapsules of PEGylated Gold Nanoparticles Prepared by Fluid-Fluid Interfacial Assembly, Nano Lett 7(2) (2007) 389-393.

[54] G. Stephenson, R.M. Parker, Y. Lan, Z.Y. Yu, O.A. Scherman, C. Abell, Supramolecular Colloidosomes: Fabrication, Characterisation and Triggered Release of Cargo, Chem Commun 50(53) (2014) 7048-7051.

[55] K.L. Thompson, M. Williams, S.P. Armes, Colloidosomes: Synthesis, Properties and Applications, J Colloid Interf Sci 447 (2015) 217-228.

[56] M.F. Hsu, M.G. Nikolaides, A.D. Dinsmore, A.R. Bausch, V.D. Gordon, X. Chen, J.W. Hutchinson, D.A. Weitz, Self-Assembled Shells Composed of Colloidal Particles: Fabrication and Characterization, Langmuir 21(7) (2005) 2963-2970.

[57] A.D. Dinsmore, M.F. Hsu, M.G. Nikolaides, M. Marquez, A.R. Bausch, D.A. Weitz, Colloidosomes: Selectively Permeable Capsules Composed of Colloidal Particles, Science 298(5595) (2002) 1006-1009.

[58] P.F. Noble, O.J. Cayre, R.G. Alargova, O.D. Velev, V.N. Paunov, Fabrication of "Hairy" Colloidosomes with Shells of Polymeric Microrods, J Am Chem Soc 126(26) (2004) 8092-8093.

[59] O.J. Cayre, P.F. Noble, V.N. Paunov, Fabrication of Novel Colloidosome Microcapsules with Gelled Aqueous Cores, J Mater Chem 14(22) (2004) 3351-3355.

[60] J.T. Tang, M.F.X. Lee, W. Zhang, B.X. Zhao, R.M. Berry, K.C. Tam, Dual Responsive Pickering Emulsion Stabilized by Poly[2-(dimethylamino)ethyl methacrylate] Grafted Cellulose Nanocrystals, Biomacromolecules 15(8) (2014) 3052-3060.

[61] V.D. Gordon, C. Xi, J.W. Hutchinson, A.R. Bausch, M. Marquez, D.A. Weitz, Self-Assembled Polymer Membrane Capsules Inflated by Osmotic Pressure, J Am Chem Soc 126(43) (2004) 14117-14122.

[62] N. Tsuda, T. Ohtsubo, M. Fuji, Preparation of Self-Bursting Microcapsules by Interfacial Polymerization, Adv Powder Technol 23(6) (2012) 724-730.

[63] M. Kobaslija, D.T. McQuade, Polyurea Microcapsules from Oil-in-Oil Emulsions via Interfacial Polymerization, Macromolecules 39(19) (2006) 6371-6375.

[64] H. Skaff, Y. Lin, R. Tangirala, K. Breitenkamp, A. Boker, T.P. Russell, T. Emrick, Crosslinked Capsules of Quantum Dots by Interfacial Assembly and Ligand Crosslinking, Adv Mater 17(17) (2005) 2082-2086.

[65] J.S. Sander, A.R. Studart, Monodisperse Functional Colloidosomes with Tailored Nanoparticle Shells, Langmuir 27(7) (2011) 3301-3307.

[66] R.K. Shah, J.W. Kim, D.A. Weitz, Monodisperse Stimuli-Responsive Colloidosomes by Self-Assembly of Microgels in Droplets, Langmuir 26(3) (2010) 1561-1565.

[67] K.L. Thompson, P. Chambon, R. Verber, S.P. Armes, Can Polymersomes Form Colloidosomes?, J Am Chem Soc 134(30) (2012) 12450-12453.

[68] W. He, X.C. Gu, S. Liu, Surfactant-Free One-Step Synthesis of Dual-Functional Polyurea Microcapsules: Contact Infection Control and Drug Delivery, Adv Funct Mater 22(19) (2012) 4023-4031.

[69] O. Shimoni, A. Postma, Y. Yan, A.M. Scott, J.K. Heath, E.C. Nice, A.N. Zelikin, F. Caruso, Macromolecule Functionalization of Disulfide-Bonded Polymer Hydrogel Capsules and Cancer Cell Targeting, Acs Nano 6(2) (2012) 1463-1472.

[70] J.W. Cui, Y. Yan, G.K. Such, K. Liang, C.J. Ochs, A. Postma, F. Caruso, Immobilization and Intracellular Delivery of an Anticancer Drug Using Mussel-Inspired Polydopamine Capsules, Biomacromolecules 13(8) (2012) 2225-2228.

[71] I.I. Slowing, B.G. Trewyn, S. Giri, V.S.Y. Lin, Mesoporous Silica Nanoparticles for Drug Delivery and Biosensing Applications, Adv Funct Mater 17(8) (2007) 1225-1236.

[72] B.J. Blaiszik, M.M. Caruso, D.A. McIlroy, J.S. Moore, S.R. White, N.R. Sottos, Microcapsules Filled with Reactive Solutions for Self-Healing Materials, Polymer 50(4) (2009) 990-997.

[73] S.A. Odom, M.M. Caruso, A.D. Finke, A.M. Prokup, J.A. Ritchey, J.H. Leonard, S.R. White, N.R. Sottos, J.S. Moore, Restoration of Conductivity with TTF-TCNQ Charge-Transfer Salts, Adv Funct Mater 20(11) (2010) 1721-1727.

[74] I.R. Nabiev, H. Morjani, M. Manfait, Selective Analysis of Antitumor Drug-Interaction with Living Cancer-Cells as Probed by Surface-Enhanced Raman-Spectroscopy, Eur Biophys J 19(6) (1991) 311-316.

[75] H. Morjani, J.F. Riou, I. Nabiev, F. Lavelle, M. Manfait, Molecular and Cellular Interactions between Intoplicine, DNA, and Topoisomerase-Ii Studied by Surface-Enhanced Raman-Scattering Spectroscopy, Cancer Res 53(20) (1993) 4784-4790.

[76] J.B. Song, J.J. Zhou, H.W. Duan, Self-Assembled Plasmonic Vesicles of SERS-Encoded Amphiphilic Gold Nanoparticles for Cancer Cell Targeting and Traceable Intracellular Drug Delivery, J Am Chem Soc 134(32) (2012) 13458-13469.

[77] X.M. Qian, X.H. Peng, D.O. Ansari, Q. Yin-Goen, G.Z. Chen, D.M. Shin, L. Yang, A.N. Young, M.D. Wang, S.M. Nie, In vivo Tumor Targeting and Spectroscopic Detection with Surface-Enhanced Raman Nanoparticle Tags, Nat Biotechnol 26(1) (2008) 83-90.

[78] C.M. Pitsillides, E.K. Joe, X.B. Wei, R.R. Anderson, C.P. Lin, Selective Cell Targeting with Light-Absorbing Microparticles and Nanoparticles, Biophys J 84(6) (2003) 4023-4032.

[79] V.P. Zharov, E.N. Galitovskaya, C. Johnson, T. Kelly, Synergistic Enhancement of Selective Nanophotothermolysis with Gold Nanoclusters: Potential for Cancer therapy, Laser Surg Med 37(3) (2005) 219-226.

[80] X.H. Huang, P.K. Jain, I.H. El-Sayed, M.A. El-Sayed, Plasmonic Photothermal Therapy (PPTT) Using Gold Nanoparticles, Lasers in Medical Science 23(3) (2008) 217-228.

[81] X.H. Huang, I.H. El-Sayed, W. Qian, M.A. El-Sayed, Cancer Cell Imaging and Photothermal Therapy in the Near-Infrared Region by Using Gold Nanorods, J Am Chem Soc 128(6) (2006) 2115-2120.

[82] X. Huang, M.A. El-Sayed, Gold Nanoparticles: Optical Properties and Implementations in Cancer Diagnosis and Photothermal Therapy, Journal of advanced research 1(1) (2010) 13-28.

[83] I.H. El-Sayed, X.H. Huang, M.A. El-Sayed, Selective Laser Photo-Thermal Therapy of Epithelial Carcinoma Using Anti-EGFR Antibody Conjugated Gold Nanoparticles, Cancer Lett 239(1) (2006) 129-135.

[84] V.N. Uversky, J.R. Gillespie, A.L. Fink, Why Are "Natively Unfolded" Proteins Unstructured Under Physiologic Conditions?, Proteins 41(3) (2000) 415-427.

[85] J.A. Yang, B.J. Johnson, S. Wu, W.S. Woods, J.M. George, C.J. Murphy, Study of Wild-Type α-Synuclein Binding and Orientation on Gold Nanoparticles, Langmuir 29(14) (2013) 4603-4615.

[86] H. Puchtler, F. Sweat, M. Levine, On Binding of Congo Red by Amyloid, J Histochem Cytochem 10(3) (1962) 355-364.

[87] H.Y. Yang, S.N. Yang, J.L. Kong, A.C. Dong, S.N. Yu, Obtaining Information about Protein Secondary Structures in Aqueous Solution Using Fourier Transform IR Spectroscopy, Nat Protoc 10(3) (2015) 382.

[88] J. Wantyghem, M.H. Baron, M. Picquart, F. Lavialle, Conformational-Changes of Robinia-Pseudoacacia Lectin Related to Modifications of the Environment - Ftir Investigation, Biochemistry-Us 29(28) (1990) 6600-6609.

[89] E. Koos, Capillary Suspensions: Particle Networks Formed through The Capillary Force, Curr Opin Colloid In 19(6) (2014) 575-584.

[90] S. Herminghaus, Dynamics of Wet Granular Matter, Adv Phys 54(3) (2005) 221-261.

[91] N.D. Rawlings, A.J. Barrett, Families of Serine Peptidases, Method Enzymol 244 (1994) 19-61.

[92] S.R. Paik, H.J. Shin, J.H. Lee, C.S. Chang, J. Kim, Copper(II)-Induced Self-Oligomerization of α-synuclein, Biochem J 340 (1999) 821-828.

[93] L.A.L. Bazydlo, M. Needham, N.S. Harris, Calcium, Magnesium, and Phosphate, Labmedicine 45(1) (2014) E44-E50.

[94] A. Binolfi, R.M. Rasia, C.W. Bertoncini, M. Ceolin, M. Zweckstetter, C. Griesinger, T.M. Jovin, C.O. Fernandez, Interaction of α-Synuclein with Divalent Metal Ions Reveals Key Differences: a Link Between Structure, Binding Specificity and Fibrillation Enhancement, J Am Chem Soc 128(30) (2006) 9893-9901.

[95] E.N. Marieb, K. Hoehn, The Cardiovascular System: Blood Vessels, Human anatomy & physiology, Pearson Education2007, pp. 703-720.

[96] E.D. Bennett, S.A. Barclay, A.L. Davis, D. Mannering, N. Mehta, Ascending Aortic Blood Velocity and Acceleration Using Doppler Ultrasound in the Assessment of Left-Ventricular Function, Cardiovasc Res 18(10) (1984) 632-638.

[97] L.O. Svaasand, C.J. Gomer, E. Morinelli, On the Physical Rationale of Laser Induced Hyperthermia, Lasers in Medical Science 5(2) (1990) 121-128.

[98] R. Rahbari, T. Sheahan, V. Modes, P. Collier, C. Macfarlane, R.M. Badge, A Novel L1 Retrotransposon Marker for HeLa Cell Line Identification, Biotechniques 46(4) (2009) 277-284.

[99] W.F. Scherer, J.T. Syverton, G.O. Gey, Studies on the Propagation in vitro of Poliomyelitis Viruses: IV. Viral Multiplication in a Stable Strain of Human Malignant Epithelial Cells (Strain HeLa) Derived from an Epidermoid Carcinoma of the Cervix, J Exp Med 97(5) (1953) 695-710.

[100] X.H. Bai, F. Cerimele, M. Ushio-Fukai, M. Waqas, P.M. Campbell, B. Govindarajan, C.J. Der, T. Battle, D.A. Frank, K.Q. Ye, E. Murad, W. Dubiel, G. Soff, J.L. Arbiser, Honokiol, a Small Molecular Weight Natural Product, Inhibits Angiogenesis in vitro and Tumor Growth in vivo, J Biol Chem 278(37) (2003) 35501-35507.

[101] J.X. Zheng, Y.J. Tang, M.R. Sun, Y.Y. Zhao, Q. Li, J. Zhou, Y.Z. Wang, Characterization, Pharmacokinetics, Tissue Distribution and Antitumor Activity of Honokiol Submicron Lipid Emulsions in Tumor-Burdened Mice, Pharmazie 68(1) (2013) 41-46.

[102] L. Dyadyusha, H. Yin, S. Jaiswal, T. Brown, J.J. Baumberg, F.P. Booy, T. Melvin, Quenching of CdSe Quantum Dot Emission, a New Approach for Biosensing, Chem Commun (25) (2005) 3201-3203.

[103] M. Babincova, P. Babinec, Magnetic Drug Delivery and Targeting: Principles and Applications, Biomed Pap 153(4) (2009) 243-250.

[104] Y.S. Kang, S. Risbud, J.F. Rabolt, P. Stroeve, Synthesis and Characterization of Nanometer-Size Fe3O4 and γ-Fe2O3 Particles, Chem Mater 8(9) (1996) 2209-2211.

[105] J.L. Lyon, D.A. Fleming, M.B. Stone, P. Schiffer, M.E. Williams, Synthesis of Fe Oxide Core/Au Shell Nanoparticles by Iterative Hydroxylamine Seeding, Nano Lett 4(4) (2004) 719-723.

국 문 초 록

알파-시뉴클레인의 자가조립을 통한 금 나노입자 마이크로캡슐의 제작 및 적재물 전달 체계로의 응용

생체 활용도가 높은 적재물 전달 체계를 확립하기 위해서는 생체 적합성, 생체내 안정성 및 목표 지점에서의 외부 자극에 의한 제어된 적재물 방출이 가능해야 한다. 본 논문에서 자가 결합성 단백질인 알파-시뉴클레인을 이용하여 금 나노입자, 은 나노입자, 양자입자, 그리고 자성 나노입자와 같은 다양한 나노 크기 입자의 표면 특성을 조절하고, 이 과정을 통해 이들 나노입자로 이루어진 피커링 에멀전을 만들기 위한 전략을 소개한다. 피커링 에멀전 형성 및 마이크로캡슐 제조의 두 과정 모두가 나노입자에 결합된 알파-시뉴클레인으로 인한 표면 특성에 전적으로 기인한다. 알파-시뉴클레인으로 나노입자를 캡슐화해 줌으로써 나노입자는 더 큰 탈착에너지를 갖게 되고, 이로 인하여 나노입자는 피커링 에멀전

구조를 안정적으로 유지시켜 에멀전의 유착이나 분해를 막아준다. 알파-시뉴클레인 분자 사이에서 유기용매로부터 유도된 베타-병풍 구조가 형성됨에 따라, 피커링 에멀전은 물리적, 화학적으로 안정적인 마이크로캡슐로 유도될 수 있다. 로다민 6G를 탑재한 마이크로캡슐은 단백질 분해 효소, pH 및 특정 금속 이온과 같은 개시인자에 의한 로다민 6G의 조절 방출을 나타내었다. 또한 금 나노입자로 구성된 마이크로캡슐의 광열 특성에 의해 야기되는 급격한 국부 발열에 관한 조사가 진행되었으며, 이 고열 요법의 유효성이 시험관내 세포 생존 실험에 의해 확인되었다. 나아가, 마이크로캡슐에 역미셀, 다른 나노입자 및 항체를 도입함으로써 상호 독립적 적재물 탑재, 영상화 및 표적화 특성과 같은 부가적인 기능을 부여할 수 있다. 종합하면, 적재물 전달 체계를 위한 금 나노입자 마이크로캡슐의 제작법이 제안되었고, 그 결과 만들어진 다기능성 마이크로캡슐은 그 활용 용도에 적합한 특성을 나타내는 이상적인 적재물 전달체로서 활용될 수 있다.

주요어

알파-시뉴클레인, 적재물 전달 체계, 금 나노입자, 복합 마이크로캡슐, 피커링 에멀전, 단백질 자가조립